LIGHTWEIGHT APPROACHES TO POLYESTER COMPOSITES: NANOCELLULOSE AND SYNTACTIC FOAMS

A Dissertation
Presented to
The Academic Faculty

by

Edward Thomas DiLoreto

In Partial Fulfillment
of the Requirements for the Degree
Doctor of Philosophy in the
Materials Science and Engineering

Georgia Institute of Technology
May 2021

LIGHTWEIGHT APPROACHES TO POLYESTER COMPOSITES: NANOCELLULOSE AND SYNTACTIC FOAMS

Approved by:

Dr. Kyriaki Kalaitzidou, Advisor
School of Mechanical Engineering
Georgia Institute of Technology

Dr. Donggang Yao
School of Materials Science & Engineering
Georgia Institute of Technology

Dr. Robert Moon
Forest Products Laboratory
USDA Forest Service

Dr. Douglas Fox
School of Chemistry
American University

Dr. Karl Jacob
School of Materials Science & Engineering
Georgia Institute of Technology

Date Approved: [April 23, 2021]

To my grandparents.

ACKNOWLEDGEMENTS

This work could not have been completed without the assistance of the many individuals both professionally, and personally. I would like to acknowledge the financial support from P^3 Nano, the U.S. Endowment for Forestry and Communities, and the 3M company, without which none of this would be possible. I would like to thank Dr. Kyriaki Kalaitzidou for providing me with a space to be creative and curious. Her support and guidance as my advisor and mentor were fundamental to my success. Also, to Dr. Robert Moon who not only provided wonderful insights and comments to my methodology and writing, but also fostered the collaborative and friendly work environment that was and is the Kalaitzidou lab. To Dr. Douglas Fox whose work was so vital to many aspects of this work: in providing both the materials and the excellent support and insights for the material. And to Dr. Karl Jacob and Dr. Donggang Yao for their suggestions on how to better shape the research and explore exciting new directions. I would like to acknowledge the specific technical support and advice provided by our 3M collaborators: Dr. Andrew D'Souza, Dr. Troy Ista, and Dr. Yong Wu. I would like to express my gratitude to the members of the Kalaitzidou lab, both new and old: Dr. Goswami, Ejaz, Arielle, Hattem, Ani, Luc, Monica, and Jamie. I will always appreciate their friendship and the many times they helped me when I found myself stuck. And to the undergraduate students, Josh, Eric, Nick, who assisted with collection of data and helped teach me how to lead a team. Finally, I want to thank my friends for the many after work pub trivia nights with the Schottkys, my parents and siblings for their love and support, and to my partner Manali who was by my side through it all.

TABLE OF CONTENTS

LIST OF TABLES

LIST OF FIGURES

LIST OF SYMBOLS AND ABBREVIATIONS

A ..... Area

BET ..... Brunauer-Emmet-Teller

CNC ..... Cellulose Nanocrystals

CNM ..... Cellulose Nanomaterials

CoNap ..... Cobalt(II) naphthenate

d ..... Diameter

D_a ..... Apparent Diffusivity

DIW ..... Deionized Water

DMA ..... Dynamic Mechanical Analysis

DSC ..... Differential Scanning Calorimetry

E ..... Elastic modulus

E' ..... Storage Modulus

E'_g ..... Glassy Storage Modulus

E'_r ..... Rubbery Storage Modulus

FRP ..... Fiber Reinforced Plastics

FTIR ..... Fourier Transform Infrared

HGS ..... Hollow Glass Spheres

I_α ..... Intensity of Loss Tangent at Alpha Transition Peak

l ..... Length

MEKP ..... Methyl ethyl ketone peroxide

MS ..... 3-(Trimethoxysilyl) propyl methacrylate

PR ..... Polyester Resin

SEM .....Scanning Electron Microscopy

SMC ..... Sheet Molding Compounds

SSA ..... Specific Surface Area

tan(δ) ..... Loss Tangent

TBPB.....tert-butyl peroxybenzoate

T_g.....Glass transition temperature

TGA .....Thermogravimetric Analysis

T_β.....Beta Transition Temperature

UV ..... Ultra-violet

V ..... Volume

v.....Volume Fraction

W_{max} ..... Maximum Water Uptake

XPS .....X-Ray Photelectron Spectroscopy

η.....Halpin-Tsai Parameter

ρ.....Density

SUMMARY

The focus of this research was to understand the effect of filler characteristics and composite processing in polyester (PR) composites on properties with the goal of realizing lightweight, high strength composites. Composites were made at both lab scale via open mold casting, and pilot scale via compression molding of sheet molding compounds (SMC). The impetus for this study is a recent trend towards lightweighting in the automotive sector, primarily driven by fuel efficiency standards.

In this study three different directions are explored, the first one is to add a high-performance nanomaterial, cellulose nanocrystals (CNC), into the composite to enhance the properties without increasing density. The second is to add a low-density material, hollow glass spheres (HGS), to reduce the density without compromising the properties. HGS were also coated with CNC and then compounded to form CNC coated HGS-PR composites. The combined effect of adding both in GF-polyester resin is also investigated. The third is to laminate SMC in a functionally graded arrangement to reduce density without compromising surface properties.

Although nanodispersion was not achieved, the ion exchanged CNCs displayed an enhanced storage modulus and improved elastic modulus, while maintaining composite density. Surface coating of HGS with CNC was successfully completed. CNC coated HGS-PR composites displayed enhanced storage modulus and reduced maximum water uptake relative to untreated HGS-PR composites. Functionally graded SMC was manufactured and showed good lamination and similar bulk properties to a monolithic formulation of similar density.

CHAPTER 1. INTRODUCTION

Much of materials science and engineering is founded on the paradigm of the materials-process-structure-properties framework (Figure 1.1), as it is the interplay between materials and processing that defines the structure of a product which in turn dictates the properties and overall performance. The material system of interest here are traditional glass fiber polyester composites, which have been used in various engineering applications for more than 50 years [1]. Such composites are made mainly using conventional sheet molding compound (SMC) technology.

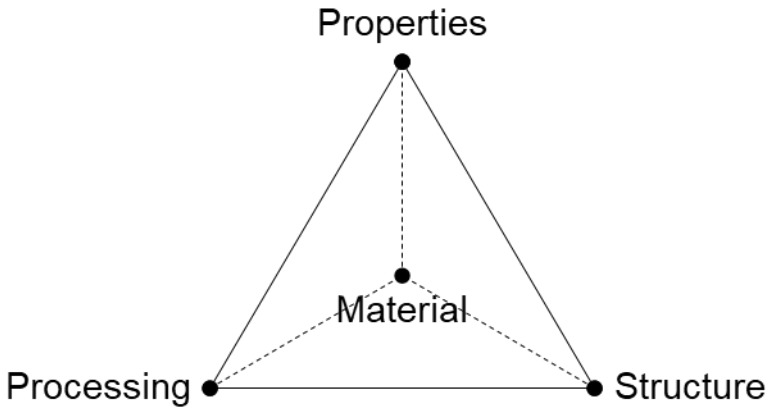

Figure 1.1 The materials science and engineering paradigm

The goal of this thesis is to provide the fundamental understanding needed to design and develop and next generation of polyester composites that are either lighter or stronger or both using scalable techniques with industrial relevance. The approach employed was to either (i) substitute, partially, constituents with a small quantity of a light but stronger material, or (ii) reduce the density of the composites by adding ultra-light fillers such as hollow glass spheres or (iii) design functionally graded composites or (iv) a combination

of i-iii. Multiple processing techniques were explored to understand the system with respect to the fundamental phenomena, including dispersion and distribution of reinforcements and fillers within the polyester resin and interfacial interactions as well as the practical performance implications of such a system. Finally, to complete the understanding of the study, the properties and structure (i.e. strength, and heterogeneity) were examined via a wide array of characterization techniques.

1.1 Background

1.1.1 Fiber Reinforced Polymers

Predominantly comprised of a polymer-based matrix, and a strong fiber reinforcement, fiber reinforced polymers (FRP) can be tailored to their specific end use. FRP, a young class of composite materials relative to other engineering materials, have found uses in a wide range of applications from the transportation to construction sectors. In addition to the core components-polymer and fiber-commercial FRP contain fillers that contribute different attributes including impact or viscosity modifiers, UV stabilizers, color pigments, low profile agents etc. [2-4].

One class of FRP known as sheet molding compounds (SMC) has risen to prominence in recent years. SMC consists of short and/or continuous fibers, generally fiberglass, and a thermoset polymer matrix. It is noted that as part of the glass fiber manufacturing process, a thin coating, called sizing, is applied on the glass fiber surface to increase the compatibility with the polymers, among other attributes. The polymer matrix is made up of a thermoset polymer and range of other commercial fillers with various purposes. Before the thermoset polymer and filler matrix is cured it is referred to as the

resin paste. A sample of these commercial fillers are outlined in Table 1.1. SMC materials are known for their formability, low cost, and adequate mechanical properties [2, 3]. As compared to oriented-long-fiber composites, SMC composites are easier to form and have substantially more isotropy in plane [3]. The wide array of variability in the SMC formulation provides avenues for advances in additives technology. This study will shed light on two specific filler materials-cellulose nanocrystals, and hollow glass spheres-and identify the principal mechanisms of their behavior.

The type of polymer resin used in the SMC has a substantial effect on the properties of the composite. The decision process for resin selection is guided primarily by cost, strength, and ease of handling. Epoxy based resin systems are widely studied in the literature but are less common in the commercial SMC composites due to their high cost. Conversely polyester, both vinyl and unsaturated, are less studied in the literature due to the material handling issues related to the vinyl crosslinker (most commonly styrene, a carcinogen), and the generally higher performance of epoxies over crosslinked polyesters [5]. Polyesters are more commonly used in commercial SMC because of the lower cost and better control of thickening time [1, 3, 6]. These circumstances provide an opportunity for inquiries. Consequently, this study examines a commercially available polyester resin (PR) and high performance-fillers from a fundamental scientific perspective with the goal of providing translatable insights to a commercial SMC application.

Table 1.1 List of types of materials commonly found in SMC composites with specific examples.

Segment	Constituent	Example	Typical Mass %
A-Side Paste	Polymer resin	Vinyl or unsaturated polyester, epoxy, or phenolic polymer	11.4
	Low-profile additive	Poly(vinyl acetate), poly(methyl methacrylate), polystyrene, polyurethane, or polyethylene	5
	Monomer solvent[a]	Styrene monomer	7
	Initiator[a]	t-Butyl peroxybenzoate, or other peroxide	0.2
	Inhibitor[a]	p-Benzoquinon	<0.1
	Mold Release	Zinc stearate, Zinc oxide	1.1
	Wetting agent	Acidic copolymers	0.2
	Fillers	$CaCO_3$, hollow glass spheres, clay particles, talc, mica, etc.	45.7
B-Side Paste	Time based thickener	Metal oxides, usually magnesium oxide	0.4
Reinforcement	Fibers	Glass, carbon, plant based, or basalt fiber	29

[a] Only included in polyester based formulations
[1, 6, 7]

Sheet molding compounds contain added commercial fillers into the matrix (Table 1.1). These additives provide a wide range of benefits to the material as a whole; including lowering cost, decreasing density, increasing mechanical properties, aiding in formability, enhancing surface finish, adding color, and assisting in clean mold release [1]. Calcium carbonate ($CaCO_3$) is the prevailing additive by mass. Derived from limestone, calcium carbonate reduces the materials cost, enhances surface finish, moderates crosslinking

exotherms, and increases processing consistency [7]. Aside from glass fibers (2.6 g/cm^3), $CaCO_3$ (2.7 g/cm^3) is the main contributor to the density of the SMC (1.8-1.9 g/cm^3). Replacing $CaCO_3$ with low density materials could increase the fuel efficiency of a finished vehicle. This study will be primarily concerned with substituting this high-density filler with lower density alternatives.

Much of the optimization and research of commercial fillers has already been completed by industry and is either patented or trade secret; however, nanomaterials have only been explored to a limited extent in some matrices [8-10]. Similarly, another open area of research is the integration of hierarchical structures (i.e. coating micron sized materials with nano sized particles, or structuring the SMC on the millimeter scale using classical models as design guides) to combat the increased density and increase the competitiveness of SMC. To explore the optimization potential, this study examines cellulose nanocrystals-polyester composites, hierarchical syntactic foams, and functionally gradient structures.

1.1.2 Cellulose Nanocrystals

Nanocomposites (composites which contain reinforcements or fillers that have at least one dimension less than 100 nm) pose a fascinating dilemma for materials researchers, there are many fundamental opportunities for improving composite material performance, but processing challenges limit translation of nanoscale properties to macroscopic structures. Theoretical research set grand expectations for fully realized nanocomposites, but empirical complications restrict progress. In the field of structural composites, the chief complication is efficiently dispersing the nanomaterial in the matrix phase. Ideally, fully

dispersing the nanomaterial takes advantage of the high surface area to volume of the nanoparticles. The interfacial volume for an ideal dispersed nanocomposite can be orders of magnitude greater than for traditional composites containing the same volume fraction of reinforcements. Properties of the matrix material at this interface are significantly different than in the bulk. As a result, even a small amount of nanomaterial by volume can significantly affect the bulk properties [11-17].

In recent times, sustainable or renewable materials including fillers, reinforcements or polymers used as matrices have become a topic of interest in the field of materials science and engineering. These family of materials are defined as being derived from a resource which are replenished through a natural process. Furthermore, overall sustainability (i.e. the environmental impact or carbon footprint) of the material system and the resulting product is of growing concern. A common approach to achieving these goals is twofold: reducing the part's mass and incorporating an increased amount of renewable materials. Critically, to be fully integrated into consumer products, these goals need to be achieved without sacrificing critical to customer properties.

Cellulose nanomaterials (CNM) have been incorporated into polymer composites for over 25 years [18]. This family of materials is attractive in a market where environmentally friendly material feedstocks are valued. Cellulose based materials have been widely used for applications ranging from food packaging to textiles. CNMs can be extracted from bulk cellulose materials (e.g., plants, trees, agricultural waste streams, recycled paper, etc.). Although CNM mechanical properties are not notably better than other nanomaterials, the biogenic, renewability, biodegradability, low toxicity, and high-volume production potential of these materials makes them particularly appealing. If used

properly, CNMs can provide strength and modulus improvements in polymer composites, and with a density of ~1.59 g/cm^3 the addition of CNM has only a slight effect on the overall composite density. Cellulose nanocrystals (CNC) are one type of CNM and are comprised of highly crystalline cellulose domains. Some basic material properties of these materials are outlined in Table 1.2, along with other comparable nanomaterials. This study will examine CNC and their impact in CNC-PR composites.

Table 1.2 General material properties of common nanofillers

Material	Aspect Ratio	Tensile Strength (GPa)	Tensile Modulus (GPa)	Density (g/cm^3)
Cellulose Nanocrystal	10-100	7.5-7.7	110-120	1.6
Carbon Nanotubes	100-500	11-63	270-950	1.3
Carbon Nanofibers	150	2.9	240	1.8
Graphite Platelet	10-10000	10-20	1000	2
Clay Nanoplatelets	0.3-1000	1	170	2-3

[13, 19, 20]

Various studies have explored CNC in thermosets such as epoxy and polyester [9, 10, 21-45]. CNC have been proven as an advantageous additive in CNC-GF-epoxy SMC systems [8-10, 37]. Work has also been done that studies a CNC-PR composite [21, 23-26, 28, 32, 46]. In surface modified CNC-epoxy composites mechanical testing revealed increases in T_g by 30°C, tensile strength by 82 %, elastic modulus by 21 %, and high temperature storage modulus by 160 % [45]. One aspect of this study is to investigate the potential of CNC as a mechanical reinforcement in PR based composites. Silane treated CNC-PR composites have shown increased tensile strength by 20 %, and tensile modulus by 11 %. [25]. In the context of SMC there are a few main avenues for introducing particulate fillers and nanoparticles: direct addition into the resin paste, coating the glass

fibers in sizing, and coatings of other fillers [1]. Previously studies have found CNC to be an efficacious sizing on glass fibers sizing for use in epoxy-based composites [37].

Reinforcement material surface chemistry can play a substantial role in how the properties of interest are transmitted to the bulk composite [5, 20]. In the world of polymer composites, surface treatment (the most common of which is silanization) of the reinforcing material is a common route. Surface treatment offers a wide range of surface chemistries to be added onto the surface in a relatively easy manner on the lab scale [40]. However, this process can be challenging to scale up when applied to nanofillers (i.e. CNC) due to their tendency to agglomerate prior to their reaction with the coupling agent. Consequently, only the agglomerate surface is modified, rather than each individual nanoparticle surface. Ion exchange is a process that has been used on CNC to exchange the cation, usually a group I element, for a more complex oligomer. The exchanged electrolyte can be bulky-to reduce CNC-CNC interactions-or selectively reactive-to encourage bonding between the CNC and matrix. Ion exchange is already in use for water purification, chemical analysis, and fuel cell manufacturing indicating the potential for this surface modification method to be commercially relevant [47]. Therefore, this study used CNC functionalized by an ion exchange process. In the previous work counterions were selected with the intent of reducing CNC-CNC interactions. CNC ion exchanged with methyl(triphenyl) phosphonium cations displayed reduced water absorption and lower desorption hysteresis and increased the peak degradation temperature indicating the potential for both better compatibility with a non-polar polymer matrix, and good environmental stability of the resulting composite. These materials were used to make CNC-epoxy nanocomposites and resulted in an increase in tensile modulus of 15 % [36].

Cellulose nanocrystals have been studied in various polymer matrices with a wide combination of other fillers [31, 34, 48-50]. These studies have predominately examined nanocomposites manufactured on the lab scale, with few striving to explore a larger scale process [8-10]. Conventional approaches to introducing nanomaterials into polymer composites-direct mixing, in situ polymerization-have proven predominantly ineffective [31]. The use of ionic surfactants or ion exchanged CNCs has only been explored in a limited number of matrix materials, and with a limited number of select counter ions. Combination treatments-i.e. using ion exchanged CNC in conjunction with traditional surfactants-has also not been examined as a potential route for CNC incorporation into polymer matrices. If the goal of utilizing sustainably sourced materials, such as CNC, is to be realized, all avenues of material incorporation must be explored.

1.1.3 Syntactic Foams

Syntactic foams are a family of materials that contain hollow spheres in a solid matrix. They are widely used in applications (i.e. automotive body panels, aircraft components, and marine structures) that require low density, radiation transparency, and high specific strengths. One material used in these foams is hollow glass spheres (HGS) which have substantially reduced densities (0.2-0.8 g/cm^3) as compared to the other components of the SMC [51]. SMC containing HGS have been in development since at least the 1970's [52]. Although these materials have been studied previously, there has been little success in generating a so called ultra-low density (~1.0 g/cm^3) SMC using HGS that also maintains mechanical strength [7, 52-54]. Much of the work in literature focuses on a system with fewer components: a reinforcement (fibers, nanofibers, or nanotubes), hollow spheres, and an polymer resin [55-57].

Many have developed numerical and computational models to explain the relationship between the properties of the constituent materials to the properties of the bulk syntactic foam [58-62]. Deviations from the ideal theoretical behavior are attributed to several sources: an imperfect HGS-matrix interface, interstitial porosity, and clustering of HGS particles within the matrix [60, 63]. An analytical model that took into account interface imperfections, parameterizing the adhesion between the HGS surface to the matrix polymer, found good agreement with experimental data up to 60 vol% HGS loading [60]. Elsewhere finite element techniques demonstrated how clustering of HGS leads to lower energy crack propagation and more rapid structural failure [63].

The interphase of syntactic foams dictates the properties of the bulk composite. Consequently, HGS are often surface modified with a range of chemistries to enhance this interphase. Silanization with methacryloxypropyl trimethoxysilane increased the flexural strength of a fiber reinforced polyester composite by 10% and the flexural modulus by 5% in SMC composites with density of ~1.3 g/cm^3. Other types of silanes were studied with similar increases to strength and modulus [64]. Elsewhere surface modified fly ash cenospheres have been studied in polymer matrices. These studies stop short of providing insight into the reinforcement-matrix chemical interactions, via dynamic mechanical analysis or Fourier Transform Infrared analysis (FTIR), and instead rely solely on imaging and bulk characterization techniques such as mechanical testing [65, 66]. A wide array of work has been published on incorporating a broad spectrum of fillers and nanofillers into the matrix phase of syntactic foams [7, 52-57, 67-70]. However, coating hollow particles prior to compounding has seem little examination in the literature [71, 72]. It is possible, and even likely that development in this area has been completed in the commercial sector,

but there is no publicly available information on the subject. Work by Zhang et al. developed HGS coated with a high specific surface area metal organic framework and, subsequently, a phosphorous containing silane. In the study they observed an increase in interfacial strength between the HGS and the epoxy matrix [73].

Extensive research has been conducted in reinforced syntactic foams [57, 74]. Various materials including glass and carbon fibers, carbon nanotubes, and clay nanoplatelets have been used in reinforced syntactic foams [57]. These filler materials have shown a general increase in mechanical properties and performance. No studies exist that explore the effect of CNC-polymer matrix syntactic foams. Other studies have shown an enhancement in the interface of epoxy-GF when CNC are added to the matrix, indicating the potential for an enhancement of polymer-HGS interface via CNC addition. The Achilles heel of syntactic foams remains the interfacial adhesion strength between the hollow particle and the matrix. Theoretical models and experimental work have confirmed the weakness of the interface [60]. The main method for enhancing interfacial strength is surface modification of the hollow particle via silanes or other chemical agents [66, 67, 75]. Prior work on coating fibers with CNCs has shown significant promise [33, 37]. Others have also explored using CNC in conjunction with silanes to enhance surface properties of glass substrates [76]. Translating the processing technology from fibers and planar substrates to hollow glass spheres will pose a challenge. Very limited work has been done in the literature on coating hollow particles for syntactic foams with nanomaterials [71]. Thus, translating GF coating technology to HGS surface treatment would greatly expand the property space for syntactic foams.

This study examines pre-processing treatment of HGS in the development of ultra-light weight SMC composites. Specifically, the chemical and physical interactions between the HGS and matrix are of interest, and the effects of CNC coatings of HGS on the properties of HGS-PR composites. Additionally, to better understand the process of developing a material from lab scale to pilot scale, this study examines HGS both in the context of a bench top idealized system, and then to a full-scale SMC, including relevant commercial additives and fillers.

1.1.4 Functionally Graded Composites

SMC manufactured with HGS have one major drawback with respect to commercial applications, a reduction in surface finish quality. After sanding the part surface, a standard step to prepare the part for painting, the HGS can be fractured, resulting in micro voids on the surface. These voids capture volatiles from paint primer and, after heating, result in paint pops. Such defects are extremely undesirable and difficult to mitigate [52-54]. As a result, some have looked towards a functionally graded, or sandwich structure, where the outer layers are free of HGS while the inner layer contains some amount of HGS. This technique improves surface quality and reduces part density [53]. Syntactic foams are also a common choice as a core material in sandwich style composites. Such composites usually have prepreg fiber mats as the outer layers with relatively significantly thicker syntactic foam cores [74, 77, 78]. Some limited studies have been done on functionally graded syntactic foams generally comprised of only epoxy and HGS. One of the main challenges noted in these studies is allowing the resin paste to thicken enough to prevent the HGS from floating to the upper layers of the resin [79-81].

This study will investigate the mechanical properties of functionally graded composites produced by SMC. A functionally graded composite part will be manufactured that utilizes HGS through processing paths developed in this study. The potential of this approach will be investigated by comparing the properties of the functionally graded composites made with the properties predicted by the lamination theory using a laminator, a commercial software for design or study laminated structures [5].

Sheet molding compounds are a thoroughly examined for commercial optimization. Unfortunately for academic interests, these studies neglect to explore the fundamental material-structure-property relationships that underlie the composite performance. Such a fundamental study of SMC is no simple task. The degrees of freedom in such an experiment would be on the order of 10-20 factors. Functionally graded SMC has been studied in brief and without consideration of fundamental relationships. Micromechanical models are a useful tool for illuminating the fundamental relationships that would be difficult to observe in a multifactorial experiment.

1.2 Thesis Aims

1.2.1 Goals and Objectives

Primarily, the goal of this work is to understand the materials-structure-property relationship in a lightweight polymer composite using CNC and HGS. This study aims to address three main objectives:

1. Understanding the effect of cellulose nanocrystal surface chemistry on CNC-PR composite properties.

2. Understanding the effect of cellulose nanocrystals on HGS-PR composite properties.
3. Evaluating methods of lightweighting SMC on composites via classical lamination theory and examining the fundamental aspects of functionally gradient structures on SMC composite properties.

In examining these questions, it will be possible to better understand the role of HGS, and CNC in composite properties as well as the development and manufacturing of advanced SMC composites, (Figure 1.2). The structure of this study is such that it bridges the gap between fundamental and applied research, thus providing an expansion of the fundamental knowledge of the field that is more directly applicable for use in industry.

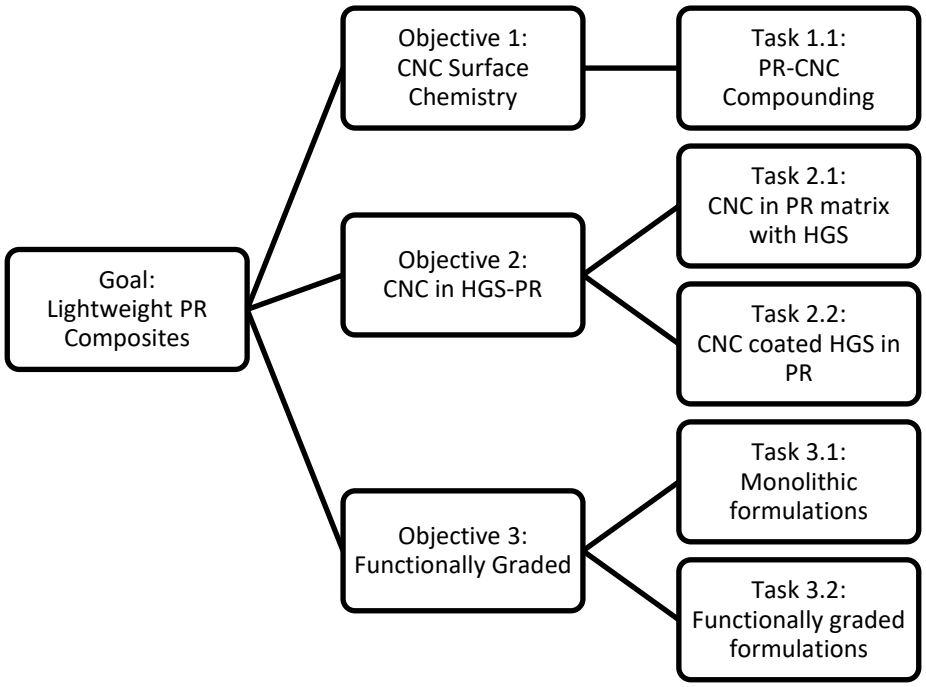

Figure 1.2 Overview of presented research on PR composites.

1.2.2 Methodology of Thesis

The structure of this manuscript generally follows the order of the thesis objectives outlined in 1.2.1. Chapter 2 outlines common materials and methods used in the work, allowing for more explicit detail to be provided in later chapters where necessary. Chapter 3 discusses results from experimental work on CNC-PR composites. Work on syntactic foam composites and reinforced syntactic foam composites is delivered in Chapter 4. Chapter 5 discusses the results of scale up and a comparison of resulting properties to predictive models. Conclusions and outcomes are stated in detail in Chapter 6.

CHAPTER 2. MATERIALS AND METHODS

2.1 Materials

2.1.1 Resin, Additives, and Glass Fibers

For the work in Chapters 3, unsaturated polyester resin POLYLITE 31608-00 was provided courtesy of Reichhold, an industrial manufacturer of unsaturated polyester resins for composites and coatings. Work in Chapter 4 and 5 used a separate commercial resin, Arotran 774/775. This two-part resin was provided courtesy of Ashland Inc., an industrial resin manufacturer. For later studies, the Arotran resin was selected due to its lower density. For lab scale studies, the initiator used, methyl ethyl ketone peroxide (MEKP), was purchased from Sigma-Aldrich. The catalyst, cobalt naphthenate (CoNap), was purchased from Alfa Aesar-53% in mineral spirits. Pilot scale trials used a higher temperature peroxide initiator, tert-butyl peroxybenzoate (TPBP). Calcium carbonate, HuberCarb W4, was supplied by Huber Engineered Materials. Surface treated glass fiber rovings, Advantex P204, was provided courtesy of Corning, (density 2.62 g/cm^3). The wet out, BYK 9010, was provided by BYK Additives and Instruments. Zinc stearate, the mold release, was purchased from Acros Organics. A styrene emission agent was used as supplied from BYK Additives and Instruments, BYK-s 740.

2.1.2 Cellulose Nanocrystals

Freeze dried CNCs with different surface functionality and dimensions were used in this study. For work in Chapter 3 as received freeze-dried powder of sulfonated CNC (SCNC), manufactured by United Stated Department of Agriculture-Forest Product

Laboratory with a degree of substitution of 0.27 mmol/g, were purchased from the Process Development Center at the University of Maine. SCNC diameter and length post-hydrolysis were 7 ± 2 nm and 134 ± 52 nm respectively [82]. Cellulose nanocrystals functionalized with Methyl(triphenyl) phosphonium (PhCNC), at a degree of substitution of 0.25 mmol/g, were provided courtesy of American University, Washington, D.C. at a concentration of 4 wt% in deionized (DI) water. PhCNC are produced from an ion exchange process. The average diameter and length of the PhCNC in solution were 6 ± 2 nm and 130 ± 67 nm, respectively. Maleic acid functionalized CNC (MCNC) were provided courtesy of the Forestry Products Laboratory at a concentration of 0.58 wt% in DI water. MCNC were produced from bleached eucalyptus pulp fibers by maleic acid hydrolysis and have a diameter of 12–15 nm and a length of 500–700 nm, and a COOH degree of substitution of 0.20–0.25 mmol/g. Methods for synthesis and characterization of the PhCNC and MCNC materials can be found elsewhere [36, 83]. The freeze dried SCNC were also used in work in Chapter 5.

For work included Chapter 3, the as received MCNC and PhCNC water suspensions were freeze-dried by first mixing with 10% tert-Butyl alcohol by volume to enhance CNC isolation in the lyophilized state [84]. The suspensions were then sonicated and placed in a −80°C freezer. Once frozen samples were lyophilized until dry using a Labconco 12L freeze-drier at approximately -45 °C and 200 μbar for 2–4 days. Freeze-dried CNC powders, consisting of micronized particles/flakes, were used without any post processing.

For work included in Chapter 4, CNC were utilized in both a dried state and in dispersion to coat HGS. The dried CNCs were supplied by Celluforce and were spray dried. The spray dried CNC particles have a diameter ranging from 1-50 μm. Celluforce CNC

have an individual particle diameter and length of 2.3-4.5 nm and 44-108 nm, respectively. The sulfate content of these CNCs is 0.246-0.261 mmol/g. Summaries of CNC used are outlined in Table 2.1.

Table 2.1 Cellulose Nanocrystal surface treatments and drying methods

Short Name	Source	Surface Treatment	Drying Method
Chapter 3			
SCNC	University of Maine	Sulfate half ester, sodium counterion	-80°C Freezing, 10% tert-Butyl alcohol, lyophilized
PhCNC	American University-University of Maine	Sulfate half ester, methyl triphenyl phosphonium counterion	
MCNC	Forest Products Lab	Maleic acid half ester	
Chapter 4			
NaCNC	Celluforce	Sulfate half ester, sodium counterion	Spray dried
NaCNC	Celluforce	Sulfate half ester, sodium counterion	Never dried, 6 wt% in deionized water (DIW)
PhCNC	American University-Celluforce	Sulfate half ester, methyl triphenyl phosphonium counterion	Never dried, 4 wt% in DIW

2.1.3 Hollow Glass Spheres

Hollow glass spheres were provided by 3M. Surface treated and untreated HGS were provided. The surface treated HGS were treated with a 3-(Trimethoxysilyl) propyl methacrylate (<1 wt%) Figure 2.1. The S32HS class HGS are comprised of a soda-lime-borosilicate glass, have a D95 of 47 µm (95% of the HGS are smaller than 47 µm), and have a volatile content of 0.5 wt%. The S38HS class HGS are of similar composition to

the S32HS HGS but have an average diameter of 44 µm and a volatile content of 0.5 wt%. The types and relevant properties of the hollow glass spheres are listed in Table 2.2. These HGS were selected based on the combination of both low density, and good mechanical strength. The rigors of processing and handling (both in benchtop scale mixing and SMC compounding) can fracture and damage some HGS. S32HS and S32HS-MAS were used in both Chapters 4 and 5 while S38HS were only used in Chapter 5.

Table 2.2 Hollow Glass Sphere Types and Properties

HGS Type	Density [a] (g/cm^3)	Diameter [a] (um)	**Surface Chemistry**
S32HS	0.32	25	Glass
S32HS-MAS	0.32	25	Methacryl silane
S38HS	0.38	44	Glass

[a] Average HGS density and diameter provided by manufacturer

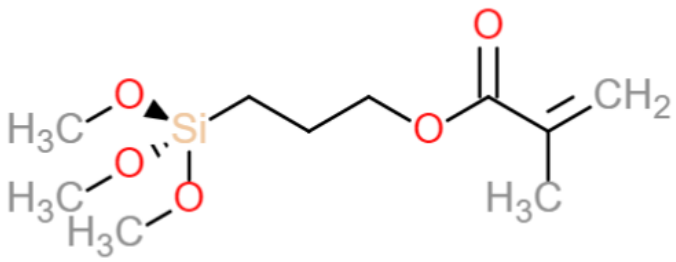

Figure 2.1 3-(Trimethoxysilyl) propyl methacrylate structure

Some HGS were further coated with CNC. This was achieved using a similar method to Pacaphol et al. [76]. CNC were dispersed in de-ionized water (DIW) at 1 wt% concentration by probe sonication. Dispersing CNC prior to the reaction increases the available reactive groups on the CNC nanoparticles. S32HS-MAS were then added in a ratio of 10:1 (HGS:CNC) by weight. Ethanol was added to produce a 1:1 ethanol:DIW

mixture. The addition of ethanol is necessary to properly disperse the relatively non-polar S32HS-MAS. Acetic acid was added to a pH of 4-5 to catalyze the hydrolysis of the silane. Samples were then stirred overnight to ensure good mixing. The mixture was then stirred and heated to 70°C for 2 hr to attempt to react the silane with the CNC. After heating the mixtures were filtered, rinsed, and dried in an oven at 120°C for 2 hr. A general reaction overview is shown in Figure 2.2.

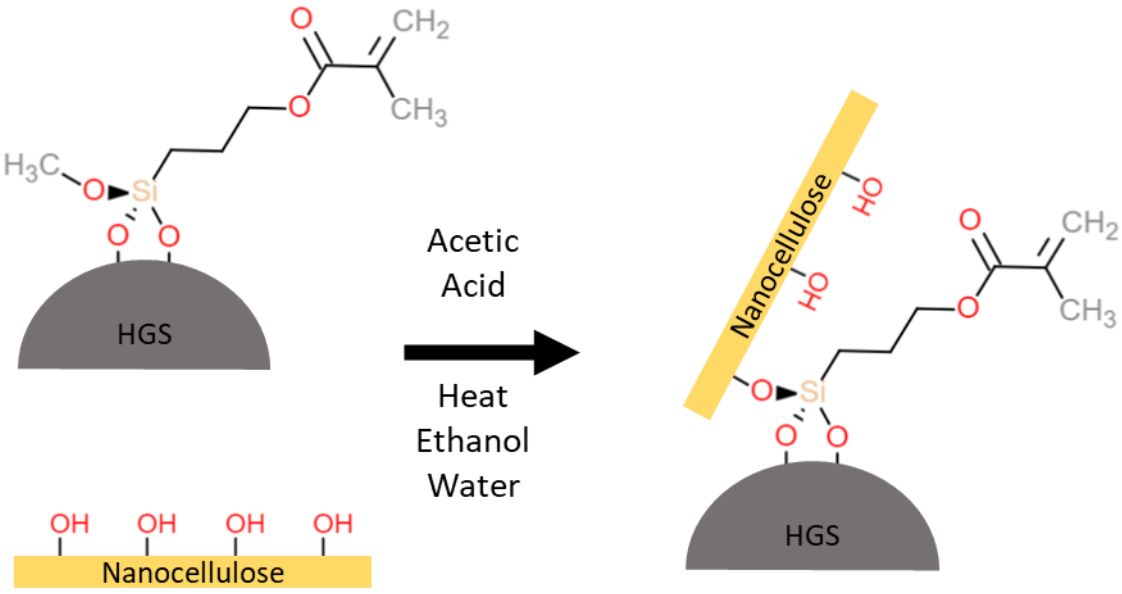

Figure 2.2 Schematic mechanism of potential chemical reaction linking CNC and HGS.

2.2 Fabrication and Manufacturing Processes

2.2.1 Lab Scale Polyester Composite Fabrication Processes

Mixtures of dried CNC powders with PR were prepared at various ratios first by manual mixing and then by probe sonication, QSonica Q-500 with ½" probe, at 50% power alternating 5 s on and 3 s off, in an ice bath, until a target energy density of 500 J/g was

reached. Samples were cooled to room temperature at intervals of 2.5 min during sonication. Subsequently, the catalyst, CoNap was added to the mixture at 0.2 wt% and the mixture was stirred. The initiator, MEKP, was then mixed at a ratio of 1.5 wt%. After mixing the system was degassed under vacuum, a small amount was set aside for optical imaging, while the remainder was poured into an open silicone mold. Samples from Chapter 3 were cured at room temperature for 3.5 h and post cured at 100°C for 30 min (Table 2.3). Samples from Chapter 4 were cured at room temperature overnight and then post cured at 120°C for 2 h (Table 2.4). Two separate cure profiles were used due to the change in resin. Samples were then demoulded. Any excess flash material was removed gently with high grit sandpaper.

Table 2.3 Formulation outline for Chapter 3

Material	Neat Resin (wt%)	1 wt% CNC (wt%)	2 wt% CNC (wt%)
Polylite 31608	98.3	97.3	96.3
MEKP	1.5	1.5	1.5
CoNap	0.2	0.2	0.2
CNC	0	1	2

Table 2.4 Formulation outline for Chapter 4

Material	Neat Resin (wt%)	1CNC (wt%)	5CNC (wt%)	15HS (wt%)	30HS (wt%)	15HS-1CNC (wt%)	15HS-5CNC (wt%)
Arotran 774	68.2	67.5	64.8	65.0	60.4	64.4	61.7
Arotran 775	29.2	28.9	27.8	27.9	25.9	27.6	26.4
MEKP	1.5	1.4	1.4	1.4	1.3	1.4	1.3
CoNap	0.2	0.2	0.2	0.2	0.2	0.2	0.2
BYK-S 740	1.0	1.0	0.9	0.9	0.9	0.9	0.9
HGS	0	0	0	4.6	11.4	4.6	4.5
CNC	0	1.0	5.0	0	0	1.0	5.0

2.2.2 Pilot Scale Polyester Based SMC Fabrication Processes

The manufacture of an SMC composite part can be divided up into three main stages: resin mixing, SMC compounding, and hot pressing. Thoroughly mixing and dispersing the fillers within the resin paste is critical in preventing heterogenous defects and achieving an isotropic resin. In an industrial setting the resin paste is mixed continuously in large vessels. After mixing is completed the resin paste is then transferred to the resin reservoirs in the SMC line (Figure 2.3). A carrier film, driven by a conveyor, pulls the resin underneath the doctor blade to produce a continuous film of consistent thickness. The thickness is adjusted by the doctor blade height and belt speed. Chopped fibers are then dropped onto the resin layer. The mass flow rate of fibers can be controlled the cutting wheel speed and belt speed. Fiber length can be varied from 6.4 to 50.8 mm (¼" to 2"). Wetting of the fiber bed is achieved when the two resin films are sandwiched in the compaction zone which is driven by a series of calendar rolls. After compaction, the SMC is collected and stored. A thickening or maturation stage is necessary to prepare the SMC for molding. The viscosity required for molding is several orders of magnitude greater than the viscosity needed to for the resin mixing and SMC compounding step. Typical maturation times are on the order of days or weeks. After the resin paste has reached a putty like consistency it is ready for forming through compression molding. Depending upon the desired part dimensions, and the flow behavior of the material, a charge of certain shape and number of layers is cut from the SMC sheet and placed into the preheated mold tool. Heated presses with metal-typically stainless steel-tooling are used to form the material. The press is then closed for a fixed time after which the part is ejected, and the process repeated until the desired number of parts has been manufactured

or the SMC consumed. Typical tool temperatures range from 100-200°C with molding times on the order of minutes [1].

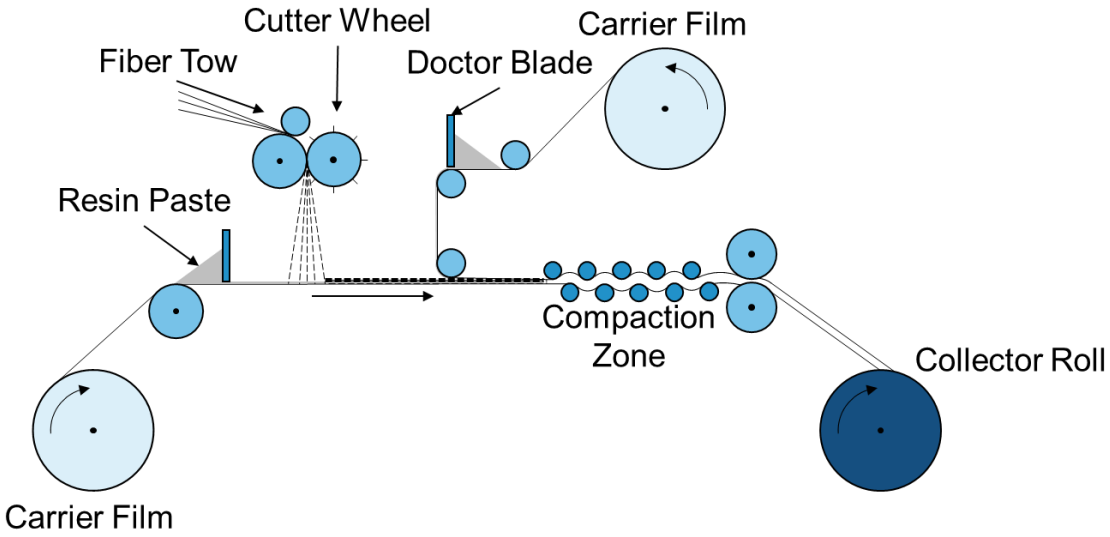

Figure 2.3 Schematic representation of a typical SMC line.

Resin paste was mixed using a Eurostar 40 cN motor in conjunction with a Cowell high shear mixing blade. The high shear mixing blade and motor were selected due to both their capability to rapidly homogenize the resin paste and the fact that this system approximates the systems used in commercial scale processes. The volume of resin mixed was approximately 2.5 L in a 4 L stainless steel vessel. A batch volume of 2.5 L was selected because it resulted in good mixing (higher or lower volumes resulted in low quality mixing vortexes), and because it allowed for manufacture of several finished plates from a single run. Various formulations were used in the study, some with and without $CaCO_3$, and some with and without HGS. Resin paste formulations are outlined in Table 2.5. When used, $CaCO_3$ added and mixed at a speed of 2,000 rpm-to break up any agglomerates-and HGS were mixed at a speed of 1,200 rpm-to avoid HGS fracture. A Finn & Fram Pilot

Scale SMC line was used. Fabrication of SMC on the pilot scale line was carried out using parameters stated in Table 2.6. Process parameters were identified over multiple iterations using a standard commercial formulation. The combination of resin bed width, and fiber drop width provided good wet out of fibers in the width that is needed for charge shaping (17-23 cm). The belt speed and glass fiber chop speed were selected to achieve the desired GF volume fraction. A GF length of 25.4 mm is considered the industry standard for most SMC materials.

Table 2.5 Resin paste formulation for samples in Chapter 5.

	S (phr)	U (phr)	M (phr)	M-CNC (phr)
A-Side				
Arotran 774 Resin	70	70	70	70
Arotran 775 Resin	30	30	30	30
TBPB	0.75	0.75	0.75	0.75
BYK 9010	1.00	1.61	1.61	1.61
BYK 740	1.00	1.00	0	0
Zn Stearate	4.50	4.50	4.50	4.50
Hubercarb W4	195	0	99.1	99.1
HGS	0	31.4	16.88	16.88
NaCNC	0	0	0	1.0
B-Side				
AM 9033	1.90	2.50	2.50	2.50
Resin Paste Density (g/cm^3)	1.75	0.70	1.23	1.23

A Wabash 50-ton hot press, model v50-1818-2tmx, was used for compression molding. The molding tool was manufactured separately and designed to produce 279.4 x 279.4 mm^2 plates. The tool dimensions were selected to optimally utilize the available SMC dimensions, (the pilot line has a maximum width capability of ~26 cm). The molding tool was comprised of three parts: the aluminum male half, the aluminum female half, and a steel punch out plate. Aluminum was chosen as the base material for the male and female

halves of the mold to manage costs. Steel was selected for the punch out as it experiences repeated concentrated impact during manual ejection and removal of the part. Typically tooling costs are the single most significant cost induced in the SMC manufacturing process. Aluminum tools have lifetimes that are orders of magnitude less than steel parts but cost substantially less. Since this project does not require high volume production (1,000-10,000s of units), aluminum was used for the body of the mold tool. Prior to introducing the charge, the mold was coated with zinc stearate release agent and pre-heated. Charge dimensions were varied to produce a 6 mm plate, but generally fell between 22 and 24 cm square (8½ and 9½" square) and used 4 plies. The plate thickness (5-6 mm) is a direct result of the mold cavity size. The plies were laid upon each other to keep the machine direction in one axis. Keeping the machine direction along the primary axis essentially controls the effect of any GF orientation bias. Once the zinc stearate coating had liquefied, indicating the mold was fully heated (zinc stearate melting point ~120°C), the charge was placed in the lower mold cavity, the top mold plate was positioned, and the entire assembly was set into the hot press. Preheating the mold is necessary to ensure that the material reaches the desired curing temperature, and no heat is lost further raising the temperature of the tool. After a final check for alignment of the mold the press was closed, and pressure was increased and held for 2 min. The mold assembly was then immediately removed, disassembled, and the finished plate was removed. Other molding parameters can be found in Table 2.6. Once cooled the plate is ready to be waterjet into specimens for testing.

Table 2.6 Pilot scale SMC line parameters

Parameter	Value
Resin Bed Width	254 mm
Fiber Drop Width	254 mm
Fiber Cutting Speed	4.4 g/s
Belt Speed	11 mm/s
Chopped Fiber Length	25.4 mm
Number of Rovings	6
Press Pressure	5.7 MPa
Mold Cavity Dimensions	279.4 x 279.4 x 6 mm^3
Molding Temperature	146°C
Molding Time	2 min

All samples were cut so that the machine direction aligned with the primary axis of the specimen. An OMAX Maxiem 1515 was used for cutting. The machining parameters were a Quality factor of 5, a high pressure setting, and a machinability setting of 700.

2.3 Characterization Techniques and Analysis Tools

Optical imaging of resin mixtures was completed using a Leica DM2500 optical microscope. The small amount of resin mixture that was set aside just after the degassing step was poured onto a glass microscope slide and covered with a glass cover slip, such that the layer of CNC-PR mixture was about 180 μm thick. Preparing samples this way provided a thin enough sample where individual CNC agglomerates could be resolved. CNC agglomerates in thicker specimens would scatter more of the light making it impossible to resolve any features. Images were collected under transmission and through cross polarizers. Due to the optically active nature of CNC cross polarizers can be used to provide increased contrast between the CNC and the polymer matrix. Optical imaging can be useful in characterizing the CNC agglomerate size and distribution in the matrix.

Imaging of pilot scale composite fracture patterns and cut surfaces was completed with a Leica DVM 6 optical microscope.

For experiments presented in Chapter 3 scanning electron microscopy (SEM) was completed using a Zeiss Ultra 60 FESEM at an accelerating voltage of 5 kV. Samples in Chapter 4 and 5 were imaged using a Phenom ProX SEM at 10 kV. For samples in all chapters prior to imaging, samples were Au/Pd sputter coated for 20-30 s at 0.1 mA using a Cressington 108 sputter coater to reduce charging effects. Fracture surface imaging is useful in identifying the source of fracture (e.g. void, agglomerate, impurity), the type of fracture propagation, the quality of the interface between filler and matrix, and the general distribution of filler material.

Mechanical testing of the tensile strength and modulus were completed according to ASTM D638 using an Instron 5982 equipped with a 100 kN load cell. For experiments in Chapters 3 and 4 a preload of 20 N was applied to remove slack from the load string, and testing was completed using displacement control with a cross-head speed of 5 mm/min [85]. Testing was completed in ambient conditions. The dogbone neck sample thickness and width were 3.3 mm, and an extensometer MTS-Model-634, with a gauge length of 12.7 mm and an axial travel range of ± 10% was used to record the axial strain. Six specimens for each CNC-PR composite type were tested. The tensile modulus was calculated in the linear elastic region. The results presented in Chapter 5, were obtained by tensile testing that was completed using a 5982 Instron with a 100 kN load cell. The specimen dimensions were set in accordance with ASTM 638 type I samples. Tests were completed at a strain rate of 5 mm/min until failure. The preload for each test was 440

N/min up to 40 N. Tensile testing was used to identify the ultimate tensile strength, and tensile modulus.

Mechanical testing of the flexural strength and modulus were completed according to ASTM D790-17 using an Instron 33R 4466 equipped with a 500 N load cell [86]. For Chapter 3 sample dimensions were 60 mm × 11.9 mm × 3.6 mm and were tested in 3-pt bending with a span length of 50 mm, and a displacement rate of 1.18 mm/min. Testing was completed in ambient conditions. At least four specimens of each CNC-PR composite type were tested. Flexural modulus was taken as the linear regression in the linear elastic region, (1.0–1.1% strain). The results presented in Chapter 5 were obtained from composite specimens with dimensions of 117 mm × 20 mm with 5–6 mm thickness and testing was performed at room temperature with a three-point bending fixture with a span length of 75 mm at a test rate of 3 mm/min. Flexural testing was used to identify flexural strength, and flexural modulus. Flexural testing is useful especially in samples where there may be property differences through the sample thickness.

From the perspective of a fundamental analysis changes in viscoelasticity can be extremely edifying. Dynamic mechanical analysis (DMA) has been extensively used to study changes in storage and loss modulus, and glass transition in polymer composites. Furthermore, DMA can be used to determine the cumulative effects of the matrix-CNC and/or matrix-HGS interactions (i.e. both chemical interactions such as covalent bonds, and physical interactions such as entanglements) on composite mechanical properties [24, 56, 87]. In conjunction with mechanical testing, DMA will be used to study chemical and physical interactions between the filler and matrix.

For Chapter 3 dynamic mechanical analysis (DMA) was used to determine the glass transition temperature (T_g) following ASTM D7028-07 [88]. DMA testing was conducted on a TA instruments Q800 DMA. The DMA parameters were standard at an oscillation of 1 Hz and a heating rate of 3°C/min, ramped from 40 to 230 °C. Sample dimensions were 60 mm × 11.9 mm × 3.6 mm, and were tested in 3-pt bending with a span length of 50 mm and a strain of 0.1%. The T_g was defined as the temperature at peak tan(δ). Glassy and rubbery modulus were taken to be the storage modulus at 80°C and 180°C, respectively. At least two specimens of each CNC-PR composite type were tested. For chapter 4 the heating rate was 5°C/min, ramped from 30 to 250°C. Glassy and rubbery modulus were taken to be the storage modulus at 50°C and 200°C, respectively. For Chapter 4 at least three specimens of each HGS-CNC-PR composite type were tested.

For samples discussed in Chapter 3 differential scanning calorimetry (DSC) was conducted using a TA Instruments Q2000 DSC on test specimens of approximately 10 mg. Samples were tested in Tzero Aluminum DSC pans and lids. To determine the residual enthalpy, two samples of each different curing cycle were ramped at 10°C/min to 200°C under a nitrogen purge of 50 mL/min. In addition to composite formulations, neat PR resin was also tested under the same parameters to acquire the total enthalpy of cure, which was used to calculate the percent cure of each sample.

Thermogravimetric analysis (TGA) was conducted on surface treated HGS to determine the amount of material deposited on the HGS surface through different coating methods. The TGA testing was conducted using a TA Instruments Q500 TGA. Test specimens were at least 5 mg in weight. The heating profile was 30 to 600°C at a rate of 10°C/min under a Nitrogen atmosphere.

ASTM D792-13 was followed to find the density of cured samples cut from the hot-pressed plates [89]. When relevant, the glass fiber content of each formulation was calculated using the Rule of Mixtures. Density measurements were completed using the water displacement technique of specimens that weighed at least 300 mg. At least 3 specimens were tested. Samples with densities less than water were weighed down using wire.

To determine the quality of the CNC surface coating on the HGS x-ray photoelectron spectroscopy (XPS) was used. To complete XPS testing a Thermo K-Alpha XPS equipped with a 1.486 KeV aluminum K-alpha x-ray source. Samples were probed for several elements, primarily carbon. XPS analysis can be used to identify relative amounts of hybridization for specific elements as well as relative atomic percentages to a high degree of accuracy and precision.

Water uptake measurements were conducted in accordance with ASTM D5229 [90]. The results are discussed in Chapter 4. Three DMA bars were used. Samples were dried in an oven at 100°C for 24 hr and stored in a desiccator until cooled to room temperature. The testing coupons were aged in 70°C DIW for 1 week. Once per day samples were removed from the water bath, patted dry, and weighed on a balance with precision to 0.1 mg. Samples weighed at least 2 g. For results in Chapter 5, 12.7x12.7 mm square pieces were waterjet from the plate material, sanded with high grit sandpaper to remove the tabs and immersed in DIW. Five samples were aged in DIW at 35 and 70°C each. The duration of the study was limited by the outbreak of the COVID-19 pandemic and subsequent campus closure. Samples were removed from the bath, patted dry, and weighed every 2-3 days. For water aged tensile samples in Chapter 5, three tensile bars

were set aside and stored in DIW at 70°C for 3.5 weeks. After the ageing period the samples were removed from the bath and subsequently tested.

All samples which were tested for significance are based on a 95% confidence interval (CI). Pairwise Tukey's test was used to determine if mean values were significantly different in test methods where statistical significance is discussed. This method for multiple comparison is useful as it has reduced error over multiple t-test comparisons. The method assumes that all observations are independent among groups, that the data is normally distributed within a group, and that there is equal within-group variance across all samples. The Tukey's test first requires an ANOVA analysis.

For glass filled or glass reinforced polymer matrix composites, a primary driving force for the absorption of water is the glass-polymer interface. In order to provide a relevant comparison for glass fiber surface area for samples in Chapter 5 which contain both HGS and GF the specific surface area (SSA) of glass was calculated. Taking the surface areas of the GF and HGS to be the surface area of a cylinder (ignoring the area of the ends), and the surface area of a sphere (A_{GF} and A_{HGS}). And taking the volumes of the GF and HGS to be that of a cylinder and sphere (V_{GF} and V_{HGS}). The specific surface area is then given by

$$SSA_i = \frac{A_i v_i}{V_i p_c} \tag{1}$$

Where A_i, V_i and, v_i are the area, volume, and volume fraction for the glass material in question, and ρ_c is the density of the composite. The resulting SSA is therefore

normalized by the total mass of the composite. To determine the total glass SSA, the SSA for HGS and GF are simply summed.

Empirical analysis of data can provide a tremendous amount of insight into material behavior; however, further knowledge can be gained by comparing the empirical data to theoretical models. Deviation between the empirical and theoretical can reveal flaws in model assumptions, or material behavior that is not captured by the model. The Halpin-Tsai equations were originally used to describe a discontinuous fiber reinforced composite but can be extended to nanorod or nanofiber type systems [91]. This model primarily describes the composite modulus through the load transfer from matrix to fiber. Higher aspect ratio, and relatively stiffer reinforcement materials perform better in a Halpin-Tsai model. Directly applying macroscale models, such as Halpin-Tsai, to a nanocomposite inevitably leads to oversight of certain phenomena. The Halpin-Tsai model does not account for interaction between reinforcement particles and assumes a perfect interface between reinforcement and matrix. These models will be used to better assess, describe, and understand the behavior of the synthesized nanocomposites.

In the Halpin-Tsai model for short fiber reinforced composites, the unidirectional elastic modulus in the direction of the fiber (E_{11}) and perpendicular to the fiber axis (E_{22}) are given by

$$E_{11} = \frac{1 + 2(l_f/d_f)\eta_L v_f}{1 - \eta_L v_f} E_f \tag{2}$$

$$E_{22} = \frac{1 + 2\eta_T v_f}{1 - \eta_T v_f} E_m \tag{3}$$

Where l_f and d_f are the reinforcement phase length and diameter respectively, v_f is the volume fraction of reinforcement, and E_f and E_m are the elastic modulus of the reinforcement and matrix material, respectively. The parameters η_L and η_T are given by

$$\eta_L = \frac{(E_F/E_m) - 1}{(E_f/E_m) + 2(l_f/d_f)} \tag{4}$$

$$\eta_T = \frac{(E_F/E_m) - 1}{(E_f/E_m) + 2} \tag{5}$$

The uniaxial aligned fiber reinforced composite properties given by E_{11} and E_{22} can be transformed to a randomly oriented reinforcement phase via

$$E_{random} = \frac{3}{8}E_{11} + \frac{5}{8}E_{22} \tag{6}$$

Classical lamination theory is often used in anisotropic composites to predict load distribution throughout the composite thickness, and overall composite properties including elastic constants, thermal expansion coefficients, and moisture expansion coefficients. Critically lamination theory takes several assumptions: that the laminate is substantially thicker than it is wide, that there is perfect interlaminar bonding, that the strain distribution in the thickness direction is linear, and that all laminas are homogenous and behave linear elastically. Derivation of these extensive system of equations is outlined elsewhere [92-94]. When examining a functionally graded SMC composite, classical

lamination theory can provide key insights into the composite microstructure. By comparing the experimental tensile and flexural properties the efficacy of the processing techniques used can be determined.

CHAPTER 3. CELLULOSE NANOCRYSTAL REINFORCED POLYESTER COMPOSITES

This chapter was adapted from a publication in *Cellulose*.

DiLoreto, Edward, et al. "Freeze dried cellulose nanocrystal reinforced unsaturated polyester composites: challenges and potential." *Cellulose* 26.7 (**2019**): 4391-4403.

3.1 Experimental Outline and Sample Nomenclature

A schematic representation of the various CNC types used in this study and their incorporation into the polyester resin outline is shown in Figure 3.1. CNC had one of three surface chemistries: sodium form sulfate half ester (SCNC), nonpolar methyl(triphenyl) phosphonium exchanged (PhCNC), or maleic acid ester (MCNC). The functionalized CNC are freeze dried and mixed within PR. MEKP was selected over other manufacturer recommended initiators because the higher temperatures required for other initiators could cause thermal degradation of the CNCs. Because of this alternative cure cycle the base properties of the neat PR were expected to vary somewhat from manufacturer reported values as their curing agent and time/temperature profile were different. The concentration of CNC within the composites was 1wt% for each surface functionalization. Loadings of 1wt% are common as it is low enough to avoid extreme agglomeration observed at >5wt% but can provide significant differences in properties that would not be observable at lower wt% [25, 31, 32, 36, 49]. Additionally, for the PhCNC material which showed the most promise in screening experiments, a higher concentration of 2wt% CNC was also produced and tested to explore the effects of CNC concertation. Samples are referred to by *nXCNC*

where *n* is the weight fraction, by total resin mixture, of CNC and *X* refers to the functionalization or type of CNC used. Baseline unfilled PR samples are referred to simply as PR.

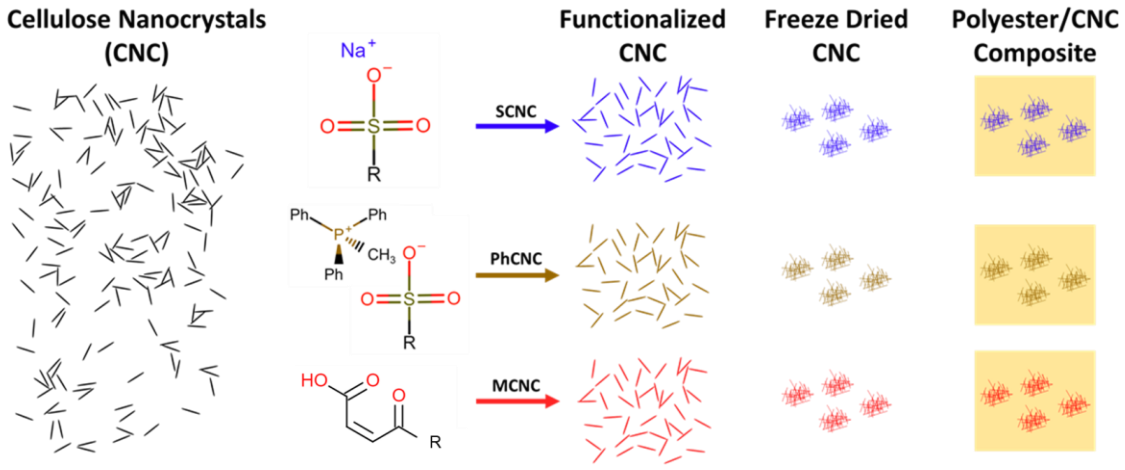

Figure 3.1 Schematic indicating the functionalization, freeze drying and incorporation of CNC into polyester resin. CNC were functionalized with either polar sulfate ester (blue), SCNC; or nonpolar methyl(triphenyl) phosphonium (brown), PhCNC; or maleic acid ester (red), MCNC.

3.2 Morphology of CNC

The freeze-dried surface functionalized CNC powders were examined via scanning electron microscopy (SEM) and characteristic images are presented in Figure 3.2 and Figure 3.3. SCNC, was comprised of ~200 µm agglomerates with little visible porosity (Figure 3.2a and Figure 3.3a). PhCNC appeared to form ~1 mm aerogel platelets with irregular surface pores 10-50 µm in diameter. These pores may be large enough for resin to penetrate; however, mixing action is still necessary to individualize and sperate the CNCs, (Figure 3.2b and Figure 3.3b). Finally, MCNC, which was lyophilized from a lower solids content suspension, showed a channel like structure with thin walls of CNC films

and some fibrillation visible at high magnification. This greater level of visible porosity could provide more access for resin to penetrate; however, favorable interactions are still necessary to fully draw resin into the structure, and, again, mixing action is necessary to disturb the agglomerate and individualize the CNCs, (Figure 3.2 and Figure 3.3 c). It is expected that these differences in dry morphology will lead to different dispersion quality or structure within the resulting polymer composite [87, 95, 96]. Notably, none of the freeze-dried CNC powders were in a nano-disperse state prior to combining with the resin and it is not expected that the resin can penetrate within the agglomerates through capillary forces alone. The freeze-dried CNC powders were mixed as outlined in Chapter 2 with the resin without any further pre-processing.

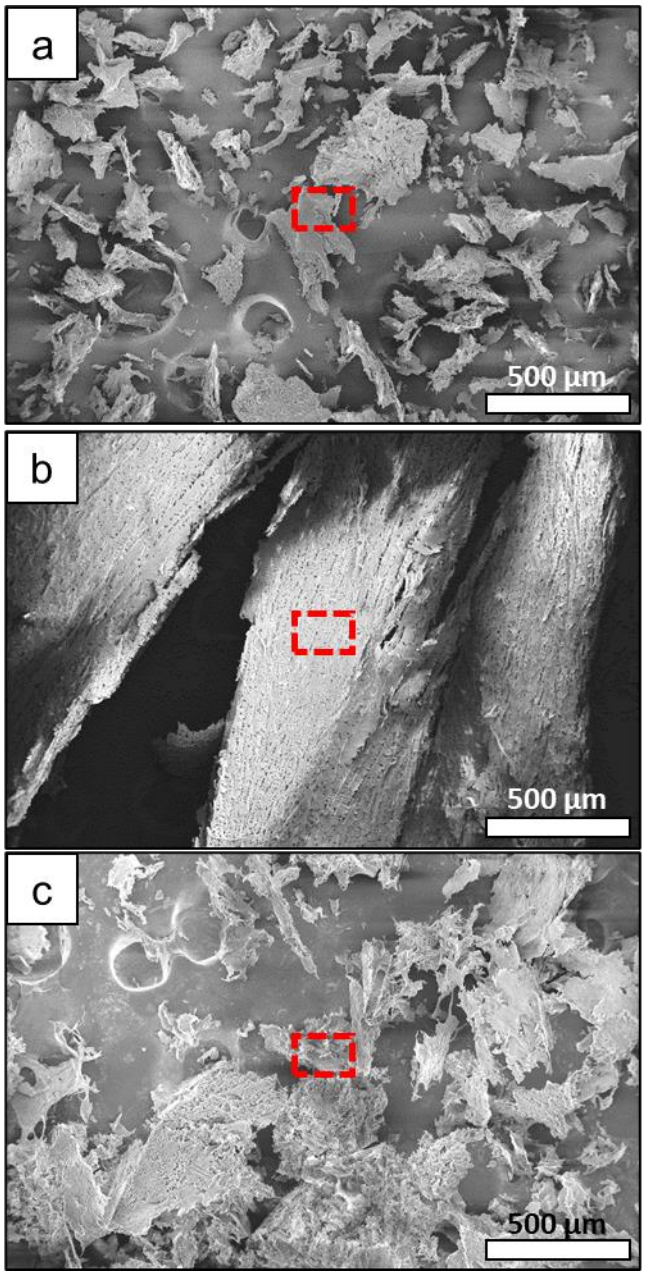

Figure 3.2 SEM micrographs of freeze-dried CNC: a) SCNC, b) PhCNC, c) MCNC. The dotted red box indicates the approximate location of the corresponding high magnification image of the sample (Figure 3.3)

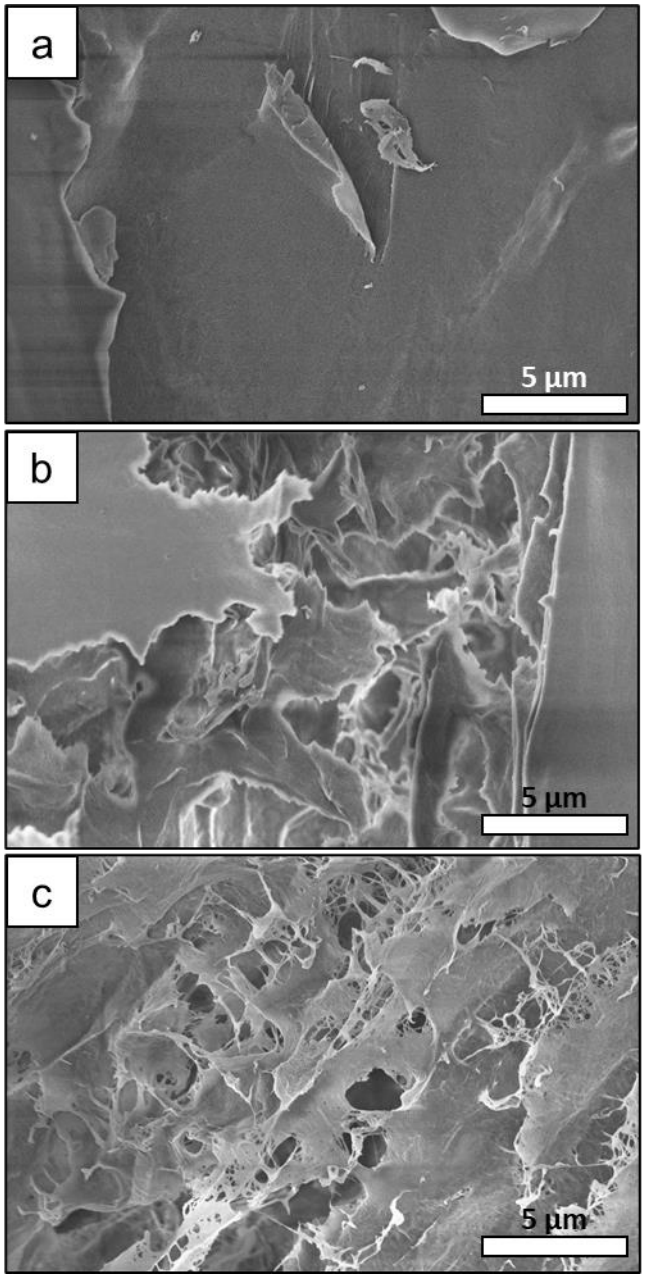

Figure 3.3 High magnification SEM images of freeze-dried CNC: a) SCNC, b) PhCNC, c) MCNC. Corresponding low magnification images are shown in Figure 3.2.

3.3 Distribution of CNC in Resin

Optical micrographs of the CNC-PR mixtures are shown in Figure 3.4. Optical imaging was done to observe the macroscopic dispersion quality of the CNC in the PR matrix. It is evident that a complete nano-scale dispersion of the CNC was not achieved, as all samples had agglomerates up to 100 μm (i.e., dark spots and flakes in the images). This CNC agglomeration is primarily a result of the inability to break up and subsequently disperse the CNC freeze-dried flakes. The consistent size in the largest agglomerates is indicative of the limited capability of probe sonication in individualizing the CNCs. The three different CNC surface functionalizations had minimal effect on this, which is interesting since the functionalization occurred before freeze-drying and should have some influence on the eutectic structure formed during freezing and thus the resulting scaffold formed after drying [97, 98]. Considering the micron-scale dispersion, the CNC agglomerates appear to be uniformly dispersed throughout the sample, and there is little influence from the different surface treatments. Because of this, the nano-scale dispersion of the CNC was not characterized, as the high degree of CNC agglomerated will dictate any mechanism responsible for changes in the mechanical properties (e.g., flaw size, critical length).

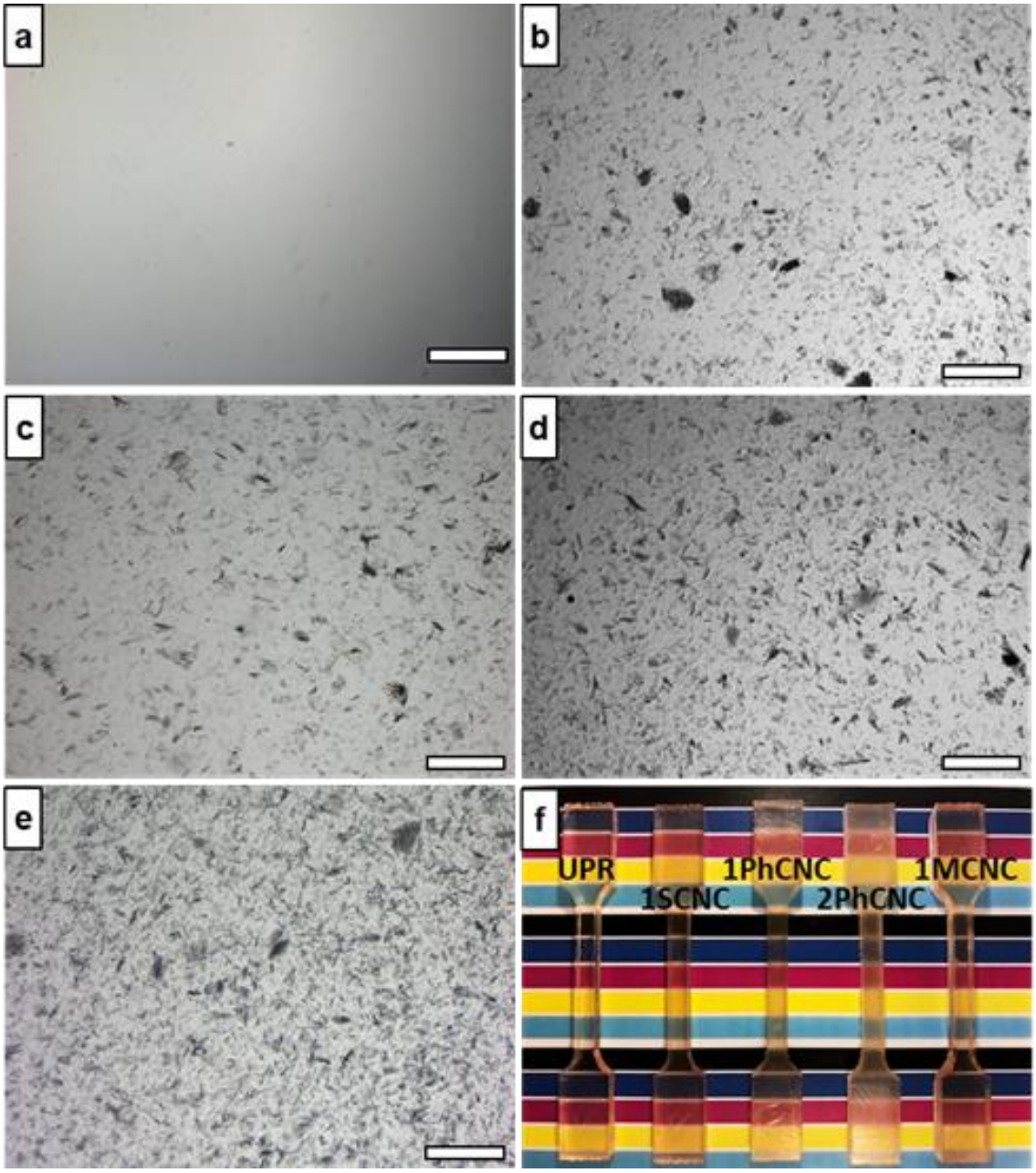

Figure 3.4 Transmitted light micrographs of CNC-PR mixtures (uncured) for: a) PR without filler, b) 1SCNC, c) 1MCNC, d) 1PhCNC, e) 2PhCNC, showing the extent of CNC agglomeration, and their flake-like morphology. Scale bars 500 µm. f) Photograph of dogbone tensile testing specimens for neat PR, 1SCNC, 1PhCNCC, 2PhCNC, and 1MCNC, respectively, showing differences in translucency between samples.

3.4 Degree of Cure, Glass Transition Temperature and Density

The material properties for neat PR and CNC-PR composites are presented in Table 3.1. The degree of cure and the Glass Transition T_g temperature were measured using DSC and DMA as describe in Chapter 2.3. The density was measured based on water displacement as described in Chapter 2.3. The CNC additions had minimal impact on the curing behavior and density. All composite samples had a satisfactory percent cure of nearly 100%, and a density of 1.23-1.24 g/mL, matching predictions from rule of mixtures. The fact that density values are consistent with rule of mixtures predictions, along with observations via SEM (Chapter 3.6), indicate that there is little to no porosity or void content in the material. Density was measured to validate the approach outlined in Chapter 1, i.e. substituting portions of the system with a small quantity of stronger material with at most equivalent density. The glass transitions of specimens were observed through the position of the tan(δ) peak in DMA measurements. No significant differences were observed in the T_g temperatures among the various samples including the PR as all values were within 1 standard deviation. As a result, it is difficult to conclude on the relative effect of CNC addition and CNC surface functionalization on the PR properties. The largest difference in T_g ~11.5°C was observed between the 1MCNC the 1SCNC composites. It is hypothesized that the shift in the 1MCNC case may be due to a restriction of the polymer chains at the CNC interface through chemical covalent crosslinks at the maleic group functional site [99, 100]. Any reduction in T_g could be related to residual water contained within the freeze-dried CNC. Water would both act to plasticize the polymer chains, and could hydrolyze the ester linkages within the polyester chain.

Table 3.1 Properties of CNC-PR composites, including degree of cure, T_g, and density.

Composite	Degree of cure (%)	T_g (°C)	Density (g/mL)
PR	99.5±0.1	156.3±9.0	1.23±0.005
1SCNC	99.2±0.3	148.5±0.7	1.23±0.003
1PhCNC	99.5±0.1	152.5±3.5	1.24±0.002
2PhCNC	98.5±0.3	140.0±10.4	1.24±0.001
1MCNC	99.2±0.1	160.0±1.0	1.24±0.002

3.5 Tensile and Flexural Properties

Mechanical properties, tensile and flexural, are shown in Figure 3.5. In general, the CNC additions were shown to increase the tensile and flexural modulus and decrease both the tensile and flexural strength and strain to failure. Specifically, there was an increase in tensile modulus for 1PhCNC, 2PhCNC, and 1MCNC samples over the 1SCNC and PR samples. A maximum increase of ~20% in tensile modulus was observed for 1MCNC over the PR baseline. Likewise, flexural modulus increased with CNC additions, with a maximum increase of ~50% for 2PhCNC. Arslan et. al. studied polylactic acid-CNC composites and attributed the decrease in flexural strength at high loadings the adverse effect of CNC aggregates [101]. Overall, the trends in tensile and flexural properties follow a similar path, (i.e. PR having the highest average strength, 1SCNC having the lowest average strength, and PR having the lowest average modulus).

The effect of CNC surface chemistry can be assessed by considering that elastic modulus in the case of composites containing discontinuous and randomly distributed and oriented reinforcements is governed primarily by reinforcement-matrix interactions, and

reinforcement aspect ratio, modulus, and volume fraction of the reinforcement [102, 103]. Taking the reinforcement phase to be of approximately similar aspect ratio (i.e. the agglomerates are of similar size) and volume fraction across all 1 wt% samples, there is no significantly different level of reinforcement-matrix interaction as measured by tensile or flexural modulus. All the CNC-PR composites had lower tensile and flexural strength as compared to PR. Mechanical strength and failure mechanisms are highly complex and can be due to multiple factors. The lowered strength in this case is believed to be due in part to the limiting strength of CNC-CNC interactions within agglomerates, i.e. the tensile strength of the agglomerate was less than the strength of the matrix, and that agglomeration of nanoparticles significantly reduces the specific surface area and thereby the level of interfacial adhesion between reinforcement and matrix (see fractography section) [104]. Kargarzadeh et. al. explored pre-dispersing surface treated freeze-dried CNC in styrene prior to composite processing. They reported a 20% increase in tensile strength and a 10% increase in tensile modulus at 2 wt% CNC over the neat PR. The key to the increase in strength was the fine nano-scale dispersion of the reinforcement phase [25]. Lastly, it should be noted that the pre-dispersion of CNC in styrene approach used by Kargarzadeh et al, was not used in the current study, as using large volumes of styrene to pre-disperse the cellulose is environmentally and occupationally hazardous and contradictory to the objective of industrially applicable process development. Based on the data an increase of loading from 1 to 2 wt% PhCNC does not seem to have a significant effect on the flexural or tensile modulus or strength. Despite the agglomeration of CNC, their addition to PR appears to be a promising reinforcement for increasing the modulus of the matrix in glass

fiber reinforced plastics, as GFRP strength is primarily driven by GF-matrix interactions and GF strength.

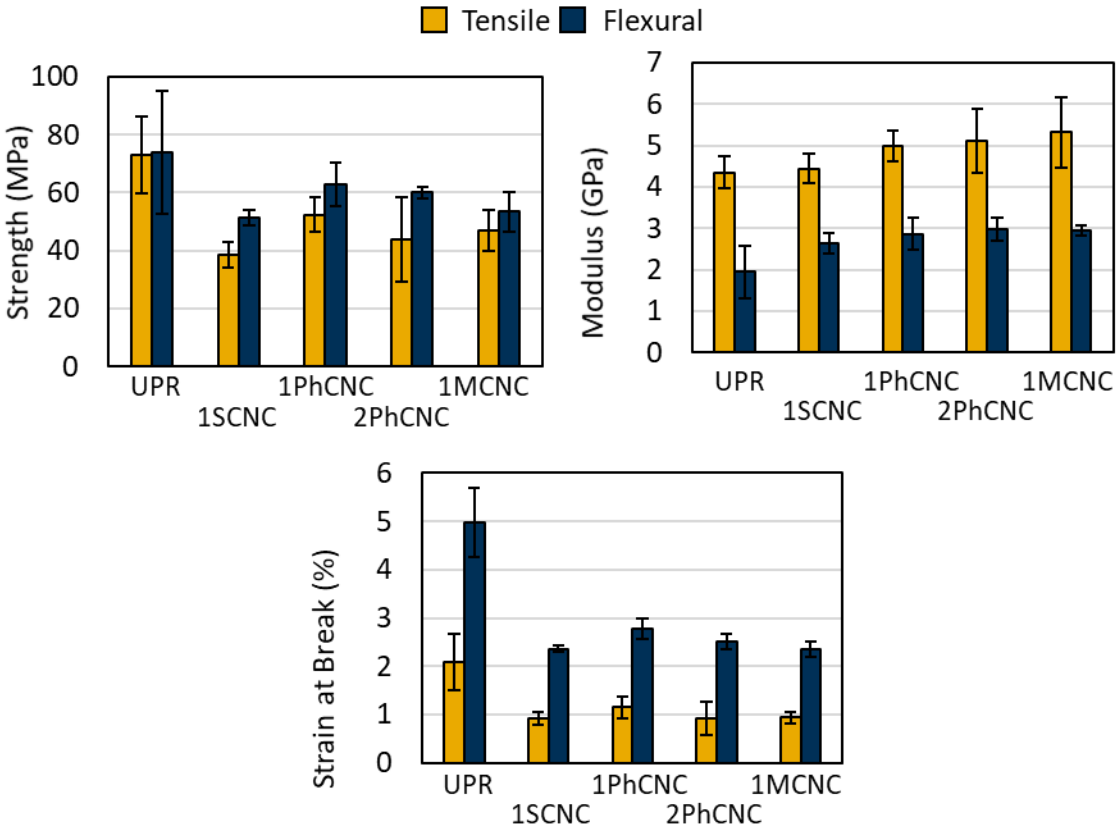

Figure 3.5 Tensile and flexural properties of neat PR, and CNC-PR composites for the three types of functionalized CNC.

Further exploration of the effects of CNC surface treatment on mechanical properties can be explored by using mechanical models. One common tool for CNC-polymer nanocomposites is the Halpin-Tsai model. The Halpin-Tsai model was originally developed for use in two phase short fiber reinforced composites [102]. Calculations for this model was completed and are outlined in Table 3.2. The tabulated values outline a "best case" and "worst case" scenario in terms of aspect ratio to provide context for agglomeration. The "best case" or idealized dispersed case assumes the CNC are

individualized and their aspect ratios are equivalent to the dimensions provided by the material supplier, (see section 2.1.2), with a modulus of 110 GPa [105]. The “worst case” assumes all material is agglomerated into approximately spherical particles with an aspect ratio of 1 and a modulus of 15 GPa [106]. The Halpin-Tsai model provided a good prediction for modulus overall. The 1PhCNC composite had a statistically significantly different measured modulus than the predicted value. Both 1MCNC and 1PhCNC moduli were significantly different than the “worst case” prediction of 1Sphere. Deviation of the measured composite modulus from the calculated value could be caused by a variety of factors. Primarily, these models do not account for interaction between matrix and reinforcement by assuming an idealized reinforcement-matrix interaction. Any changes in the stiffness in the interphase could be the result of several effects: orientation of chains around CNC, changes in crosslink density, reduction in free volume of chains around CNC [21, 107-110]. Further studies (atomic force microscopy, molecular dynamics models, etc.) would be necessary to conclusively determine the cause of the differences between the model and measured values.

Table 3.2 Comparison of elastic modulus as measured by tensile testing to mechanical models.

Sample	E_c (GPa)	E_{HT} (GPa)
1SCNC	4.45±0.37	4.52
1PhCNC	4.99±0.38	4.53
2PhCNC	5.11±0.82	4.70
1MCNC	5.32±0.89	4.55
1Sphere		4.40
2Sphere		4.45

E_c: measured composite tensile modulus with 95% confidence interval, E_{HT}: Halpin-Tsai calculated modulus, Assumes E_{CNC}=110 GPa, $E_{agglomerate}$=15 GPa, E_{PR}=4.36 GPa, Aspect ratio of CNCs are 19, 22, 44, and 1 for SCNC, PhCNC, MCNC, and Sphere respectively, CNC density is 1.6 g/cm^3.

To assess possible mechanisms for the reduced tensile and flexural strength of PR from the CNC additions the fracture surfaces of the tensile samples (Figure 3.6) were examined. For the PR, a flat and smooth fracture plane perpendicular to the direction of loading was observed and is indicative of a brittle fracture behavior of polymer materials and is expected for the type of PR used in this study. The PR samples show crack initiation sites located at the edge of the test specimen (Figure 3.6a), which indicates a homogenous material with a defect size smaller than what is at the surface of the test specimen. In contrast, for all CNC-PR composites, crack initiation occurred within the bulk of the test specimen at a localized stress concentration point (Figure 3.6f, g, and h). These crack initiation sites are of a similar size-scale to that of the CNC aggregates, (Figure 3.4), indicating that the CNC aggregates are causing property limiting defects within the composites. However, the fracture surface away from the initiation point (Figure 3.6 b, c and d), appeared to be more textured as compared to the PR, indicating more resistance to crack propagation. This suggest that if the larger defects can be removed, and thus increase

the CNC-PR interfacial area, it may be possible to increase the strength of PR by CNC additions. The effect of CNC surface chemistry was not overwhelmingly apparent, however, for SCNC-PR it was easier to see the flake shaped CNC aggregates and interfacial delamination to the PR (Figure 3.6 d, Figure 3.7), which were not as apparent for the PhCNC and MCNC composites. This may suggest stronger bonding between PhCNC and MCNC to the PR as compared to the SCNC.

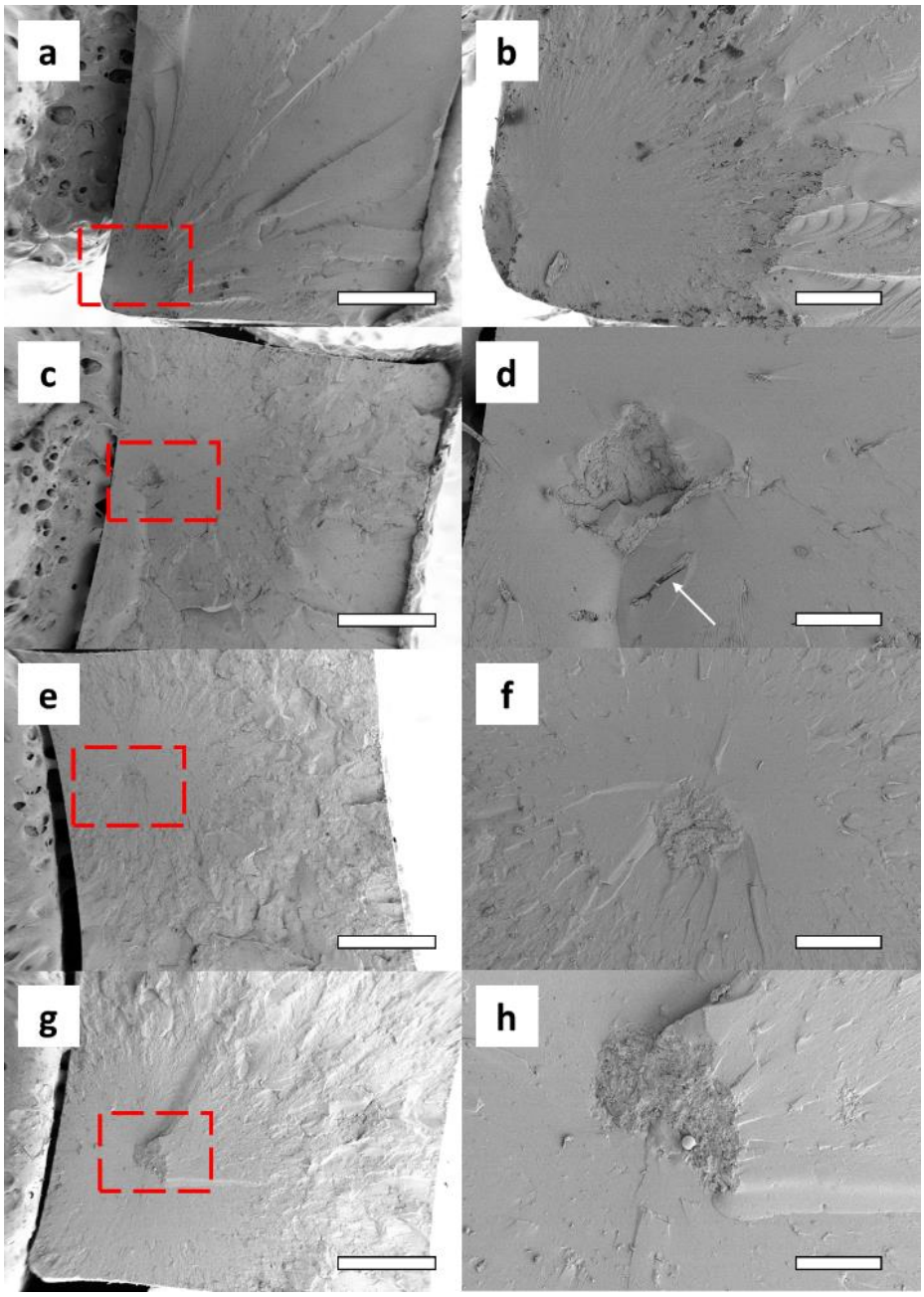

Figure 3.6 SEM micrographs of tensile fracture surfaces for: a,b) neat PR, c,d) 1SCNC, e,f) 1PhCNC, and g,h) 1MCNC composites. Images a, c, e, and g, (scale bar 1 mm), show entire fracture surface, images b, d, f, and h, (dotted red box insets), show the corresponding crack initiation sites, (scale bars 200 µm). The dotted red box shows the location of the crack initiation point, and the location of the corresponding higher magnification images. The white arrow in (d) indicates delamination at CNC agglomeration-PR interface.

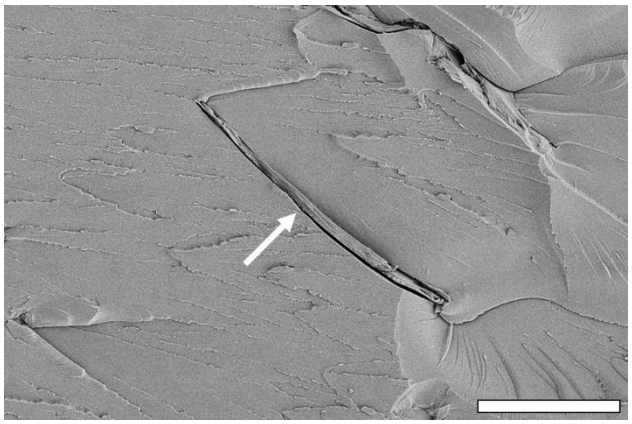

Figure 3.7 SEM micrograph of tensile fracture surface for 1SCNC, showing CNC agglomerate flake (indicated by the arrow) and delamination along the interface with the PR matrix. Scale bar 500 µm.

3.6 Composite Thermomechanical Properties

To help assess the interaction between CNC agglomerates and the PR matrix, and the effect of CNC surface chemistry, DMA analysis was conducted. This technique provides an approach to probe the filler-matrix interface and interphase region within the system. For the CNC-PR system, the interphase region extends from the CNC-PR interface to some depth within the PR, this region would be expected to have different physical properties than the bulk PR. The stiffness and volume of this interphase are expected to depend on the surface chemistry of the CNC, and the exposed surface area of CNC or dispersion quality. It is generally expected that polymer chains located in this interphase have a more restricted range of motion resulting in more elastic behaviour as compared to the bulk. Furthermore, the temperature dependence of interphase stiffness, which can provide further insight to the matrix-filler interaction are probed by DMA. A weaker interaction could result in a smaller interphase by volume, or a less stiff interphase, either of which would cause a reduction in storage modulus, while strong interactions can produce an increase in storage modulus, and higher thermo-mechanical stability (i.e. less

change in modulus with temperature). For example, a fully crosslinked and nano-disperse filler would be expected to have a high storage modulus and a smaller reduction in storage modulus above the T_g, relative to a similar system without any crosslinking. By assessing shifts in storage modulus associated with CNC additions, the effect of the CNC surface chemistry can be observed [21, 32, 111, 112].

DMA measurements at 80°C, assessed the glassy storage modulus, in which the 1MCNC and 1PhCNC showed a 61% and 66% improvement, respectively, in glassy storage modulus over the neat PR sample (Figure 3.8). Notably, the 1MCNC and 1PhCNC are also shown to have higher glassy storage modulus as compared to 1SCNC. Taking the particle dispersion level and the exposed surface area of CNC to be equal across all samples, the similar magnitude of the 1MCNC and 1PhCNC glassy modulus indicate that the surface chemistries produce a similar effect. With respect to 1MCNC it is possible that a more elastic interphase is the result of chemical crosslinking of the polymer matrix through the maleic group on the CNC surface. Mechanisms for radical polymerization of styrene and maleic acid and crosslinking of CNC have been explored elsewhere [113, 114]. As shown previously, the phenyl groups in PhCNCs sterically hinder CNC-CNC interactions [36]. It is conceivable that a reduction in CNC-CNC interaction energy potential would lead to relatively more CNC-matrix interfacial area. Assuming the PhCNC-matrix interactions are favorable for stiffening the interphase, this phenomenon could result in a larger interphase volume relative to an SCNC case and as a result a higher storage modulus. Note that the CNC agglomeration in this study reduces the effective volume of the interphase region and is expected to result in a smaller effect on the storage modulus, as compared to a fully nano-scale CNC dispersed within the PR system.

Interestingly, the glassy modulus of the 2PhCNC is 32% lower than that of 1PhCNC, while the tensile and flexural moduli are consistent between the two samples. The difference in length scales of the techniques may be the source of an explanation. DMA probes the filler-matrix interface within the system, while tensile and flexural testing examine the bulk. DMA is a more sensitive technique than tensile and flexural testing, allowing for differences to be significant in the former but not the latter. Furthermore, the temperature at which the glassy modulus is given, 80°C, is elevated to the flexural and tensile testing, which were conducted in ambient conditions.

DMA measurements taken in the rubbery plateau region, assessed the rubbery storage modulus, and revealed somewhat similar results, in which the 1MCNC and 1PhCNC showed the greatest increase in storage modulus, 65% and 48%, respectively, over the PR baseline. Here MCNC appears to provide a moderately more effective reinforcement as compared to the PhCNC. One explanation for this effect is that the MCNC-PR interactions are to some extent more thermally stable than the PhCNC-PR interactions.

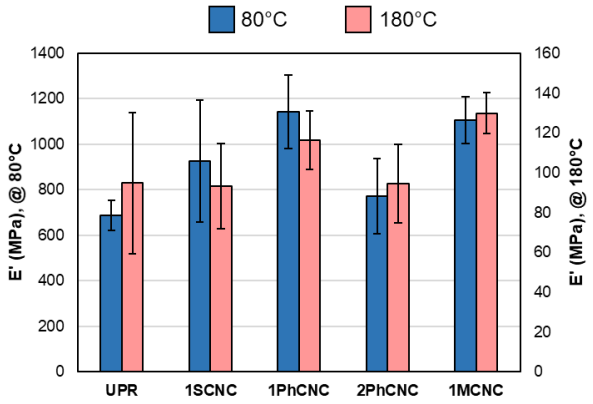

Figure 3.8 Storage moduli of CNC-PR composites in the glassy (at 80°C) and rubbery states (at 180°C).

3.7 Conclusion

The effect of surface functionalized of cellulose nanocrystals: sulfate ester (SCNC), methyl(triphenyl) phosphonium (PhCNC), and maleic acid ester (MCNC), on freeze-drying CNC agglomerate morphology, and the resulting properties of unsaturated polyester (PR)-CNC composites was studied. The addition of freeze-dried CNC powders into PR, resulting in micron-sized CNC agglomerates, were shown to enhance the flexural and tensile modulus by up to 50% and 20%, respectively, but decreased the tensile strength by up to 40%. The 1PhCNC-PR and 1MCNC-PR composites showed a 66% and 61% increase in glassy modulus and a 65% and 48% increase in rubbery modulus over the PR baseline, respectively. Additionally, the glass transition increased by 4.5°C and 12°C for 1PhCNC and 1MCNC over 1SCNC, respectively. Overall, PhCNC and MCNC displayed potential for use in polyester resin composites, proving to be effective reinforcements even at low concentrations.

While ideal nano-scale dispersions of CNC in PR were not achieved, the results in this work reflect potential in the use of functionalized CNC agglomerates as an additive in PR systems to produce composites with high moduli and good thermo-mechanical stability without dramatically affecting overall cure performance. They also serve to outline a processing pathway for CNC-PR composites while identifying key challenges along said pathway that must be addressed in any work involving the use of CNC as a nanofiller, such as the redispersion of freeze-dried CNCs in PR resins.

CHAPTER 4. LIGHTWEIGHT POLYESTER COMPOSITES VIA NANOREINFORCED SYNTACTIC FOAMS

As discussed in Chapter 1, syntactic foams are a readily available method for light weighting composites. Many works have already explored the use of HGS, cenospheres, and other hollow particles in a wide range of matrices from polymers to metals. Recent studies have also explored the use of nanomaterials in the matrix phase including clays, nanotubes, and nanofibers and the effects on the syntactic foam composite mechanical and structural properties. The study outlined here aims to accomplish three main goals: first, to determine what, if any interaction there is between CNC mixed in a PR matrix and HGS, second, to identify interaction effects between HGS loading and HGS surface treatment for the system used here, and finally to investigate the effect of coating HGS with CNC on bulk composite properties.

4.1 Experimental Outline and Sample Nomenclature

A schematic representation of the various composite samples examined in this study is outlined in Table 4.1 and Figure 4.1. Four different cases of HGS were used: (i) HGS without any surface treatment, (ii) HGS treated with methacryloxypropyl trimethoxysilane (MS), (iii) HGS treated with MS and coated with CNC with sodium counterion (NaCNC), and (iv) HGS treated with MS and coated with CNC with methyl(triphenyl) phosphonium counterion (PhCNC). All HGS used in this study had a density of 0.32 g/cm^3 and were either S32HS or S32HS-MAS as described in Chapter 2. Different HGS are referred to as follows: HS for untreated HGS, HSMS for MS treated

HGS, HSMSNaCNC for MS and NaCNC coated HGS, and HSMSPhCNC for MS and PhCNC coated HGS. NaCNC were selected due to it being one of the most common surface chemistries for commercially available CNC. PhCNC were selected on the basis of previous studies on coating GF with CNC which indicated that PhCNC provided improved interfacial shear strength over NaCNC coatings [33, 115]. Details on CNC types used, and processing of CNC is outlined in Chapter 2.

Table 4.1 Samples names and filler content and surface modification for samples in this study.

Sample	CNC content (wt%)	HGS content (vol%)	HGS surface modification
Neat Resin	0	0	
1NaCNC	1	0	
5NaCNC	5	0	
15HS	0	15	Glass
30HS	0	30	Glass
15HSMS	0	15	MS
30HSMS	0	30	MS
15HS-1NaCNC	1	15	Glass
15HS-5NaCNC	5	15	Glass
15HSMSNaCNC	0	15	MS, NaCNC
15HSMSPhCNC	0	15	MS, PhCNC

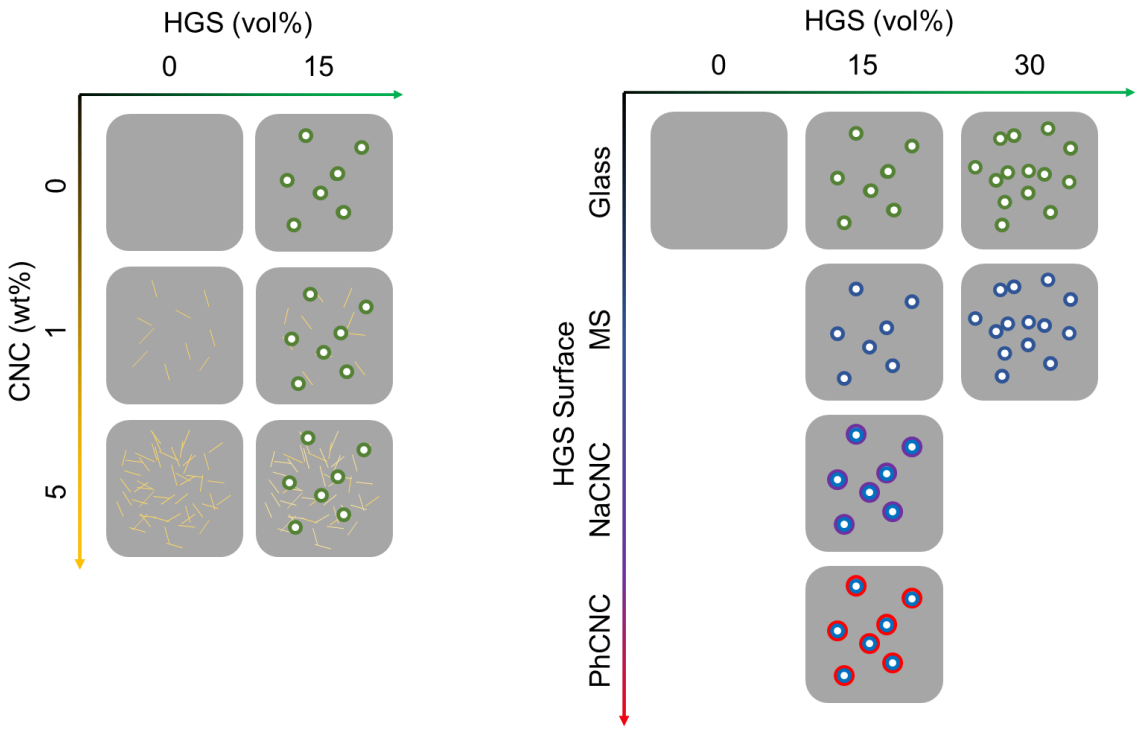

Figure 4.1 Schematic overview of samples used in this study. Primary axes of study were HGS content, CNC content, and HGS surface modification.

This study aimed to examine three main effects as measured by various techniques: is there any interaction between HGS and bulk mixed CNC, is there any interaction between HGS loading and HGS surface treatment, and what are the effects of coating HGS with CNC. For the sake of ease of discussion, the samples in this study are broken down into three subsets: the first subset explores interactions between CNC in the matrix and HGS in the matrix (i.e. HGS-CNC-PR composites), the second subset explores interactions between HGS content and HGS surface treatment with MS, and the third subset explores the effects of coating HGS with CNC (i.e. CNC coated HGS-PR composites). Methods for surface coating of HGS by CNC and composite compounding are outlined in Chapter 2.

4.2 Characterization of Surface Modified Hollow Glass Spheres

To determine if CNC were successfully coated on the HGS surface various tests were conducted. XPS analysis was conducted on each of the four types of HGS (Figure 4.2). The control HGS sample shows some carbon present on the surface near 285 eV. This is likely adventitious carbon but may also be due to a proprietary post treatment of the HGS by the manufacturer. Silane treated HGS presented an increase in intensity in the 285, 286, and 288 eV, indicating the presence of C-C, C-O, and C=O respectively. These signals reflect the stoichiometric composition of the silane (~5:1:1 for C-C:C-O:C=O) [116, 117]. Samples coated with CNC displayed nearly overlapping XPS signals in this range. With the addition of CNC there was a relative increase in C-O intensity as compared to C-C and C=O bonding, again as expected by the stoichiometry of the cellulose monomer (i.e. ~100% C-O) [118].

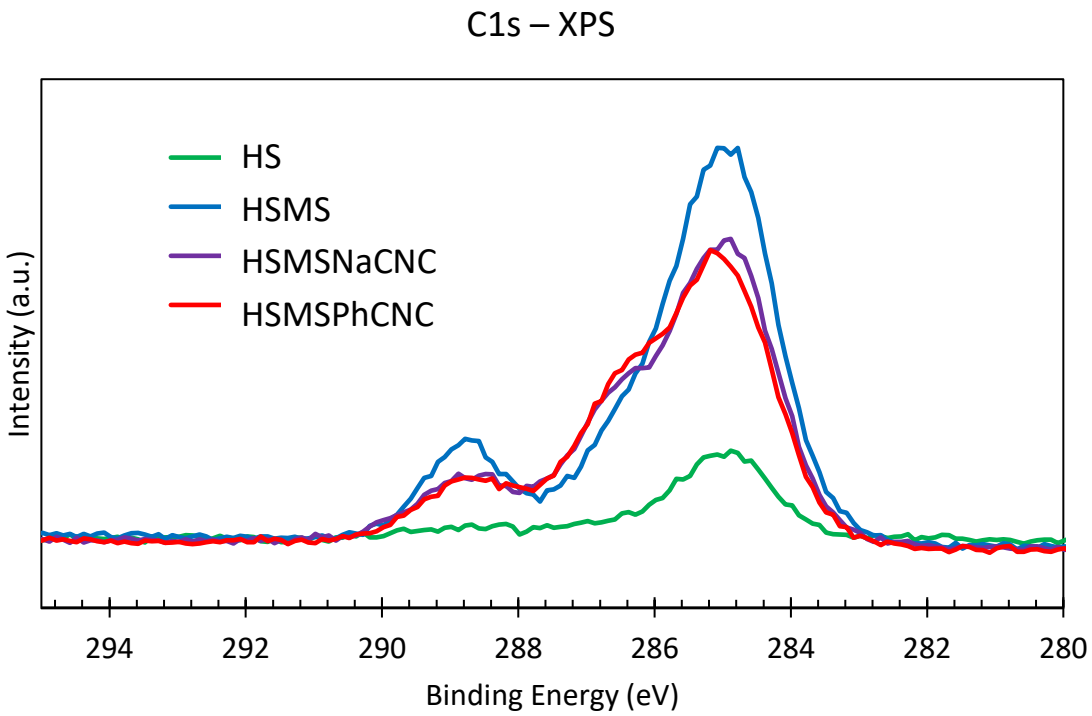

Figure 4.2 XPS scan of C1s for various surface modifiecations of hollow glass spheres.

Thermogravimetric analysis was also used to determine the weight content of any material coated on the HGS particles Figure 4.3. The weight residue for HS, HSMS, HSMSNaCNC, and HSMSPhCNC samples were 100, 99.2, 98.7, and 95.6 wt% respectively. The base HS displayed nearly no mass loss in this temperature range as would be expected from a borosilicate soda lime glass material. The silane treatment reduces the residue content slightly, and the CNC coated samples reduce it further. Interestingly the PhCNC coated sample displayed significantly lower residual mass relative to the NaCNC coated samples. This could be an indication of an increased amount of CNC on the surface of HSMSPhCNC samples, or a relatively lower thermal stability of PhCNC than NaCNC. The initial study that presented PhCNC indicated a char yield of 12 % for PhCNC and 22 % for NaCNC when pyrolyzed under nitrogen [36]. These results are indicative of the

presence of less thermally stable material and provide further evidence of surface coating with CNC.

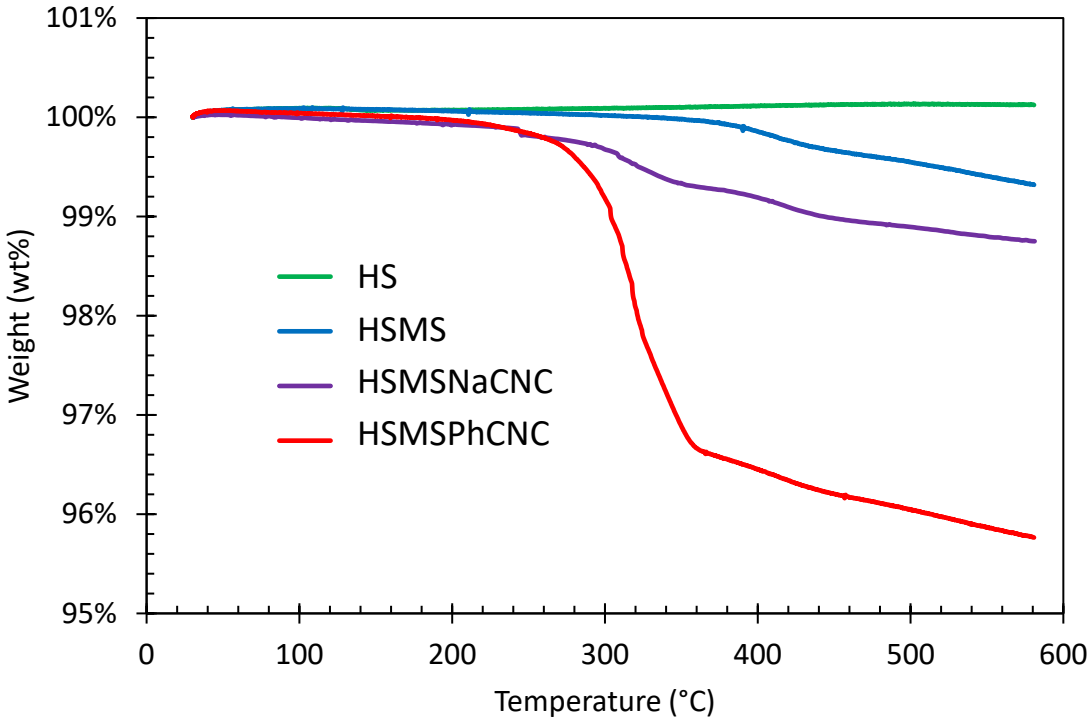

Figure 4.3 TGA data for various surface modification conditions of hollow glass spheres.

To examine the topographical structure of any surface treatment on the HGS, SEM imaging was conducted, (Figure 4.4 and Figure 4.5). The baseline untreated HGS, (Figure 4.4a and b), have relatively smooth surfaces with only small amounts of electrostatically attached dust. HGS treated with the MS, (Figure 4.4c, and d), had a slightly roughened appearance, likely due to surface inhomogeneities caused by the MS. The silane treated sample also displayed some agglomerated particles. Samples which were coated with CNC show film like structures on the surface (Figure 4.5). Additionally, the CNC surface coated samples did not show severe agglomeration of particles. Notably, all samples had a

minimal number of broken HGS indicating that the surface modification processing did not damage the spheres material substantially.

Although the results outlined herein do not conclusively indicate whether the CNC were covalently bonded to the HGS surface there are several qualitative factors that strongly indicate the presence of CNC-HGS bonding. Initial studies which involved simple mixing of CNC and HGS followed by a DIW rinsing step resulted in no observable CNC present on the HGS surface. Considering the hydrophilicity of CNC particles, if there were any CNC not covalently bonded to the HGS surface, they would be expected to go into suspension in the DIW. Further work is needed to conclusively determine the chemical nature of the CNC-HGS interactions.

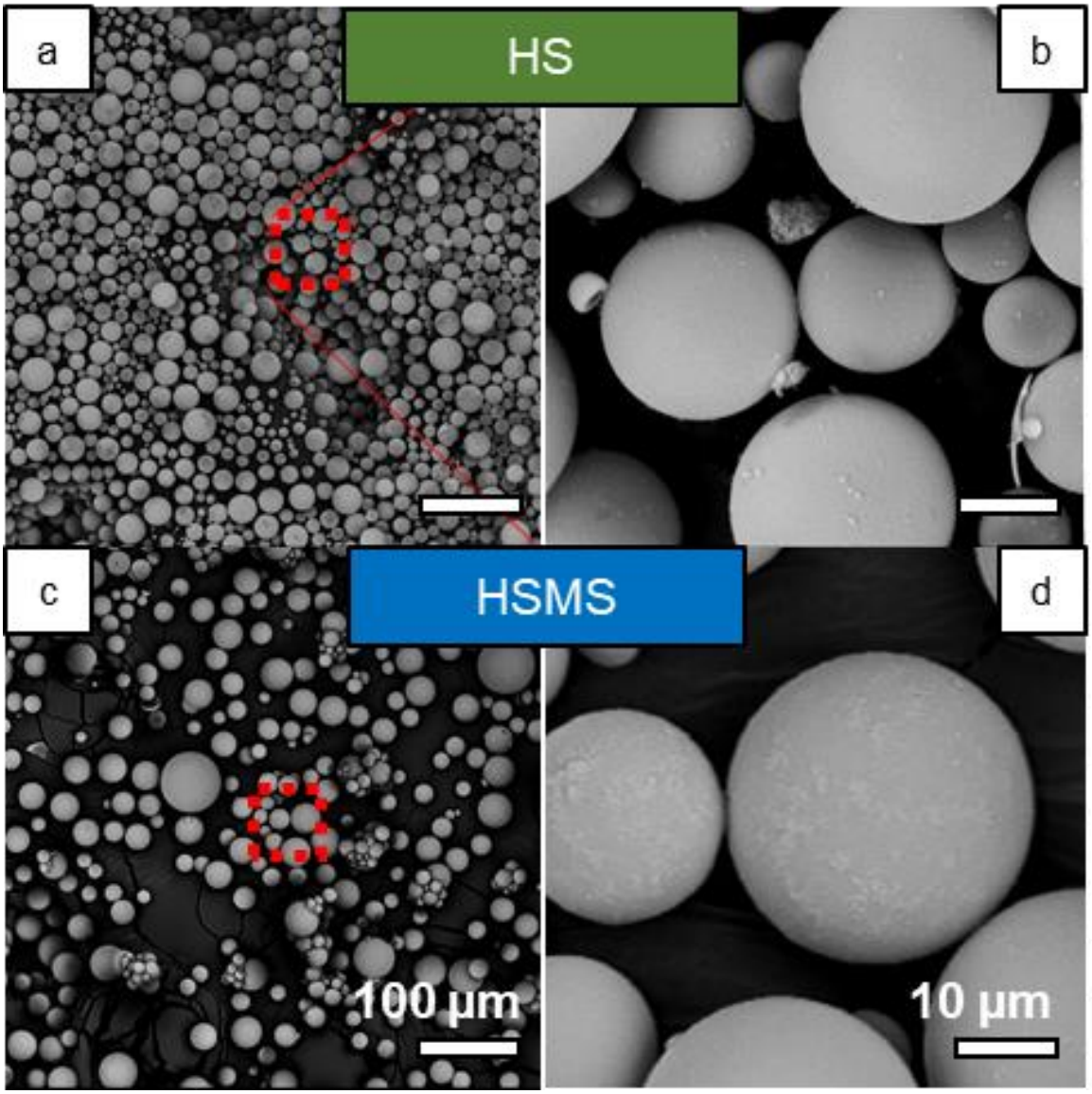

Figure 4.4 Electron microscope images of HS (a, b) and HSMS (c, d). Scale bars are 100 and 10 µm for low and high magnification, respectively.

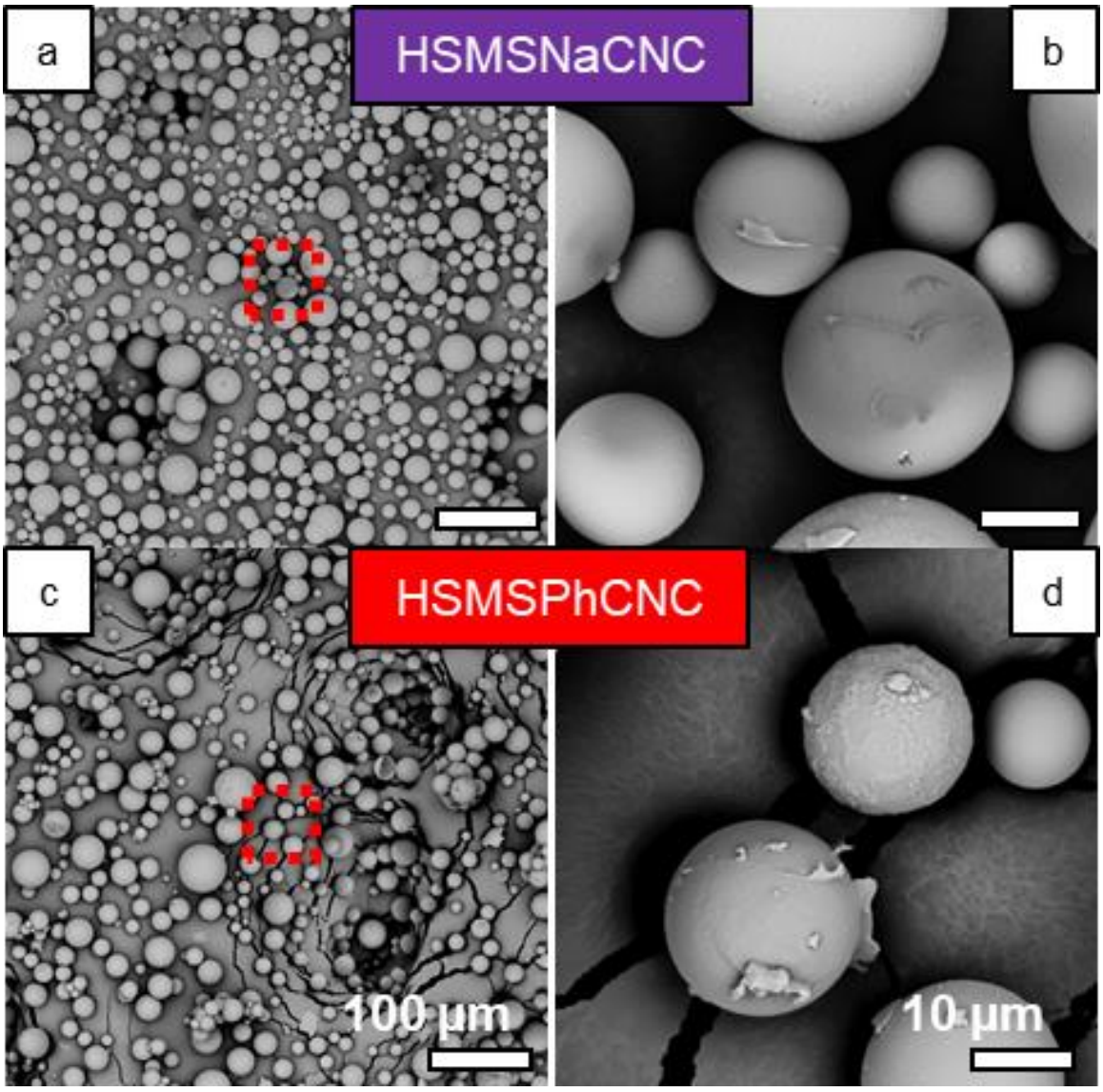

Figure 4.5 Electron microscope images of HSMSNaCNC (a, b) and HSMSPhCNC (c, d). Scale bars are 100 and 10 µm for low and high magnification, respectively.

4.3 Composite Mechanical Properties

The tensile properties of composites, containing HGS, CNC (either as a coating or a reinforcement in the matrix), and PR, were examined to investigate the effect of different fillers and different filler surface treatments on the composite. In multi-phase composite structures the tensile modulus is determined by several factors: the elastic modulus of each

constituent phase, the ability for load to be transferred from one phase to the next, the aspect ratio of each phase, and finally surface chemistry and structure of the constituent materials (i.e. interphase effects).

It should also be restated that the base matrix material and formulation is different from that in Chapter 3. As a result of the change, the properties of the control PR are different and in the case of tensile strength and elastic modulus are lower. In brief: the decision to change the resin and formulation was a result of the desire to select a material that was more directly relevant to the SMC process and was readily available to the researchers.

Various studies have examined both the PR-CNC and PR-HGS system and discussed them thoroughly; however, to the author's knowledge no studies have explored interaction effects between CNC and HGS [21, 24-26, 29, 31, 46, 119-121]. As in Chapter 3, the CNC are expected to be agglomerated and poorly dispersed within the resin matrix. The first set of samples of interest are those which combine CNC in the matrix with HGS in the matrix (HS, NaCNC, and HS-NaCNC samples). No treatments were applied to HGS in this subset. The tensile modulus and strength of these samples are shown in Figure 4.6. The addition of spray dried CNC (1NaCNC, and 5NaCNC) did not significantly (95% confidence level) decrease the tensile strength relative to the base polyester. For these samples, the elastic modulus was observed to significantly increase upon addition of 5 wt% CNC but not 1 wt% CNC. The addition of 15 vol% HGS did not significantly decrease the tensile strength but did significantly increase tensile modulus. Maintaining tensile strength indicates that the dispersion of the HGS did not detrimentally affect the strength (i.e. uniform dispersion). The increase in tensile modulus is consistent with previous studies

based on the S32HS wall thickness and density [122]. The HGS-NaCNC-PR composite samples did not show any interaction effect with respect to tensile strength or elastic modulus as determined by a multiple linear regression analysis, (i.e. the regression coefficient was not significantly different from zero at a 95% confidence level). The tensile strength for both 15HS-1NaCNC and 15HS-5NaCNC was significantly lower than the neat resin sample (20.8, 22.8, and 27.2 MPa respectively). This could possibly be caused by agglomeration of HGS, as the addition of NaCNC into the resin increases the viscosity and could limit the dispersion quality of the HGS during mixing. Agglomerations would cause stress concentrations that could decrease strength of the composite. Entrapped voids or dry spots within agglomerated particles would also significantly reduce strength. Overall, there was no significant interaction effects observed between HGS and NaCNC. The combined use of spray dried CNC and HGS can produce a low-density composite with an increase in elastic modulus of more than 20%. When considering the mechanical properties in conjunction with the density of the composite, the benefits of syntactic foams become clear Figure 4.9. 15HS-1NaCNC and 15HS-5NaCNC show an increase in specific tensile modulus of 70% and 25% over their respective CNC-PR composites, with approximately equivalent specific tensile strengths.

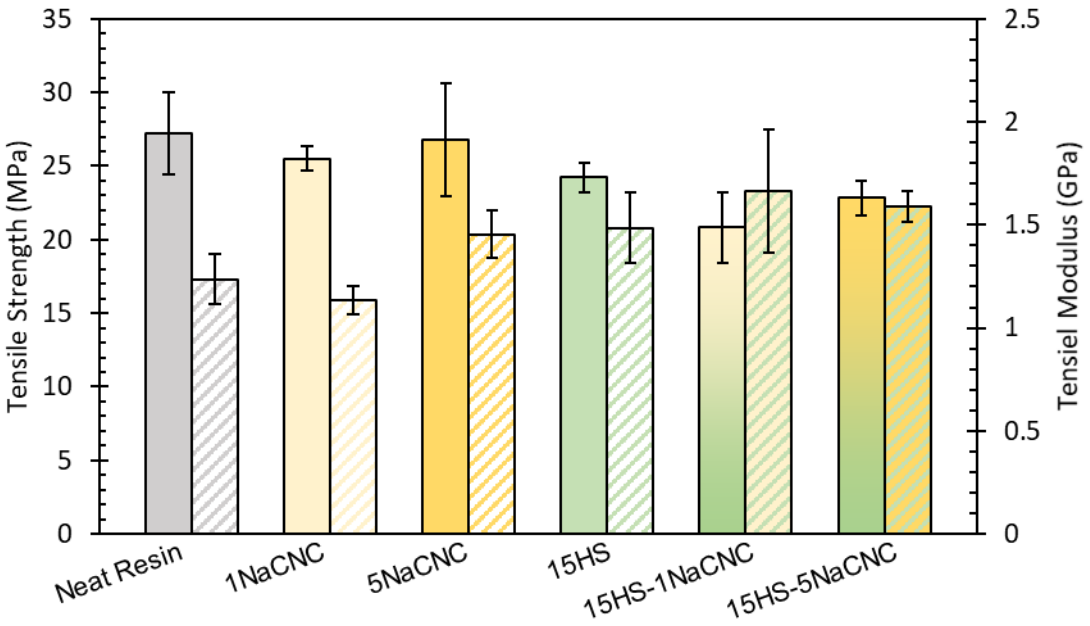

Figure 4.6 Tensile strength (solid bars) and elastic modulus (patterned bars) as a function of spray dried NaCNC as a reinforcement phase and HGS in PR.

The second subset of samples was selected to elaborate on any interaction effect between the HGS vol fraction and the HGS surface treatment (Figure 4.7). In every case the addition of HGS decreased the average tensile strength of the composite. 15HSMS displayed lower average tensile strength than 15HS, 18 MPa vs 24 MPa (statistically significant at 95% confidence level), this could potentially be due to agglomerated silane treated HGS. The average tensile modulus of 15HSMS was higher than 15HS, 1.7 GPa vs 1.5 GPa, though not to a statistically significant level. Both samples containing 30 vol% HGS had similar tensile strengths. The reduced tensile strength in each case is likely due to porosity within the samples (see Section 4.4 Composite Morphology). The similar tensile strength and observations of entrapped porosity indicate similar failure mechanisms. The specific tensile modulus is increased by 38% and 16% for HS and HSMS composites, respectively, upon increasing the HGS content from 15 vol% to 30 vol%. The

specific tensile strength is reduced by 39% and 26% for HS and HSMS composites respectively. Although the addition of more HGS has the potential to increase the HGS-PR composite stiffness and specific stiffness the significant reduction in tensile strength was a decisive factor to keep the HGS content to 15 vol% as the benchmark for further testing of surface treated HGS-PR composites. The specific tensile properties for these composites could be improved by further optimization of the process method to eliminate defects including agglomerates and voids; however, such a process optimization study is outside the scope of this work.

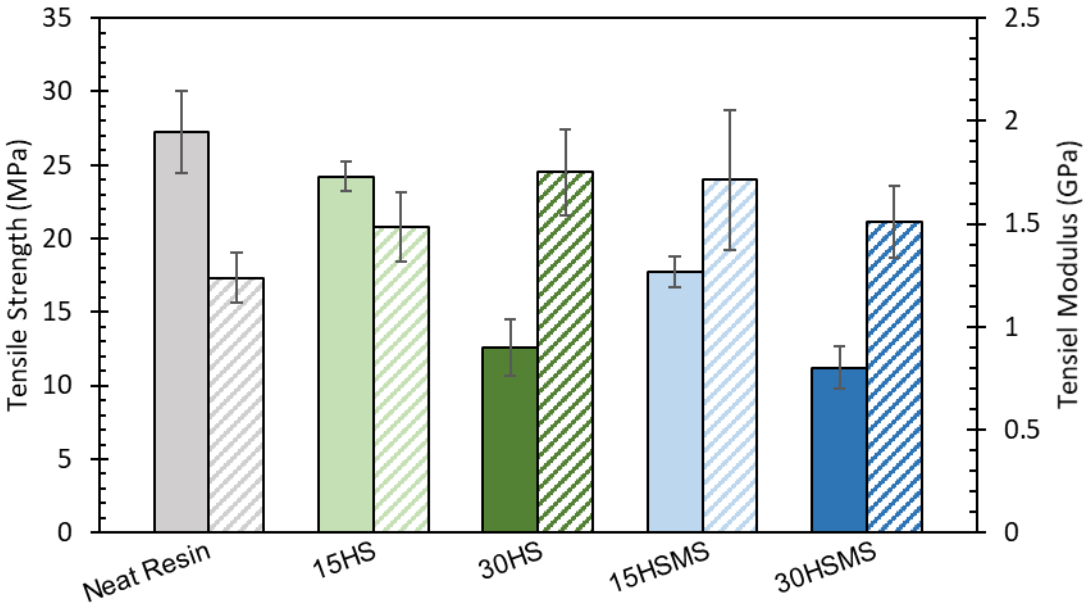

Figure 4.7 Tensile strength (solid bars) and elastic modulus (patterned bars) for Neat Resin and HGS-PR composites as a function of HGS content (vol%) and surface treatment.

The third subset of samples is centered around exploring the effect of various surface treatments, (silane, NaCNC, PhCNC), on composite tensile strength and elastic modulus (Figure 4.8). As in the previous sample subset, the addition of HGS decreased the HGS-PR composite tensile strength in every case. Surface modification of HGS with

PhCNC (15HSMSPhCNC) did somewhat reduce tensile strength as compared to the 15HSMS case (15 MPa vs 18 MPa). Reduction in tensile strength could be caused by a variety of factors, but when taking the context of the processing route, the most likely source is either further agglomeration of HGS or an increase in the number of fractured HGS. Tensile modulus measurements showed no significant differences between HGS surface treatments. Only 15HSMS displayed a statistically significant higher modulus from the baseline resin, (1.7 vs 1.2 GPa).

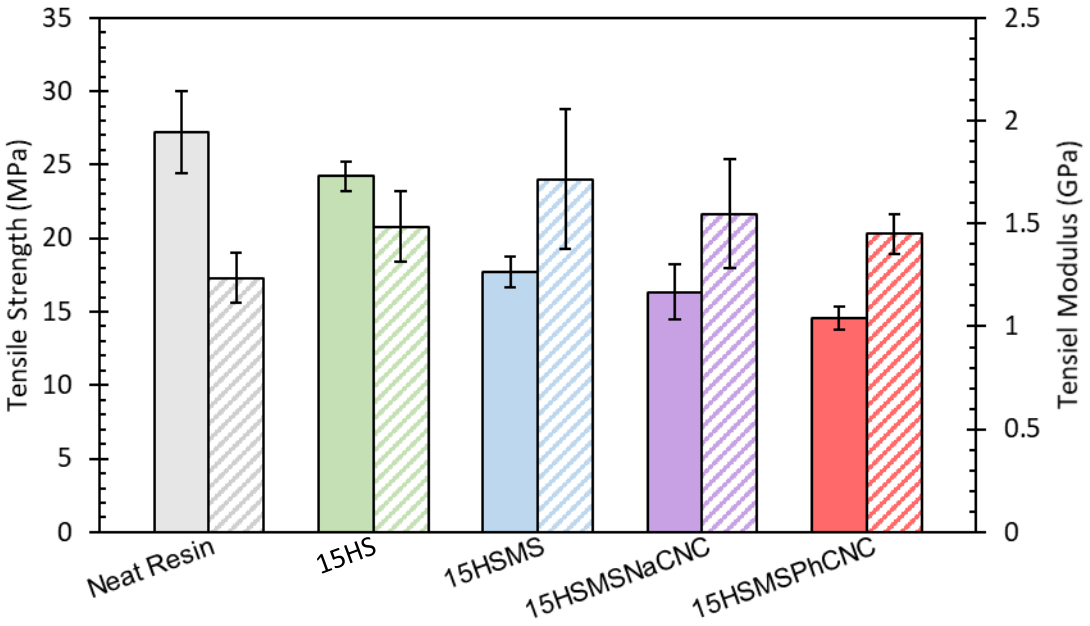

Figure 4.8 Tensile strength (solid bars) and elastic modulus (patterned bars) for HGS-PR composites with various HGS surface treatments.

Specific mechanical properties are outlined in Figure 4.9. The specific mechanical properties help highlight the benefits of syntactic foam composites over traditional composites or nanocomposites. The reduction in density achieved from adding in the low density HGS can significantly enhance the specific mechanical properties, especially specific tensile modulus.

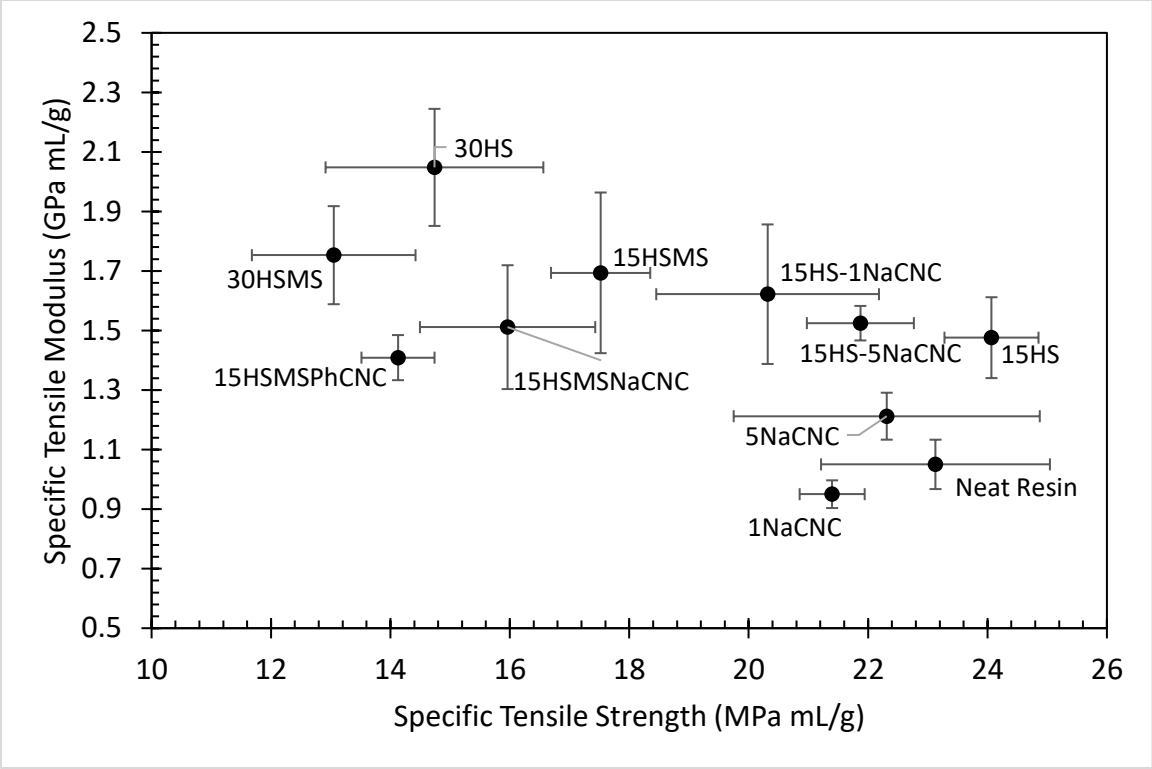

Figure 4.9 Specific tensile strength and specific tensile modulus for samples in this study. Error bars are 1 standard deviation.

Although tensile testing is a useful tool for determining bulk mechanical properties, the precision of the test is low relative to other techniques such as DMA. Further analysis can shed light on the subtleties of HGS-PR interactions and changes thereof by surface modification with CNC.

4.4 Composite Morphology

Scanning electron microscopy (SEM) was conducted on tensile fracture surfaces to explore relationships between the composite microstructure, properties, and processing. Interpretation of the composite fracture surface, along with other supporting techniques such as DMA and tensile testing, can provide useful information on particle-matrix

interactions, as well as general material features including particle agglomeration and porosity.

In examining the first subset of samples the agglomeration of NaCNC spray dried particles within the PR is immediately evident, Figure 4.10 and Figure 4.11. Within 1NaCNC and 5NaCNC samples the spray dried CNC particles are readily visible within the PR in a form almost identical to that of the raw material, indicating that the sonication mixing had minimal effect on disrupting the spray dried aggregate structure. Similar particles were also observed in 15HS-1NaCNC and 15HS-5NaCNC composite samples. Failure points were clearly identified in samples containing HGS as either being areas with a high local density of HGS, porosity near the surface, or both (Figure 4.12 and Figure 4.13). With respect to HGS-PR interactions, the addition of spray dried NaCNC to the PR had no effect as observed by SEM, corroborating other methods which showed no interaction between spray dried NaCNC and HGS (tensile, DMA, water uptake). The untreated HGS seemed to debond from the matrix cleanly (i.e. a smooth cavity was produced from HGS pullout), indicating a low interfacial energy between HGS and PR. Tensile results corroborate these results as the tensile strength and modulus is within statistical error across 15HS, 15HS-1NaCNC, and 15HS-5NaCNC samples.

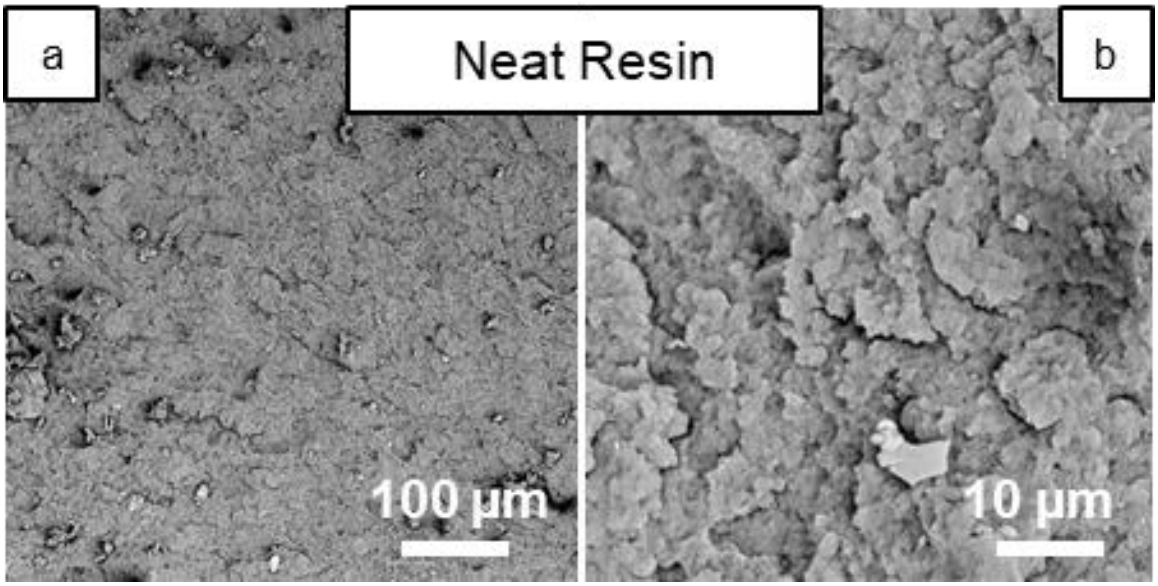

Figure 4.10 SEM images of the Neat Resin fracture surfaces. Scale bars are 100 and 10 µm for the low and high magnification images, respectively.

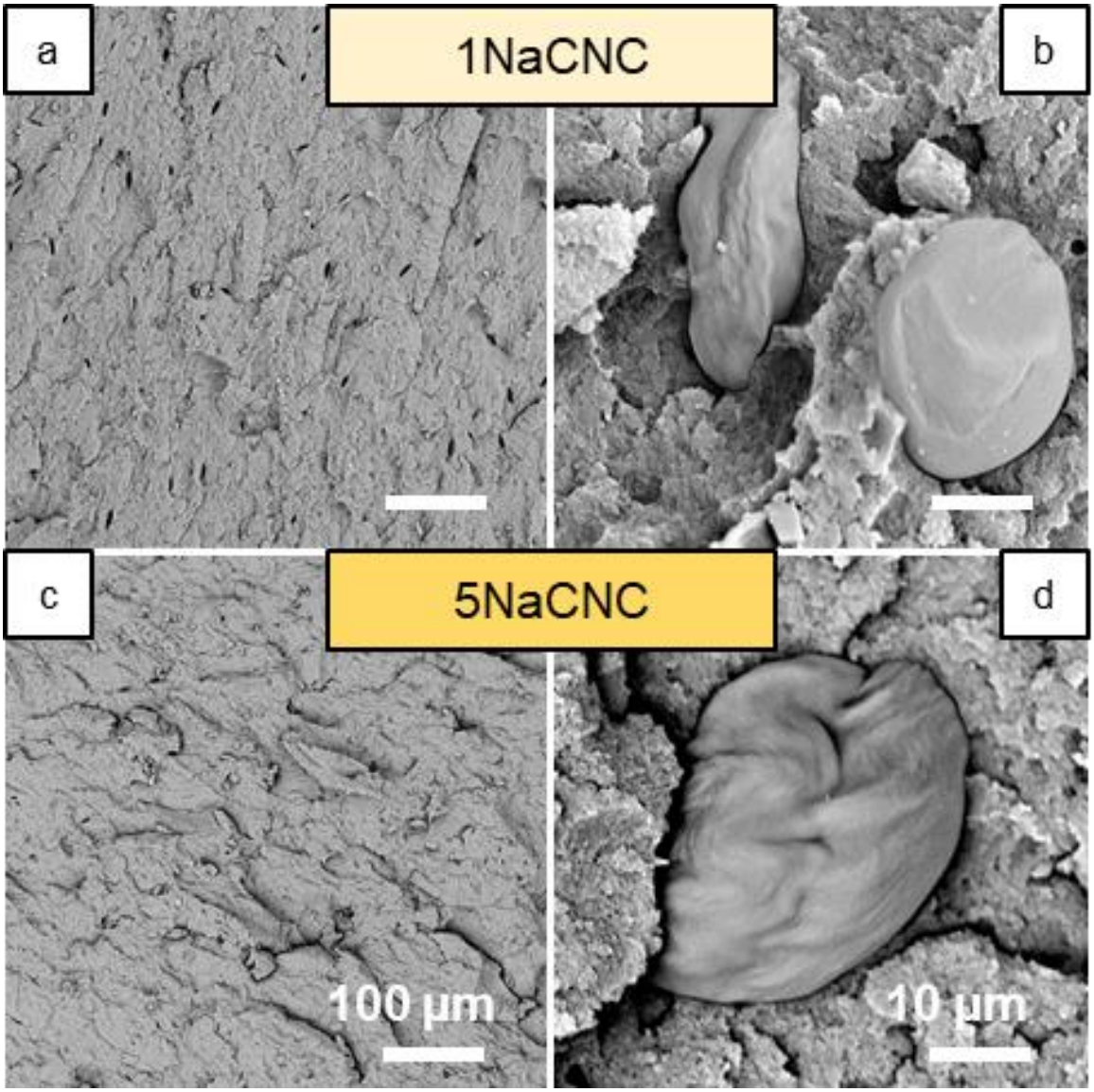

Figure 4.11 SEM images of the 1NaCNC and 5NaCNC fracture surfaces. Scale bars are 100 and 10 µm for the low and high magnification images, respectively.

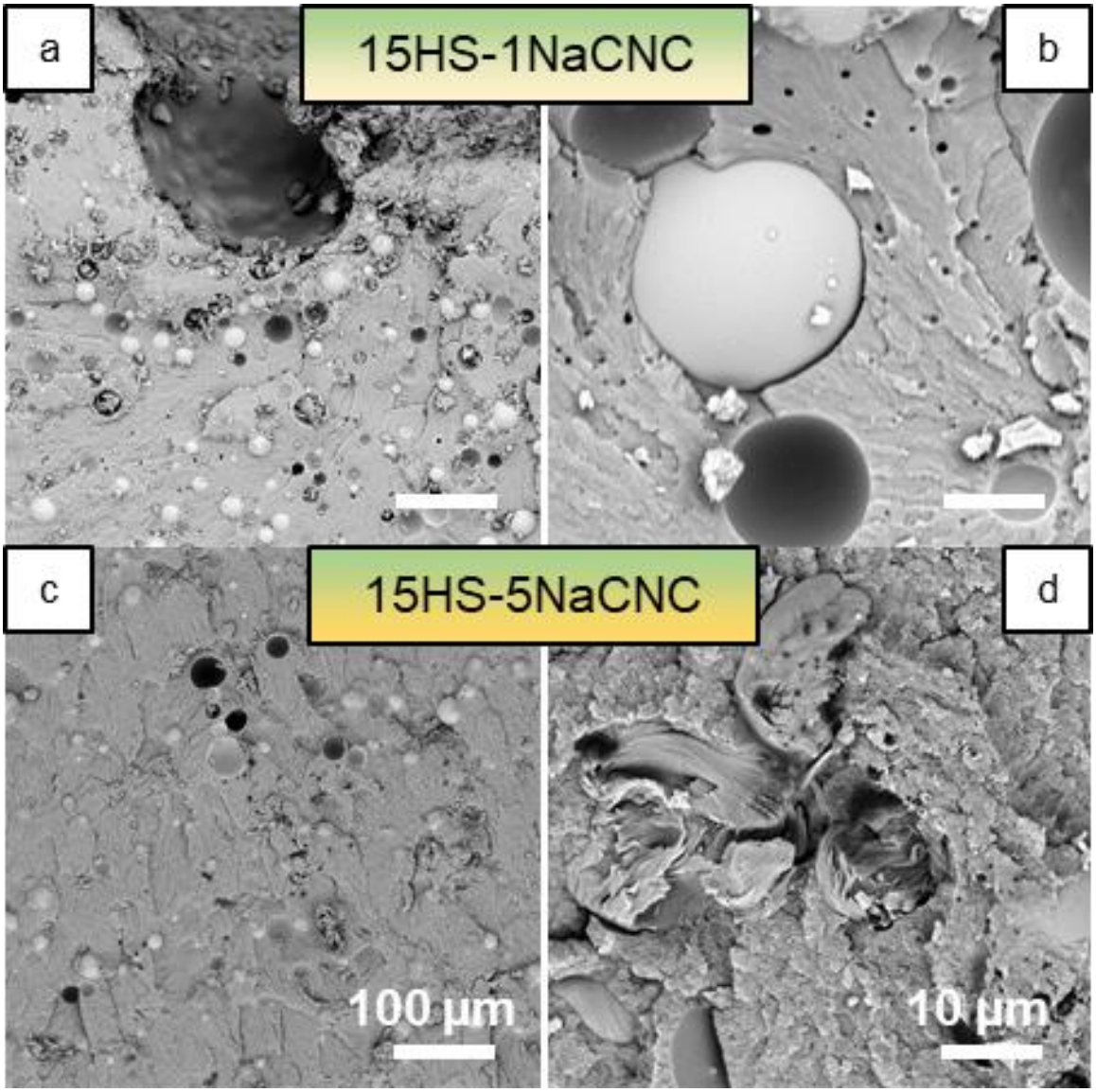

Figure 4.12 SEM images of the 15HS-1NaCNC and 15HS-5NaCNC fracture surfaces. Scale bars are 100 and 10 µm for the low and high magnification images, respectively.

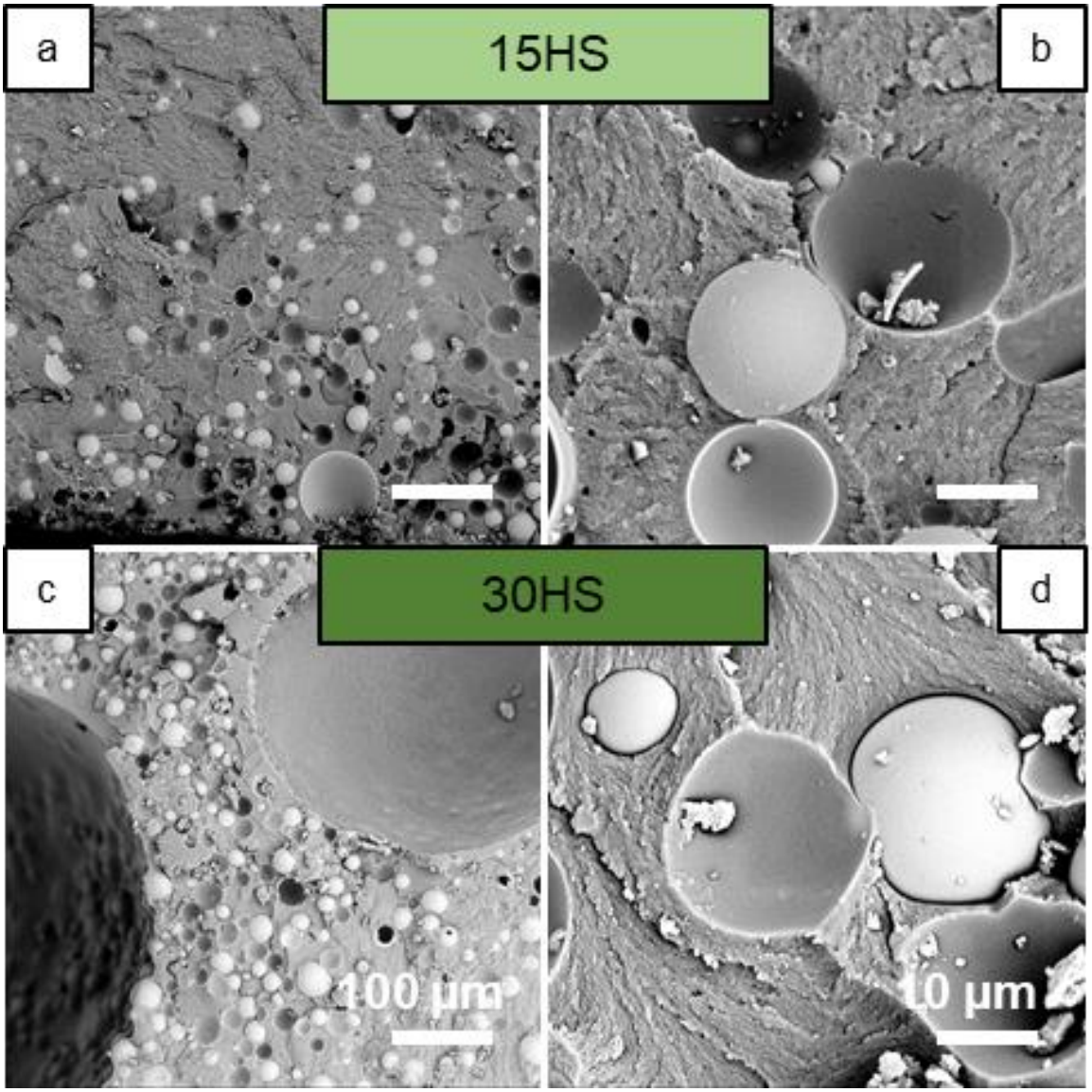

Figure 4.13 SEM images of the 15HS and 30HS fracture surfaces. Scale bars are 100 and 10 µm for the low and high magnification images, respectively.

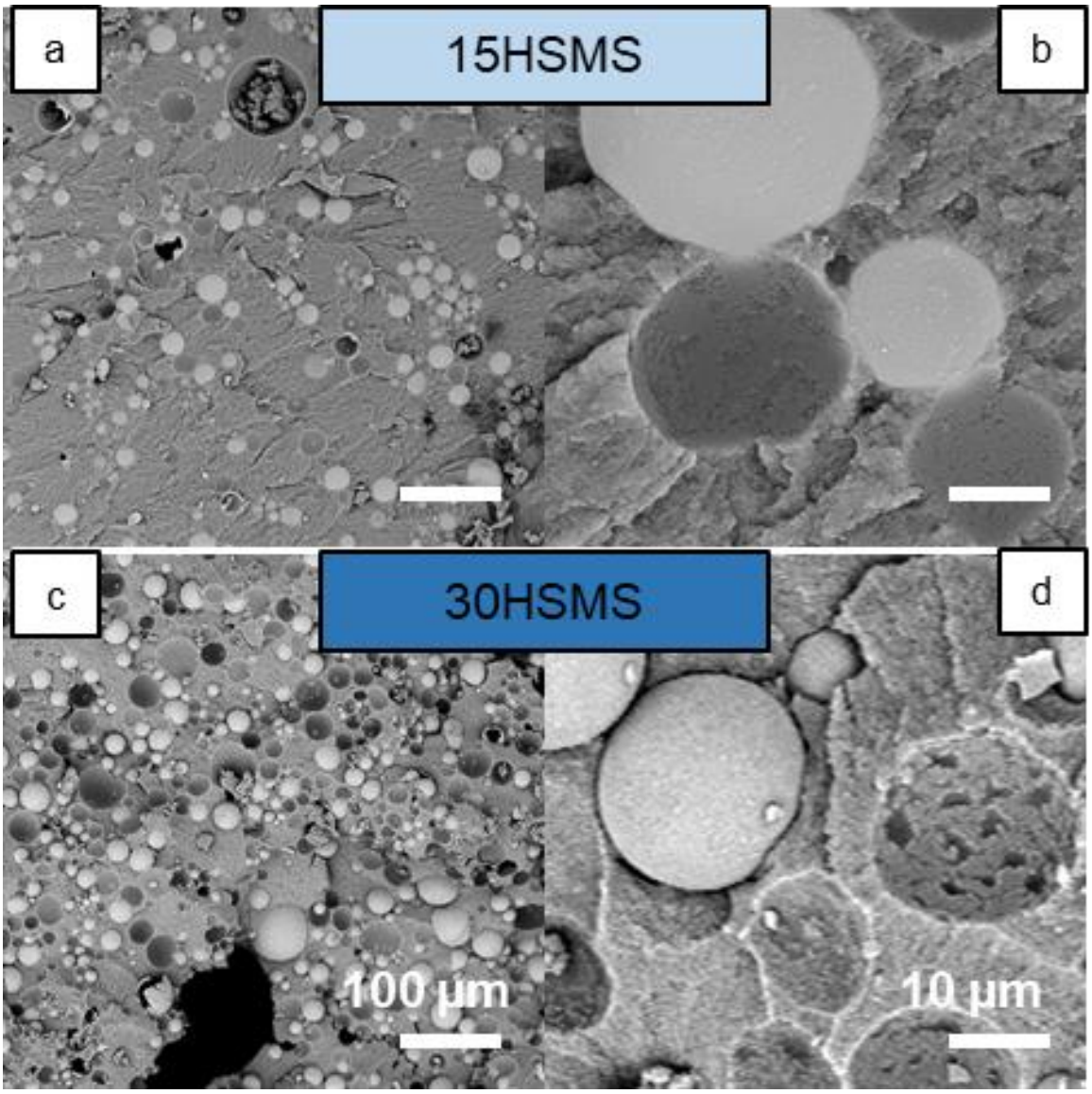

Figure 4.14 SEM images of the 15HSMS and 30HSMS fracture surfaces. Scale bars are 100 and 10 µm for the low and high magnification images, respectively.

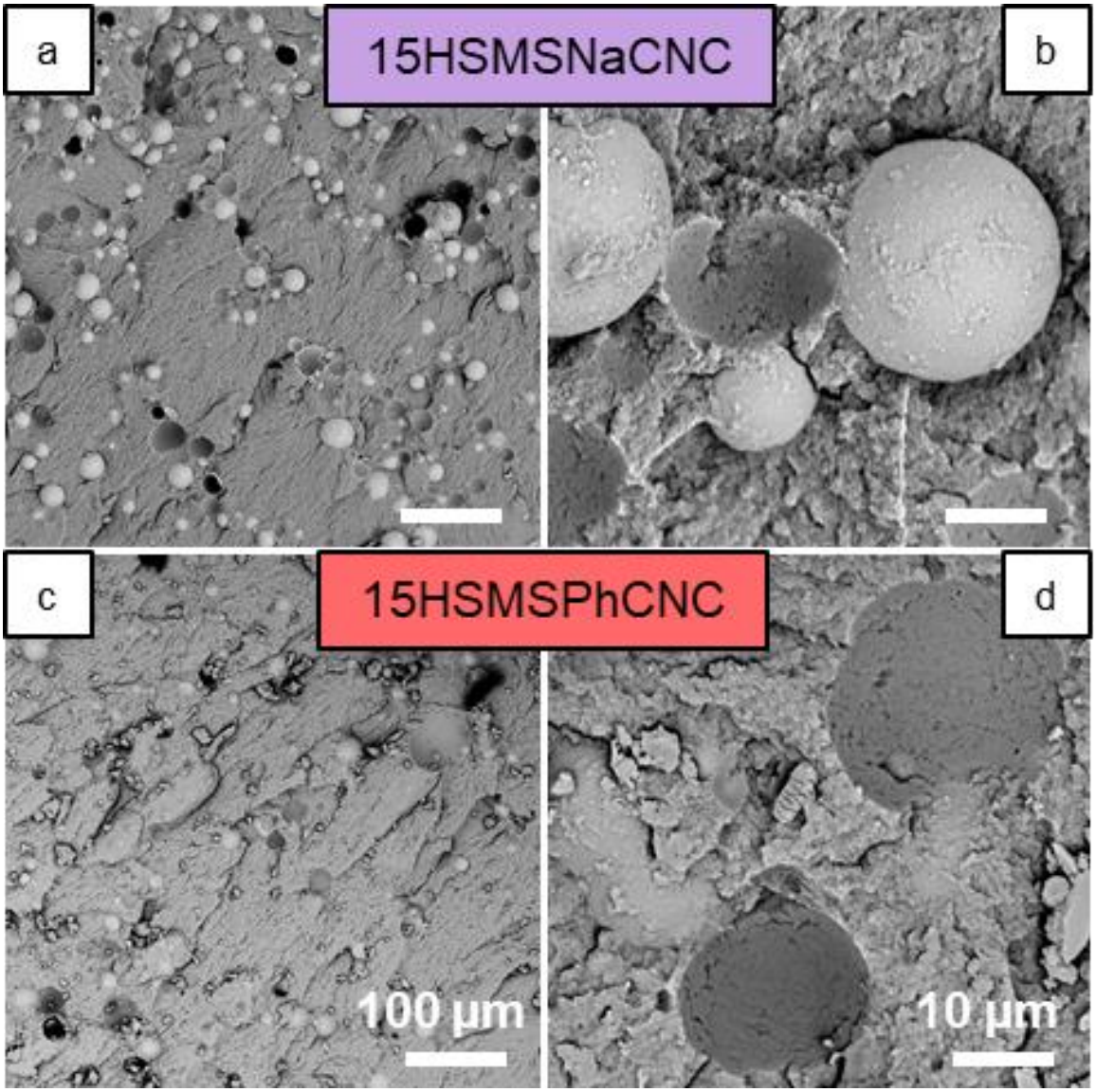

Figure 4.15 SEM images of the 15HSMSNaCNC and 15HSMSPhCNC fracture surfaces. Scale bars are 100 and 10 µm for the low and high magnification images, respectively.

Within the second subset of samples, the localized accumulation of HGS and porosity are more pronounced in the 30 vol% HGS samples as anticipated from tensile testing results, (Figure 4.13 and Figure 4.14). Pores ~100s of µm in diameter were observed and showed clear signs of being the fracture initiation point. Surface treatment of the HGS

with MS also resulted in distinct differences in the HGS pullout cavity morphology. 15HSMS and 30HSMS samples showed noticeably rougher HGS pullout cavities than 15HS and 30HS samples, indicating a higher energy interaction between HGS and PR. The effect of surface treatment on pullout features has been reported in other studies to be related to interfacial shear strength, (i.e. a rougher pullout surface indicated a relatively higher interfacial shear strength) [9, 10].

SEM images of the final subset of samples clearly supports the findings of other characterization techniques (Figure 4.15). CNC coated HGS-PR composite samples, 15HSMSNaCNC and 15HSMSPhCNC, display highly textured HGS pullout surfaces. Other studies involving GF, CNC, and epoxy matrices have shown that after adding CNC into the polymer matrix, the elastic modulus of the material increased, and an increase in roughness of the fiber pullout cavity was also observed. These results indicated that samples containing CNC had higher fiber-matrix adhesion [9, 10]. Overall, these observations are in good agreement with other experimental techniques used in this study and indicate the beneficial effect that CNC treatment has on HGS-PR interactions.

4.5 Composite Thermomechanical Properties

Dynamic mechanical analysis (DMA) was conducted to determine the composite materials' performance as a function of temperature. Methods for DMA are outlined in Section 2.3. DMA also provides insight into the relaxation behavior of polymer chains in the composite and can be significantly influenced in situations where there is a large volume of interphase between a filler and matrix (i.e. nanocomposites and microcomposites). The glassy plateau in storage modulus (E') was not observed due to a

lack of a cooling unit in the available testing equipment. Furthermore, at high temperatures the loss modulus decreased to nearly zero. This is believed to be due in part to thermal decomposition of the composite based on observations of discoloration in composites after testing and mass loss of specimens after testing. A note on the Neat Resin prior to discussion of composite samples: along with the primary glass transition or T_g there is a secondary, beta transition observed in the loss tangent curve centered near ~70°C (T_β). Beta transitions are usually associated with transitions relating to the localized polymer chain or side groups. It's presence here could be indicative of differing relaxation behavior for the main polyester backbone and the interconnecting polystyrene chains [123]. For the sake of discussion, the rubber modulus is taken at 50°C (E'_g), the glassy modulus at 200°C (E'_r), the glass transition (T_g) as the maximum in the loss tangent, and the maximum of tan(δ) at that transition (I_α). Data is averaged over 3 sample runs.

The first subset of samples which explore any interaction effect between spray dried NaCNC and HGS in the PR matrix are discussed here. Examining the results of the first subset: there is little difference between the E'_g of the Neat Resin, 1NaCNC, and 15HS samples (Figure 4.16). The 5NaCNC sample is incrementally higher followed by a step increase to 15HS-1NaCNC and 15HS-5NaCNC. This trend matches, for the most part, the results of the elastic modulus as measured by tensile testing. The main difference being that 15HS is more comparable in modulus to the Neat Resin by DMA than by tensile testing. At elevated temperatures above T_g the difference in E' of the samples are more noticeable. Samples containing HGS, (15HS, 15HS-1NaCNC, 15HS-5NaCNC), display higher E'_r than those without. These effects are easily explained through Halpin-Tsai like concepts on mixtures of materials with differing stiffness. Similar results with respect to

CNC-PR composites have been observed in other works [21, 24, 29]. The T_g increased from 128.8°C in the Neat Resin to a maximum of 135.9°C in 15HS-1NaCNC. Glass transition shifts are often explained via changes in the mobility of polymer chains. In this case it is possible that, although a majority of the NaCNC is agglomerated, some amount of the NaCNC is nanodisperse in the resin at this concentration and is reducing the polymer free volume. Furthermore, the addition of HGS acts to generally increase the composite rigidity and reduce polymer chain motion. Along with the increase in T_g all samples showed varying degrees of suppression of the beta transition shoulder. Suppression of this shoulder is likely the result of HGS and/or CNC restricting polystyrene side chains in the network.

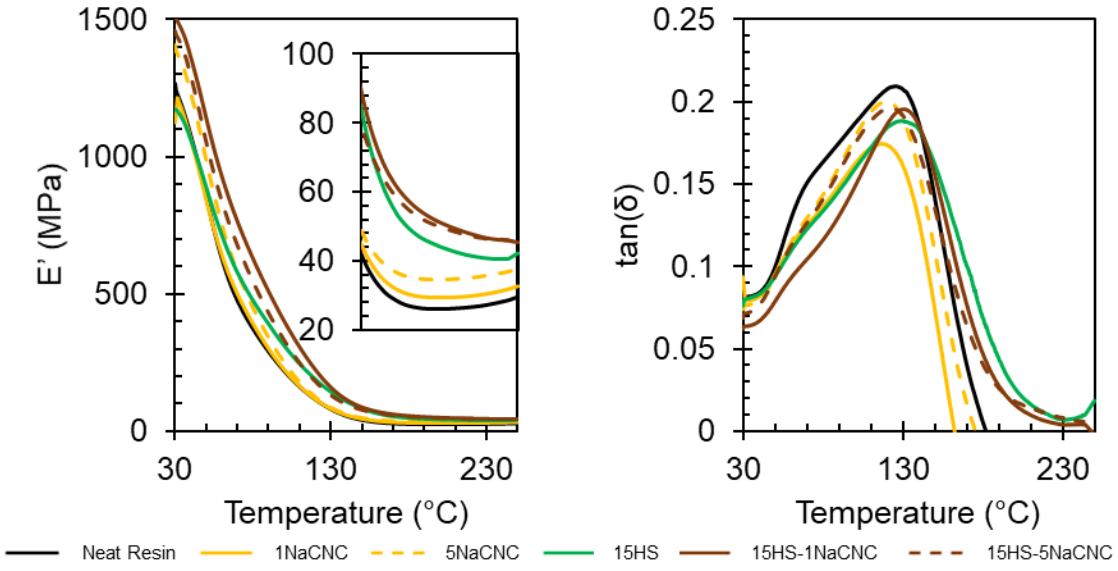

Figure 4.16 Effect of CNC content (wt%) on the elastic modulus and tan(δ) of PR, CNC-PR, HGS-PR, and HGS-CNC-PR composites.

The second subset of samples, which aim to explore the interaction between HGS surface treatment and HGS content (vol%), in order of increasing average E'_g were: Neat Resin, 15HS, 15HSMS, 30HSMS, and 30HS (Figure 4.17). This trend is somewhat similar

to that observed during tensile testing in that 30HS had both the highest average elastic modulus and E'_r. Both 15HS and 15HSMS E'_g were deemed not statistically significantly different from the Neat Resin sample. At elevated temperature, the E'_r of samples stratified into three distinct tiers: Neat resin, 15HS and 15HSMS, and 30HS and 30HSMS. Among this sample subset the trend seems to indicate that the primary factor driving E'_r is the HGS content. This observation follows with the understanding of each constituent materials performance at elevated temperatures. Glass, having a significantly higher service temperature than PR, would be expected to improve the high temperature stiffness for polymer matrix composites. The T_g of composites was generally increased by further increase of HGS. The MS surface treatment also led to an increase in T_g over untreated samples. Higher HGS loadings also led to a suppression of the beta transition. Higher amounts of HGS material would likely result in further restriction of chain motion and an increase in the activation energy for the transition. The I_α increased with higher HGS content. The I_α is often associated with the interphase volume and subsequently the dispersion quality of the fillers. Therefore, the increase in I_α in 30 vol% samples over 15 vol% samples is indicative of possible particle agglomeration. These results show the customizability of syntactic foam composites to specific application requirements. Strong consideration should be taken for surface treatment of the HGS for enhanced bonding as has also been revealed in other studies [65, 66].

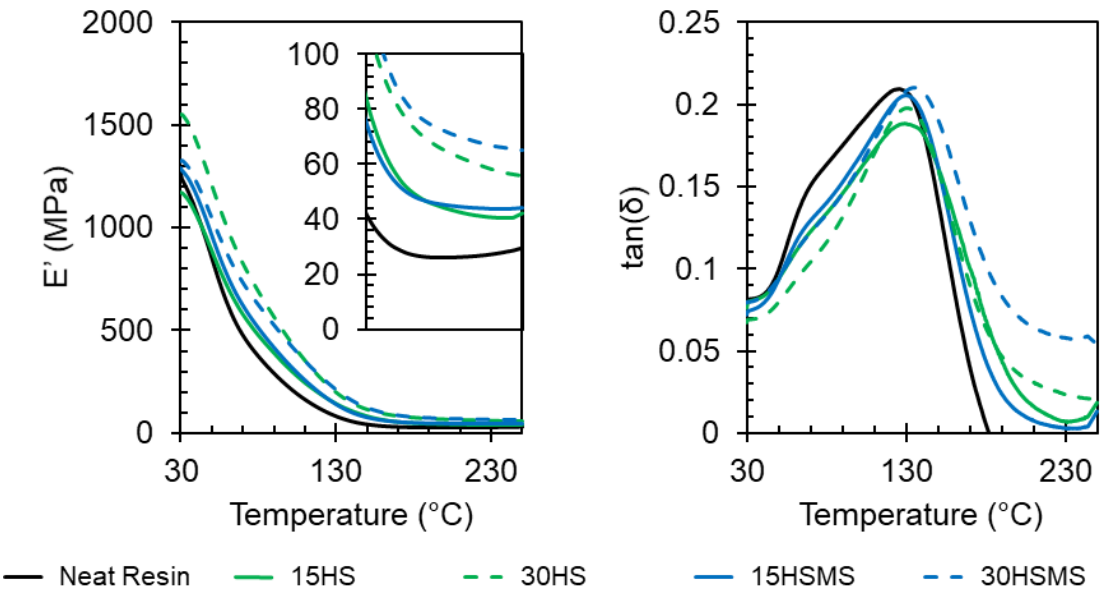

Figure 4.17 Effect of HGS surface treatment and loading on storage modulus and tan(δ) of PR and HGS-PR composites.

The final subset of samples provided interesting insights into the HGS-PR interphase and the effects of various surface treatments on composite behavior (Figure 4.18). In order of increasing E'_g were: Neat Resin, 15HS, 15HSMS, 15HSMSNaCNC, and 15HSMSPhCNC. As stated earlier, DMA can provide a more sensitive analysis in the linear elastic strain range than tensile testing. At elevated temperatures the samples, in order of increasing E'_r were: Neat Resin, 15HS, 15HSMS, 15HSMSNaCNC, 15HSMSPhCNC. Interestingly, the 15HSMSPhCNC displayed a statistically significantly higher E'_r than 15HSMS (59.7 MPa vs 45.2 MPa), suggesting that CNC surface coated HGS can outperform covalent crosslinking from the MS treated HGS at elevated temperatures. The similarity between HGS surface treatments in this respect indicates similar effects on polymer chain vibration activation energies. The beta transition observed in the Neat Resin appears to be suppressed somewhat by the addition of the HGS, and further by CNC coated HGS. As mentioned before, this phenomenon is likely related to

restriction of smaller vibrational modes in the polymer network. A highly textured particle, such as the CNC coated HGS, could disrupt the styrene linkages within the matrix and increase the T_β. The I_α is lowest in 15HSMSNaCNC samples indicating an increase in the interphase volume relative to other HGS samples. A larger interphase volume could be caused by different degrees of interaction effects between the NaCNC-PR and PhCNC-PR interfaces; however, considering the tensile strength data the likely cause of this difference is agglomeration of PhCNC coated HGS.

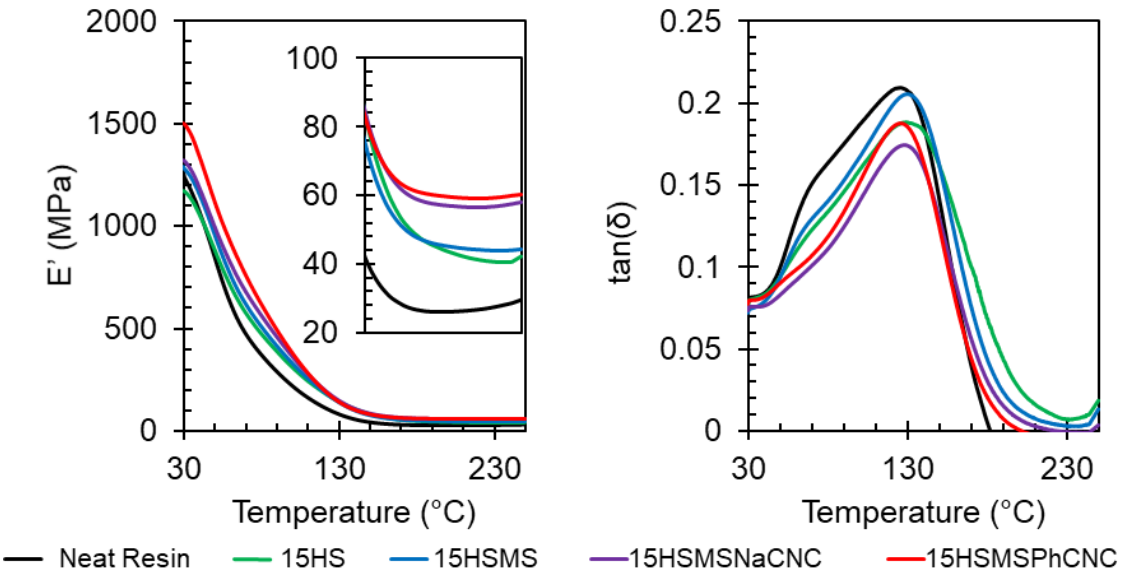

Figure 4.18 Effect of HGS surface treatment on storage modulus and tan(δ) of PR, and HGS-PR composites.

Considered as a whole, the treatment of HGS with CNC produces new effects on the HGS-PR composite behavior that are not observed in HGS-CNC-PR composites, (when CNC is dispersed in the PR resin), including increased E'_r and a reduction of the T_β shoulder. DMA also revealed that PhCNC coated HGS-PR composites at a statistically significantly higher storage modulus than the MS treated HGS-PR composite at high temperature and untreated HGS at lower temperatures. The DMA results outlined here also

provide a higher resolution of analysis than was observed via tensile modulus testing, and a more wholistic impression than provided by SEM analysis. These DMA results are also generally consistent with the results outlined in previous sections: spray dried NaCNC do not have an interaction effect with HGS, higher levels of HGS loading lead to an increase in stiffness, and surface treatment of HGS with CNC has some effect on HGS-PR interactions.

4.6 Composite Environmental Stability

The environmental stability of the composites was also explored using water uptake analysis following the protocol outlined in Section 2.3. Water uptake data is comprised of two primary parameters: apparent diffusivity (D_a), and maximum water uptake (W_{max}). The diffusivity value, taken to be the slope of the initial linear region of the mass uptake vs time$^{1/2}$ plot, is dependent on multiple factors including temperature, pressure or concentration gradients, porosity, and the activation energy for diffusion (e.g. how readily water interacts with components of the material). The W_{max}, taken to be the maximum of the mass gain measurements, can be considered to be related to the balance of the chemical potential for water in the composite, and the increased mechanical stress applied for each unit of water absorbed [124].

Increases in the maximum water uptake value would indicate a composite that would undergo a higher degree of swelling, a higher degree of strain, and subsequently a higher degree of stresses on the composite. Such stresses have often been determined to be detrimental to polymer matrix composite mechanical performance and so should be minimized [125, 126].

The water uptake behavior of the first subset of samples is outlined in Figure 4.19. Under these environmental conditions for the Neat Resin sample the linear region which is characteristic of the D_a is brief, completing within 1-2 days of initial submersion. The W_{max} for the Neat Resin is the lowest for all samples studied at 3.3 wt%. This value is within the range that has been reported in similar studies [127-131]. The NaCNC-PR composites displayed higher W_{max} and D_a than the Neat Resin. Considering that most of the CNC particles are likely still agglomerated, this result agrees with results of other studies that have examined water uptake of cellulose-polymer composites. The NaCNC agglomerates could provide sites for water to enter and swell the particles that are more readily available and thermodynamically advantageous. The HGS-PR composite, 15HS, displayed a substantially higher maximum water uptake over the base resin (9.0 wt% vs 3.3 wt%) and a much clearer linear region. The addition of the high surface area glass particles is the likely source of this dramatic increase. Syntactic foams have been shown to significantly increase the water uptake behavior as compared to the base polymer matrix [132-134]. Glass, being significantly more hydrophilic than PR, has been shown to increase the D_a and W_{max} for PR composites. Adding CNC into the matrix of the HGS-PR composite had a small but noticeable effect on the water uptake behavior. In the case of 15HS-1NaCNC, the D_a increased somewhat but the W_{max} is still within error of the 15HS sample. The addition of 5 wt% NaCNC (15HS-5NaCNC) both increased the D_a and the W_{max}. These results seem to indicate that the presence of the HGS is the dominant driving force in the water uptake behavior for HGS-PR composites.

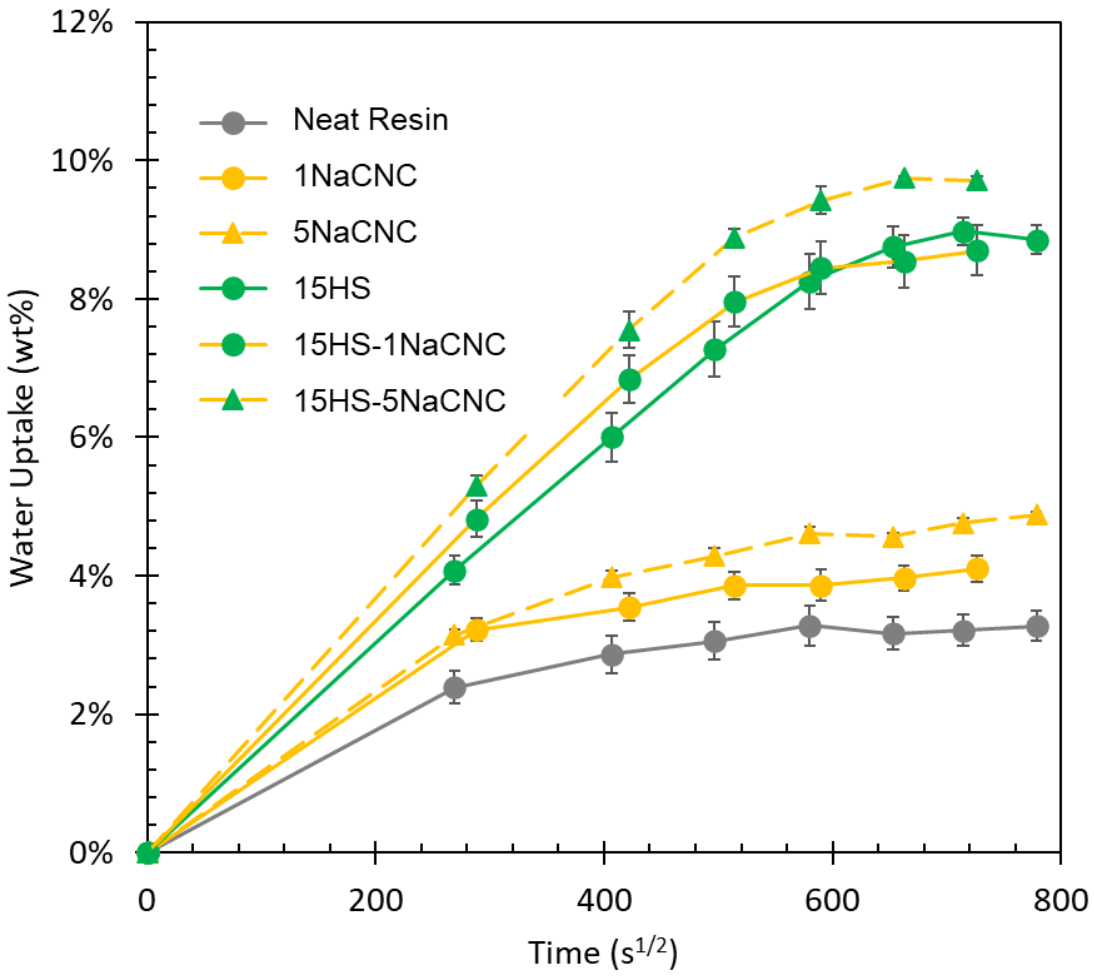

Figure 4.19 Water uptake for Neat Resin, CNC-PR, HGS-PR, and HGS-CNC-PR composites.

The second subset of samples further reinforces some of the concepts observed within the first subset (Figure 4.20). Primarily that the high surface area HGS are a dominant driver in HGS-PR composite water uptake behavior. In both the MS treated and untreated HGS case, the presence of more HGS increases the W_{max}. However, the MS silane treatment does significantly reduce the W_{max} between samples with similar HGS content: 31% and 36% for 15 vol% and 30 vol% respectively. As discussed earlier, the W_{max} is, in part, related to the propensity of the material to swell and accept new water molecules. If the MS treatment of HGS induces crosslinking between the HGS and matrix,

as other data in this study and studies elsewhere have suggested, then the polymer immediately surrounding the HGS particles would be more constrained and unable to swell to accept as many water molecules. Interestingly, the D_a is similar among samples with the same content of HGS. This would seem to indicate that the kinetics of water absorption are at least energetically similar (e.g. similar activation energies). Other studies have also found that silane treatment reduces the maximum water uptake by as much as 20% in HGS-epoxy composites with 40 vol% of 60 μm diameter HGS, but also does not significantly change the D_a in the initial region of the water uptake regime. They attribute these differences to the hydrophobic coating formed by the silane around the HGS, thereby limiting the primary vector for water ingress into the composite [134].

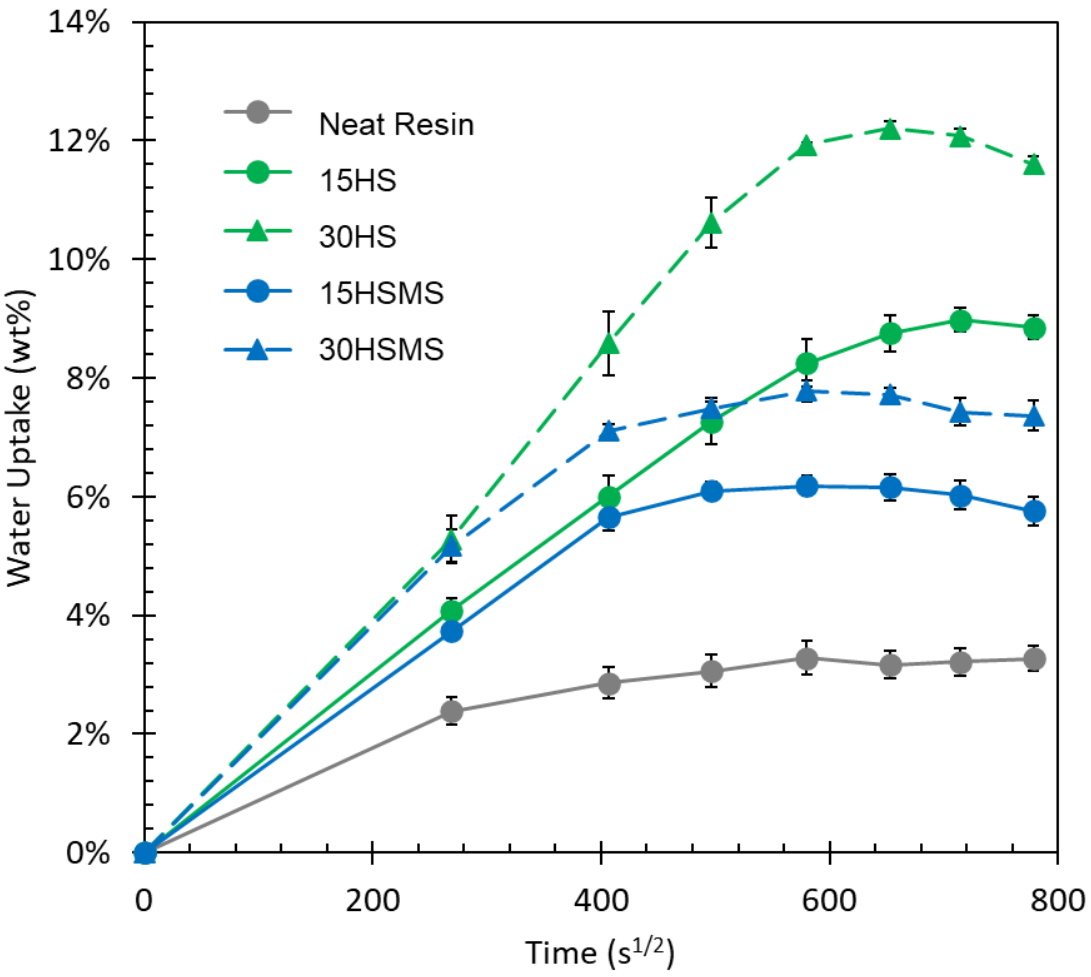

Figure 4.20 Water uptake for Neat Resin and HGS-PR composites with different HGS loading levels and HGS treated with MS.

The final subset of samples examined the effect of treating HGS with CNC on water uptake behavior (Figure 4.21). The addition of a CNC layer onto the HGS prior to compounding with PR significantly reduced W_{max} and D_a beyond what was observed even in the 15HSMS case and nearly to a level comparable with 5NaCNC. The water uptake curves for 15HSMSNaCNC and 15HSMSPhCNC composites displayed a nearly colinear D_a in the initial region but separated somewhat in the plateau. The W_{max} for 15HSMSNaCNC and 15HSMSPhCNC composites was 4.4 wt% and 5.1 wt% respectively, averaged over 3 samples. In the initial study of ion exchanged PhCNC, the material

displayed improved moisture resistance as compared to the sodium form [36]. The W_{max} result is therefore at first perplexing; however, when considering other results from this study, the likely source of this difference is an increased degree of agglomeration in the PhCNC coated HGS. The over 50% reduction in W_{max} and significant reduction in D_a for CNC coated HGS-PR composites could be connected to the water uptake behavior of nanoparticle thin films. Nanoparticles have been found to reduce the permeability of materials when introduced in a nanodisperse state or as tightly packed thin film coatings. The source of this improved barrier behavior is attributed to the increased tortuosity that many, high aspect ratio particles produce. Furthermore, cellulose films have been shown to have a higher water contact angle than glass, indicating that although both materials would be considered hydrophilic, glass has a higher chemical potential for interaction with water [135]. In the case of this study, the CNC are acting as a barrier layer and decreasing the availability of the relatively hydrophilic HGS particles. This finding provides a tremendous opportunity for enhancement in syntactic foams utilized in underwater environments or in environments with sustained humidity.

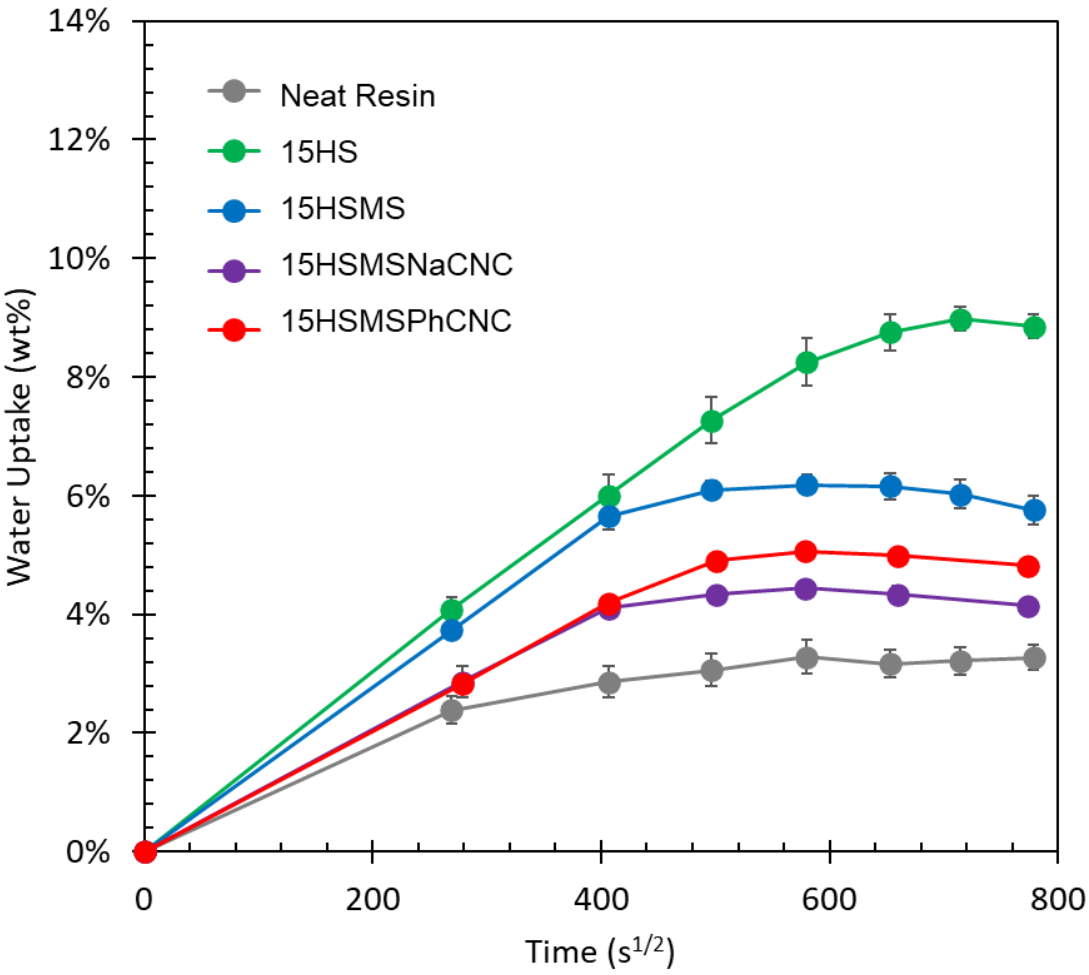

Figure 4.21 Water uptake for Neat Resin and HGS-PR composites with various HGS surface treatments.

4.7 Conclusions

The results outlined here provide a framework development and processing of 3 phase syntactic foams comprised of polyester resin, hollow glass spheres, and cellulose nanocrystals. The resulting properties of these composites were examined. The addition of spray dried CNC into the PR matrix did not have any significant interaction effects with HGS as observed by the methods used here. Based on the processing methods used here, the presence of HGS at a level of 30 vol% significantly reduced, by as much as 50%, the

tensile strength when compared to similar materials with 15 vol% HGS. Coating HGS with did not significantly increase the elastic modulus as measured by tensile testing but did increase the storage modulus both at low temperatures above the base HGS and, at elevated temperatures beyond that of the MS treated HGS composites. Furthermore, coating the HGS with CNC significantly reduced the maximum water uptake and rate of water absorption as compared to samples with untreated HGS or MS treated HGS. The results indicate that CNC coatings on HGS can lead to stronger HGS-matrix interactions. The CNC coating could be influencing mechanical properties through several mechanisms including interpenetration of the resin into the CNC coating increasing the toughness of the interphase and increasing HGS-PR debonding resistance [33]. The reduced water absorbance behavior could be explained by an increase in the tortuosity of the HGS-PR interphase by the CNC coating and by the relatively lower surface energy between CNC and water as compared to that of glass and water [136, 137].

Overall, coating HGS with CNC proved to be an effective means for tuning the HGS surface and modifying the bulk properties of the composite. These results provide a roadmap for further studies on modification of HGS with other nano or micromaterials. Regarding the overall thesis these results show the potential for this method to be used as a technique for reducing the density of PR based composites and increasing specific modulus of the composite.

CHAPTER 5. UNDERSTANDING DENSITY-STRENGTH TRADEOFFS IN SYNATCIC FOAM SMC

The final aspect of this thesis examines functionally graded composites and provides an initial study into the realm of nanoreinforced syntactic foam SMC. SMC composites are generally comprised of a single formulation. Within the formulation there are various fillers, a binding polymer phase, and the reinforcement phase-usually glass fibers. The development of techniques for lightweighting SMC composites is of interest. Furthermore, a reduction in density should not come at the cost of other critical material properties (specific strength, specific modulus, environmental stability, etc.). The addition of HGS into SMC formulations has been proven to reduce the density of the composite, but at the cost of lower quality surface finish. In some applications, (e.g. external auto body panels), a smooth finish and good aesthetic quality are of high importance to the customer, and any defects are carefully avoided. To overcome this issue, it is possible to stack the SMC sheets such that the outer layers are traditional SMC composition, while the interior consists of syntactic foam-SMC. The study detailed here aims to investigate the consequences on material properties of these lightweighting approaches and provide a blueprint for more expedient design and development of such functionally graded materials.

5.1 Experimental Outline and Sample Nomenclature

This study examined five composite compositions. A schematic representation of the composites is outlined in Figure 5.1. A standard density formulation (S) was produced to provide a baseline comparison to a material of similar composition and density to

commercially available SMC. The S formulation uses low cost $CaCO_3$ as a filler and no HGS. The mid density formulation (M) was selected as it is comparable to current state of the art formulations that utilize HGS. The M formulation uses both HGS and $CaCO_3$ as fillers. The ultra-low density formulation (U) is a high end composite formulation that is not as commonly found in industry due to the high material cost [138]. To investigate the effect of CNC on composite properties, 1 phr of freeze dried NaCNC was added to the M formulation (M-CNC). This study also explored a functionally graded composite specimen (SUUS) which was comprised of S and U SMC laminates stacked with the standard density (S) formulation on the outer surfaces and the ultra-low density (U) formulation as a reinforced syntactic foam core. These SMC composite samples should provide a good insight into the variety of formulation and materials design options available to commercial SMC manufacturers and the following results will allow for a thorough discussion and investigation of processing-structure-properties relationships.

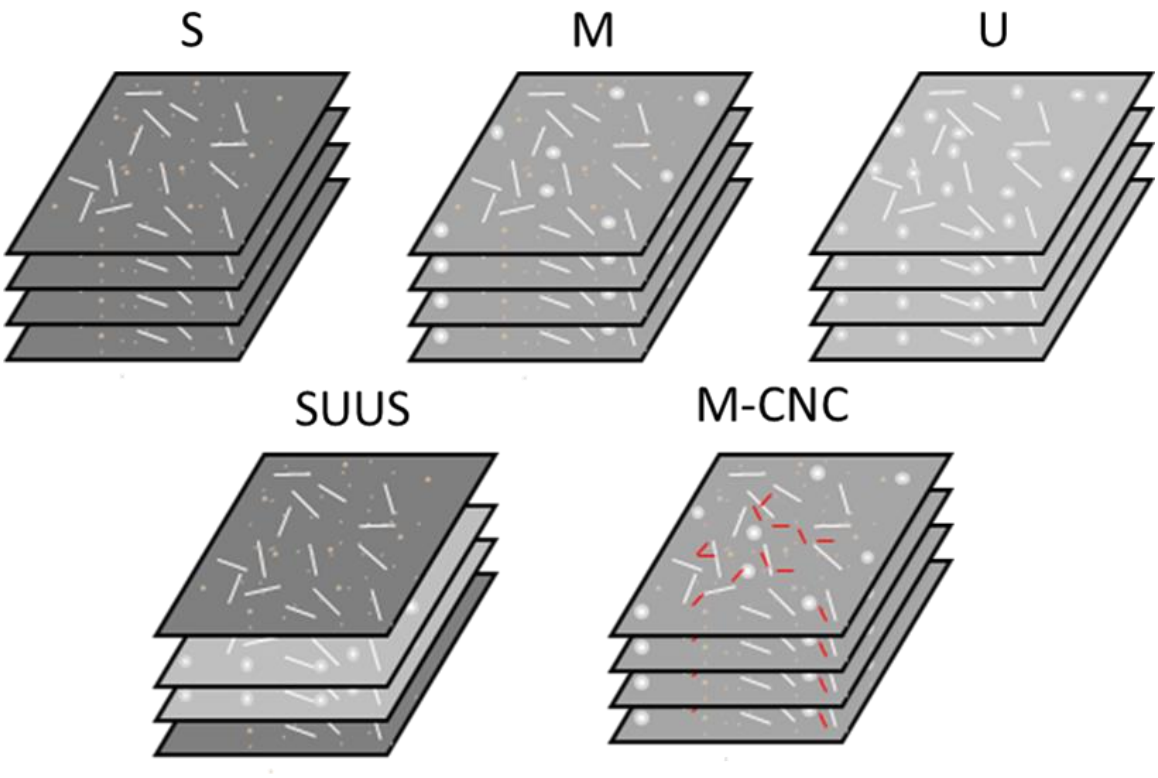

Figure 5.1 Schematic representation of composite samples in this study. GF, $CaCO_3$, HGS, and CNC represented by white lines, tan dots, light grey circles, and red lines respectively.

Resins were processed in accordance with SMC pilot scale procedures outlined in Chapter 2. Briefly: wet components of resins were first weighed and premixed at high rpm, followed by the addition, and mixing of $CaCO_3$ at high rpm or HGS at a reduced rpm (depending on the formulation). Subsequently the material was transferred to the SMC line where it was compounded in line with chopped glass fibers (25.4 mm in length). The collected SMC thickened for 7 days after which it was compression molded. The charges for homogeneous samples were comprised of four plies of identical material, while the functionally graded samples contained two outer plies of standard density (S) formulation and two inner plies of ultra-low density (U) as indicated in Figure 5.1. All samples showed

good mold filling and no macroscopic surface defects. All specimens for testing were waterjet from the square molded plates.

5.2 General Material Properties

The general material properties for composites in this study are outlined in Table 5.1. Density measurements were taken by water displacement measurements and averaged over at least three samples as described in Chapter 2. Other material content including GF, HGS, and $CaCO_3$ was calculated based on the resin paste formulation and reported densities for each component of the resin paste. There is some variation in GF content across samples (16-20 vol%) but is overall within the acceptable limit typical of SMC fabrication, (run to run variation for a given SMC formulation is on the order of 1-2 vol%). The SUUS density is comparable to that of the M. M and M-CNC have similar formulation densities indicating consistent processing between samples. As similar process parameters (i.e. doctor blade height, belt speed, GF cut speed, etc.) were used, the similar composite densities and GF content are positive indicators towards similar behavior of the resin paste during SMC manufacturing. In other words: the addition of 1phr NaCNC did not affect the resin paste viscosity enough to force a change in process parameters.

Table 5.1 Composite density, and reinforcement and filler content for samples in this study. All error bars are 95% confidence interval (CI).

Sample	Density (g/cm^3)	GF content (vol%)	HGS content (vol%)	$CaCO_3$ content (vol%)
S	1.88±0.11	16	0	35
U	1.05±0.07	18	40	0
SUUS	1.48±0.25	17	20	18
M	1.51±0.04	20	20	16
M-CNC	1.51±0.05	20	19	16

5.3 Mechanical properties

Flexural and tensile mechanical testing was conducted on all samples Figure 5.2. The loading conditions of flexural testing are such that the mechanical load is carried by the outer layer of the composite. Within functionally graded specimens, the standard density layer (S), being the outer layer, is expected to define the mechanical behavior in a flexural loading condition.

The standard density (S) formulation displayed the highest strength and modulus both in flexural and tensile loading conditions. Standard density composites have previously been shown to have better mechanical performance (higher strength and modulus) [53, 119, 139]. SUUS displayed similar strength and modulus performance to M. The similar performance in properties between SUUS and M is a positive indication for the competitiveness of the SUUS to other formulations that could have lower quality surface finish. Additionally, the fact that SUUS is competitive with a formulation of similar density indicates that there was no substantial compressive buckling of the U core within

the functionally graded composite. The addition of 1 phr NaCNC did not have a significant effect overall to M mechanical properties. At this loading, 1 phr or 0.3 vol%, the amount of CNC is not enough to significantly impact the mechanical properties.

Failure behavior of composites can be of interest in applications where the material needs to “fail safe” or not fail catastrophically (i.e. retain some strength after initial fracture occurs). To investigate the role of fracture behavior in these composites, particularly the functionally graded material, the individual stress-strain curves for 3 point bending testing were examined, Figure 5.3. Most S samples displayed an immediate substantial drop in strength (as much as 60%) after maximum stress was reached. All U samples displayed a more gradual failure behavior, some displaying a small drop in stress before continuing to increase until ultimate failure. All but one of the functionally graded SUUS composites display failure behavior more characteristic of the U sample. These observations seem to indicate that SUUS can provide a more gradual failure than S.

The mechanical properties of the composites normalized by density are outlined in Figure 5.4 and Figure 5.5. As expected based on previous studies, the standard density formulation has the lowest specific properties and the U formulation has the highest [139]. This is primarily due to the high amount of HGS present in the U formulation. Although the HGS reduce strength and stiffness of the composite, the reduction in density counterbalances this effect when examining specific mechanical properties. Again, the SUUS formulation shows comparable average specific strength and modulus to the M samples. Further indicating the promise of a functionally graded composition for components where high surface finish is desired.

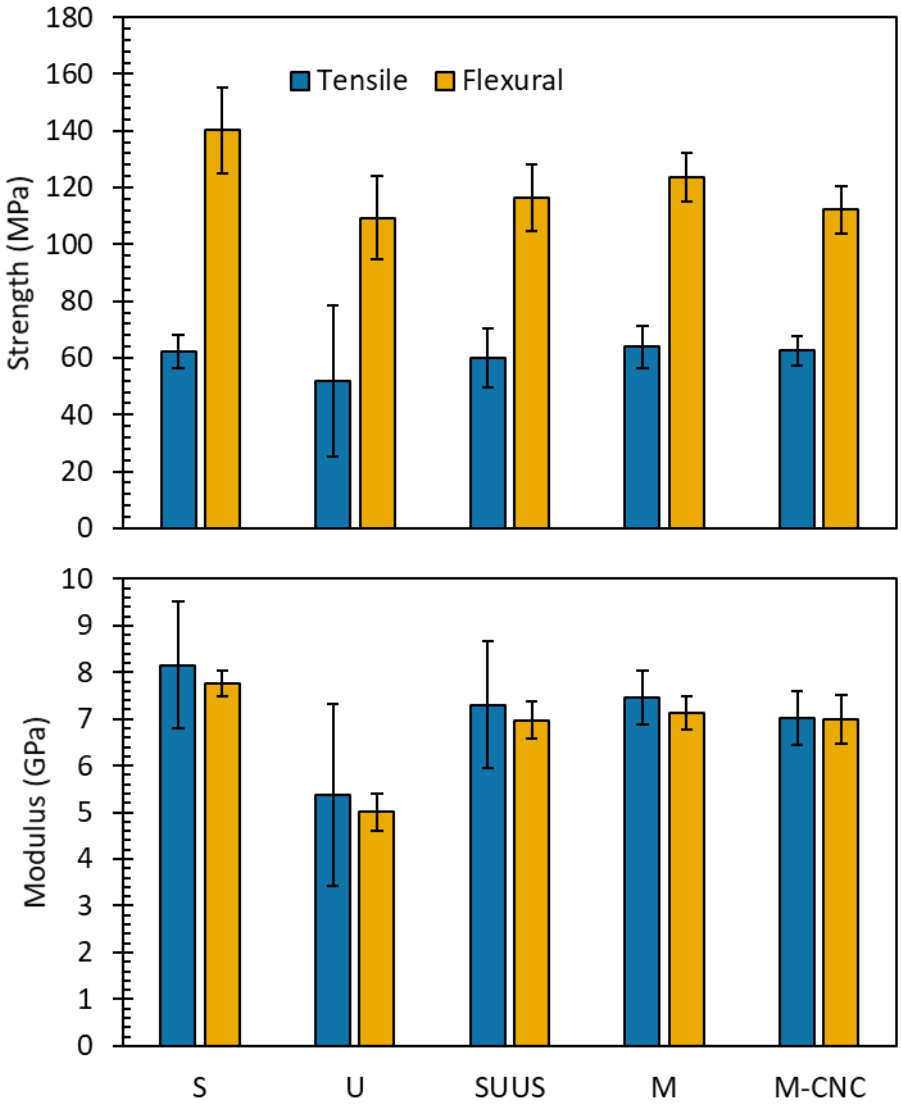

Figure 5.2 Flexural and tensile properties for various SMC compositions in this study. Error bars are 95% CI.

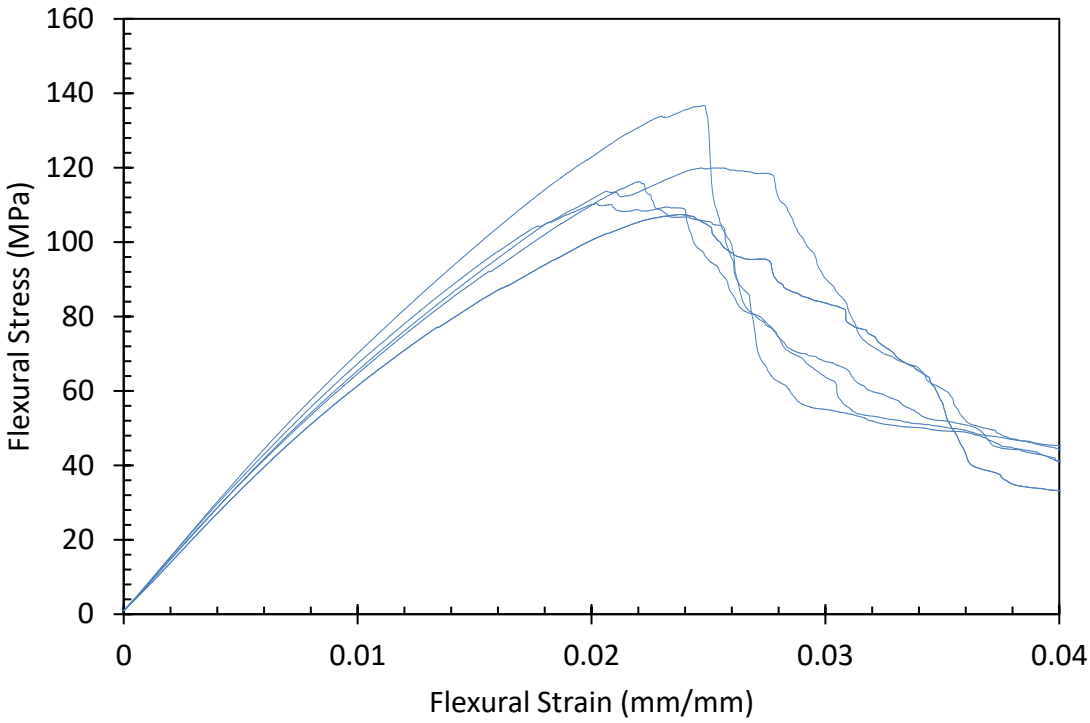

Figure 5.3 Stress strain curves for 3 point bend samples comparing monolithic S (black), U (red), and functionally graded SUUS (blue) failure behavior.

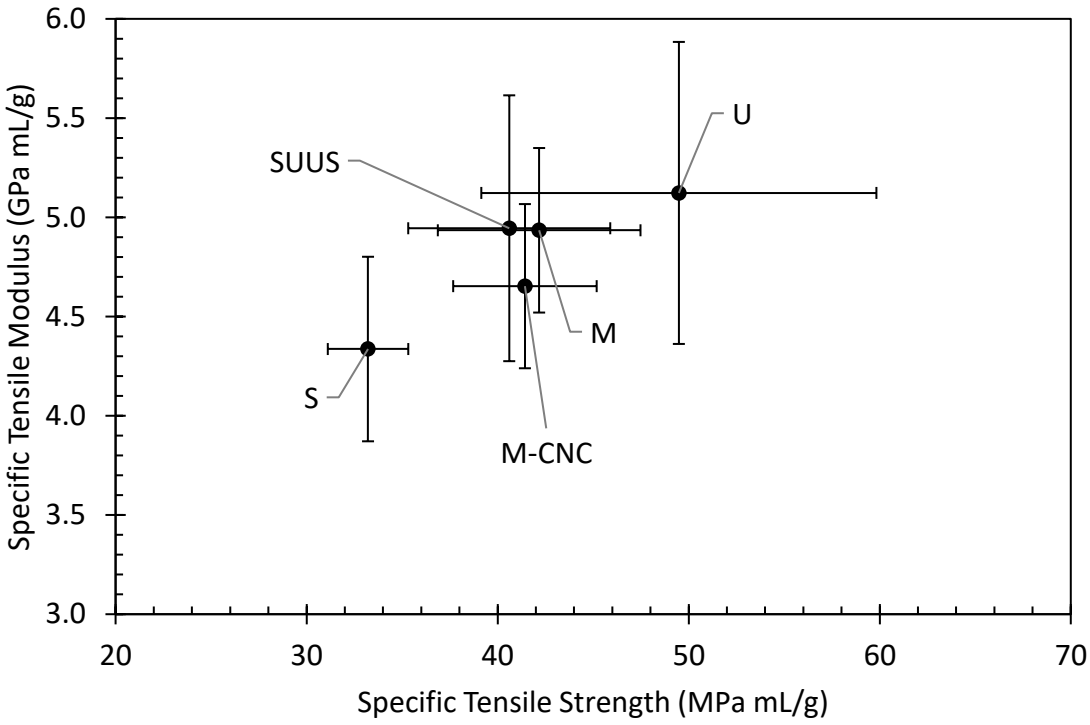

Figure 5.4 Specific tensile strength and specific tensile modulus data for samples in this study. Error bars are 1 standard deviation.

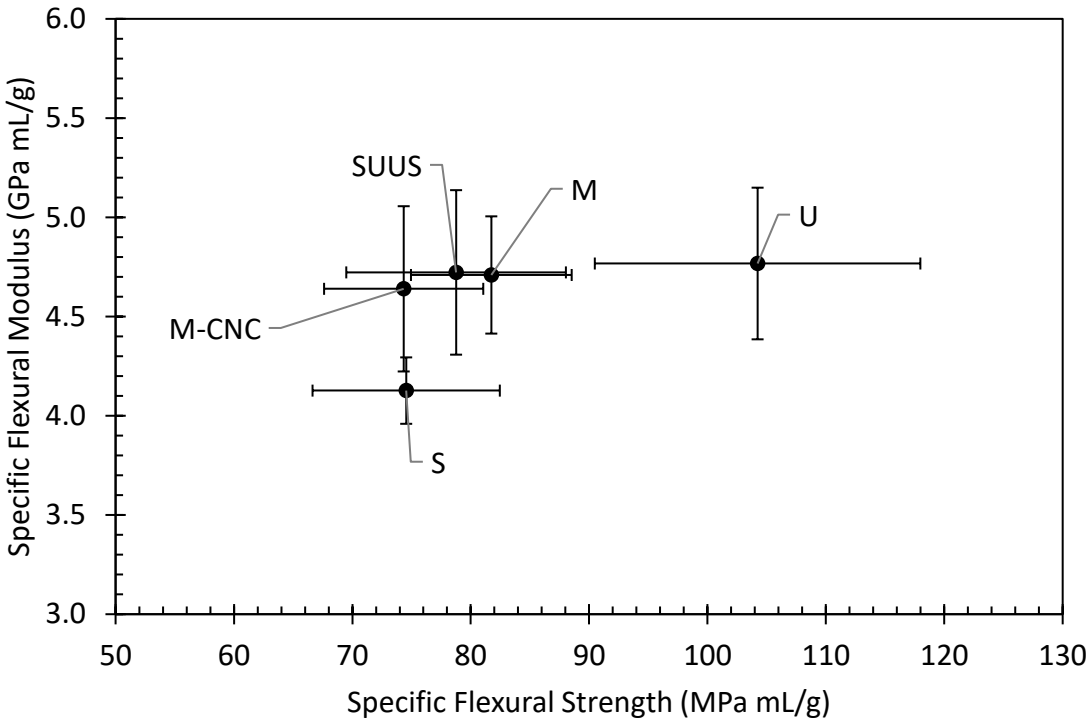

Figure 5.5 Specific flexural strength and specific flexural modulus for samples in this study. Error bars are 1 standard deviation.

5.4 Microstructure

In the development of this functionally graded composite, ensuring that the various material formulations are distinctly distributed and consistently spaced is of interest. If, during compression molding, the S and U layers were to mix and comingle, the objective of this study would be unfulfilled. Optical and electron microscopy was conducted to examine the boundary layer between the different layers of the composite. Furthermore, imaging was done on tested 3-point bend specimens to examine if there is any change in fracture behavior, i.e., compressive vs tensile failure or failure along the S-U interface.

Optical microscope images of the S, U, and SUUS samples are shown in Figure 5.6, with high magnification images shown in Figure 5.7. The S sample shows crack

propagation to a depth of approximately 2.5 mm into the sample while the U sample shows cracking and failure throughout the thickness. This indicates that S could have superior fracture toughness or a higher crack propagation energy over U. A similar observation is born out when comparing S to SUUS (Figure 5.6a and c). The core U material within the SUUS composite displays significant cracking. This observation may be of interest in applications where failure modes are of interest but is likely not relevant for structural components that are only expected to experience elastic deformation. All samples displayed signs that the primary mode of fracture was from tensile failure on the side opposite of the applied flexural load. No buckling behavior was observed. With respect to fracture behavior the final point of interest is the presence or lack thereof of delamination at the S-U interface within the SUUS composite. The upper region of initial failure (Figure 5.6c and Figure 5.7b) does not show signs of delamination between component material layers (the tan S layers from the white U layers). At the S-U interface closer to the compression side, Figure 5.7a, there is some degree of delamination between layers. This may be due to the different crack propagation behavior between S and U. As the crack propagated through the middle U layers, it ran into the S layer and was inhibited. As a result, the crack deflected more in the horizontal direction parallel to the S-U interface. Further testing, such as impact testing could provide more insights into this behavior.

The S-U interface was also examined both by SEM and optical microscopy. Optical imaging showed mostly even stratification of S and U layers. There were some observed perturbations (~500 μm variance across ~10 mm of length), but none substantial enough to interact with the outer material surface, Figure 5.6d, and Figure 5.7c. Examining the interface more closely, the boundary layer can be clearly distinguished and no HGS

particles appear to have mixed in with the S layer Figure 5.8. These observations are evidence of satisfactory processing techniques for manufacturing a functionally graded composite.

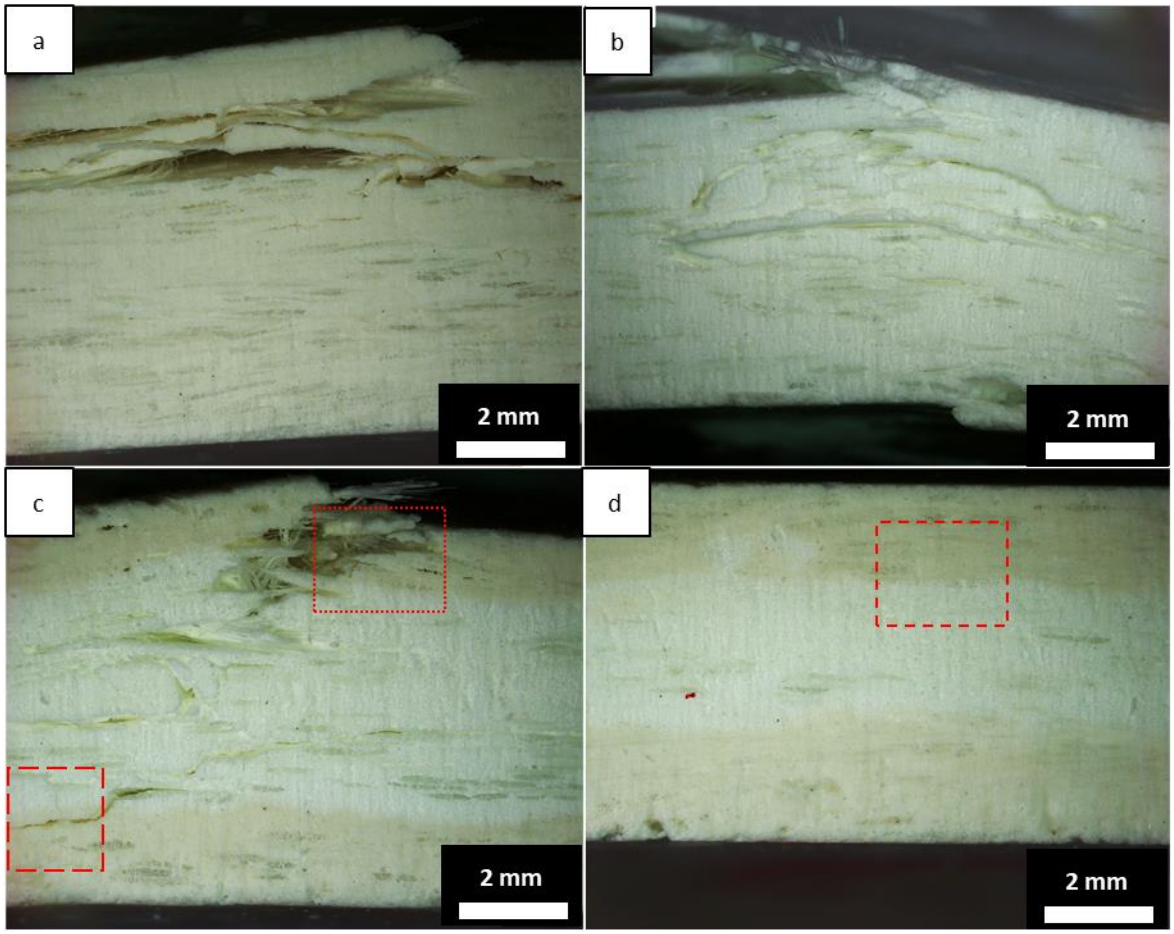

Figure 5.6 Representative fracture images for 3 point bend specimens a) S, b) U, c) SUUS. Upper surfaces were in tension while lower surfaces were in compression during testing. d) Un tested region of SUUS specimen showing segregation between tan S layers and white U layers. Areas outlined in red boxes are shown in Figure 5.7

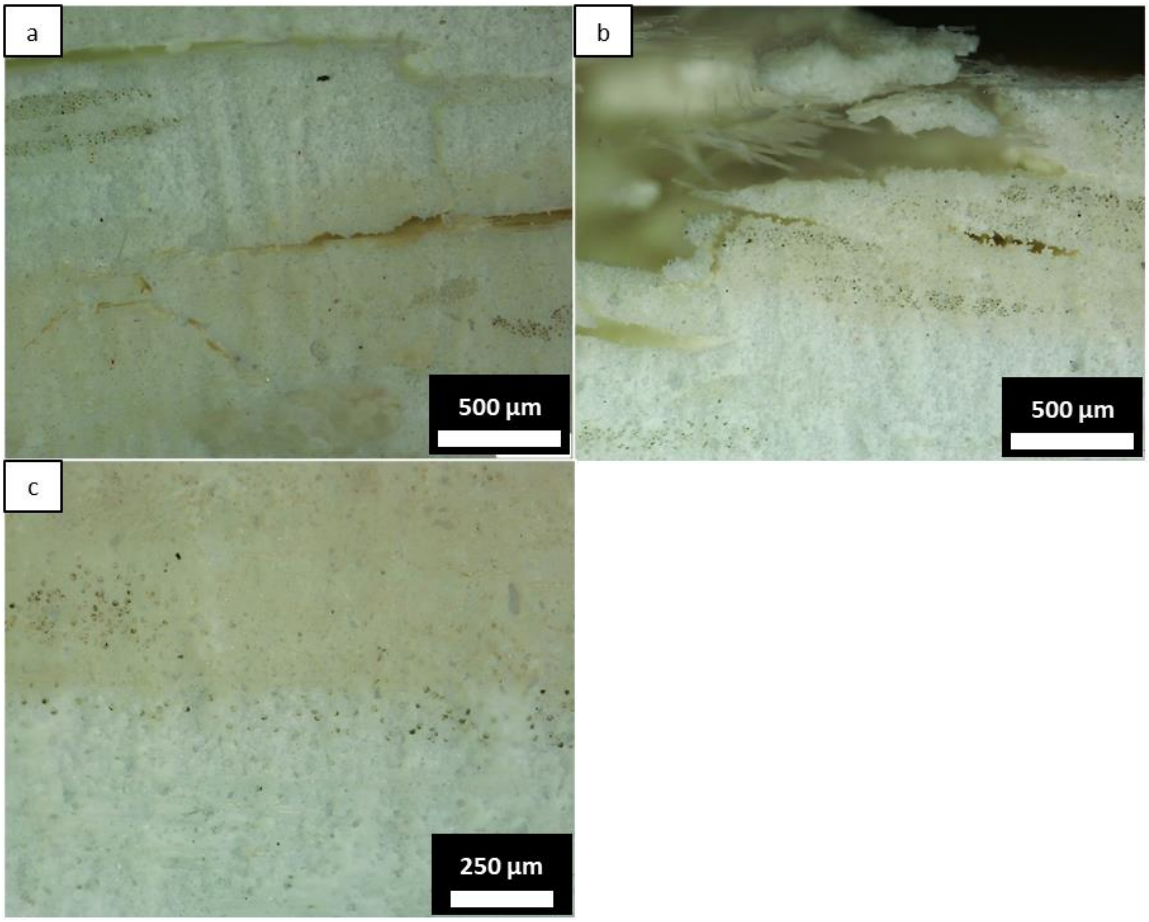

Figure 5.7 Higher magnification optical microscope images of a) dashed box and b) dotted box in Figure 5.6c. Images of c) dashed box in Figure 5.6d.

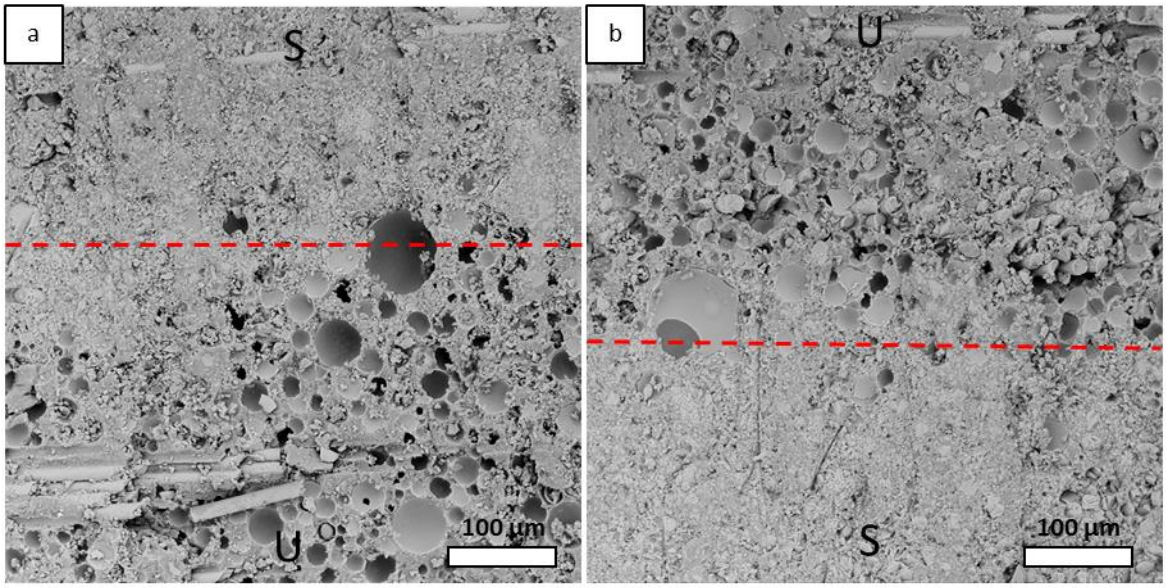

Figure 5.8 Electron microscope images of S-U interface. Dotted red lines indicate approximate boundary between different layers. a) and b) depict the two boundary layers of the SUUS composite. Scale bars are 100 µm. Exposed surface prepared via waterjetting.

5.5 Water Uptake Properties

Water uptake of the SMC composites was characterized at two temperatures, 35 and 70°C to observe the material performance under different acceleration conditions. Two models are useful in understanding the water uptake behavior of materials: the Fickian Diffusion model, and the Langmuir Adsorption model. Water uptake behavior following Fick's second law is characterized by a linear initial region followed by a level equilibrium water uptake plateau. The Langmuir Adsorption model is characterized by more logarithmic like behavior with no plateau. For fiber reinforced composites the primary driver of composite water uptake is glass fiber content. The main avenue for water uptake is via diffusion along the surface of the glass fiber. Glass specific surface area (SSA) or area of glass surface per unit mass of composite, for both GF and HGS were calculated from methods outlined in Chapter 2. The glass SSA values are outlined in Table 5.2.

Although SUUS and M have similar HGS vol% (Table 5.1), the differences in diameter between the HGS types used leads to differing HGS SSA values. Critically, these calculations assume a monodisperse size distribution equal to the reported GF and HGS dimensions. As described in Chapter 4, increased water uptake leads to swelling of polymer chains and delamination of the matrix from the glass surface, resulting in reduced mechanical properties. As a result, minimizing water uptake is of critical interest.

Table 5.2 Calculated specific surface area for glass surfaces found within various composites in this study.

Sample	GF SSA[a] (m^2/kg)	HGS SSA[b] (m^2/kg)	Total Glass SSA (m^2/kg)
S	23	0	23
U	48	5.1	53
SUUS	32	1.8	34
M	38	1.0	39
M-CNC	37	1.0	38

[a] Assume GF diameter of 14 µm. [b] Assumes HGS diameter as reported by supplier in Chapter 2.

The resulting water uptake data is outlined in Figure 5.9 and Figure 5.10. At 35°C the water uptake behavior of all samples is largely coincident. In order of increasing average maximum water uptake the samples are M, M-CNC, SUUS, S, and U. The consistent water uptake behavior across samples at this temperature is an indication of the good moisture stability of the samples at relatively mild conditions. At elevated temperatures (70°C), the samples begin to differentiate more strongly, Figure 5.10. The U sample, containing MS treated HGS and no $CaCO_3$ displays significantly higher maximum water uptake. There are multiple factors that could lead to this effect. First, the significantly increased glass surface area presented by the relatively high loading of HGS would be expected to increase the total amount of water absorbed by the composite, Table 5.2. Second, at elevated temperatures and extended times, the HGS can leech minerals into the

DIW and allow water to permeate the previously entrapped void within the HGS. As a result, the water uptake will increase substantially as the entrapped voids are filled with water. Interestingly, the SUUS does not increase proportionally to the same extent as the U, even though it contains a significant amount of HGS. SUUS more closely mimics the behavior of the S and M samples. The addition of 1phr NaCNC to the M formulation does not seem to significantly affect the water uptake behavior. The primary driving force behind the water uptake remains the glass surface area for M-CNC. The reduced water uptake behavior of S relative to U indicates that in the case of an infinitely wide plate (i.e. where there is limited diffusion through the edges of the material), the water uptake should more closely mimic the behavior of the S material. Future studies are needed with samples generated specifically for this purpose, as this study was constrained both by the sample geometry (12.7 x 12.7 mm^2 squares), and the time (the lockdown due to the COVID-19 pandemic).

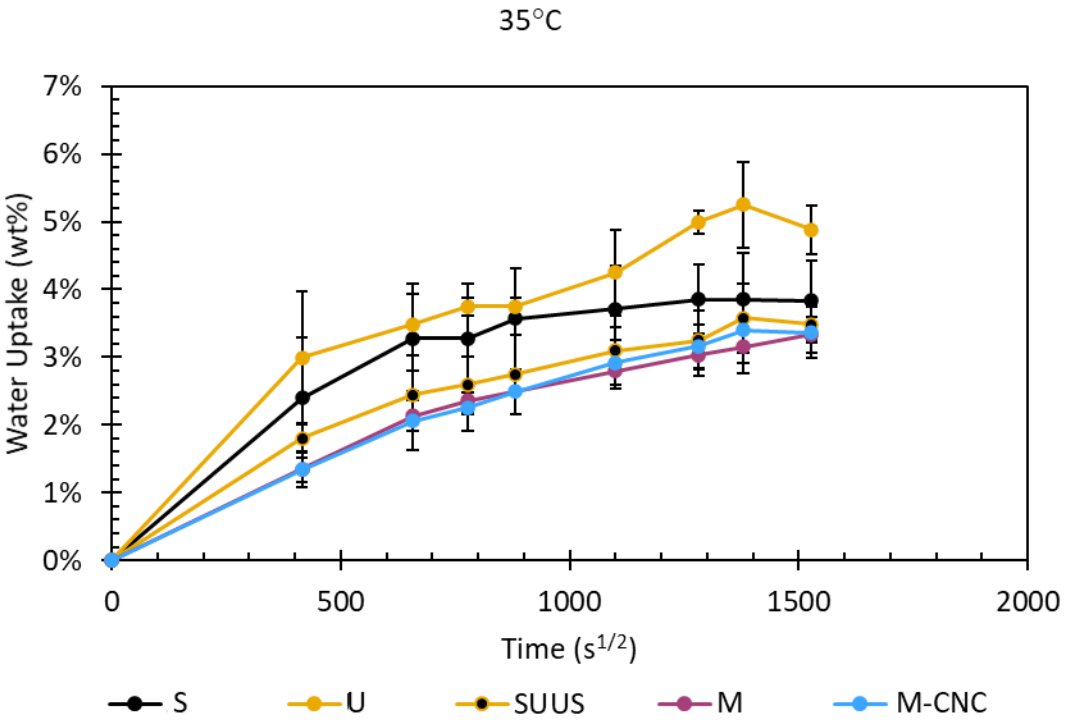

Figure 5.9 Water uptake curves for samples in this study conditioned at 35°C in DIW. Error bars are 1 standard deviation.

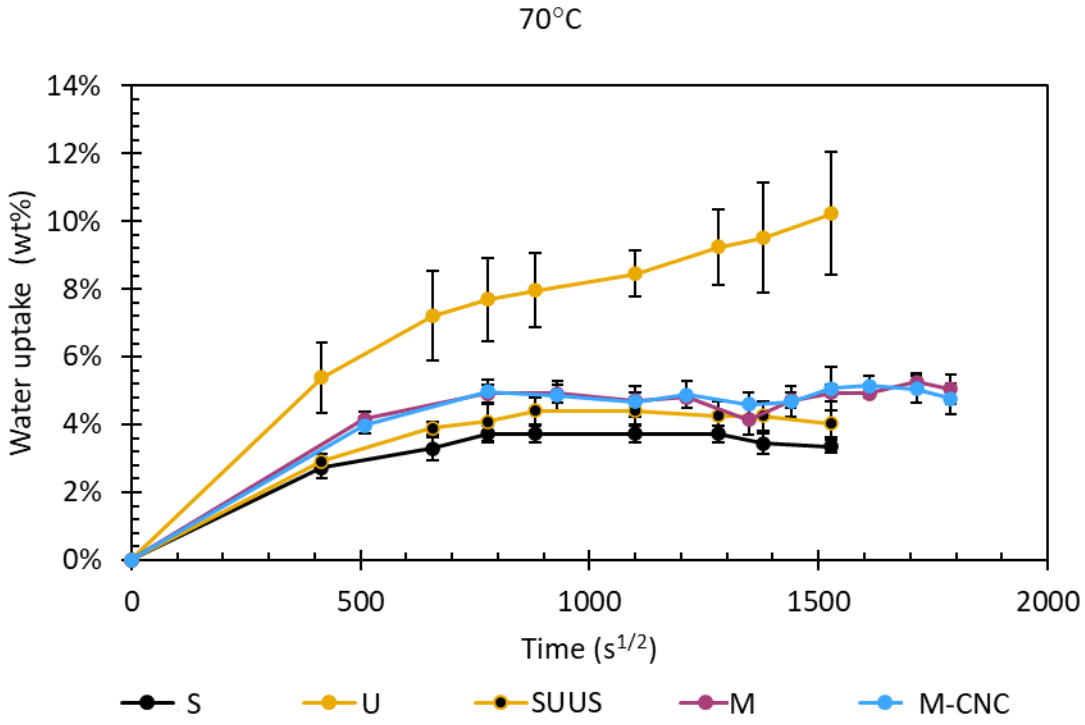

Figure 5.10 Water uptake curves for samples in this study conditioned at 70°C in DIW. Error bars are 1 standard deviation.

The wet aged material properties were also examined for composites. Samples were aged in 70°C DIW for 3.5 weeks and subsequently tested without drying. The dry and wet aged tensile properties are given in Figure 5.11. All samples had a reduction in tensile strength and most samples showed a reduction in tensile modulus. The only exception being U, which displayed an increase in average tensile modulus; however, the shift is small (<10%) and not statistically significant. During water uptake, each material will swell in accordance with the amount of water absorbed, and the elasticity of the matrix. Essentially, if the swelling behavior of S and U is different, then hygrothermal ageing would induce residual stresses within the composite. The SUUS sample did not display significantly lower wet properties than either the material with similar density (M), or the

baseline S. This appears to indicate that the macroscopic layering structure does not make the material more susceptible to mechanical losses during water uptake. The M-CNC sample is not statistically different from the M sample in wet mechanical properties. This indicates that at this loading of CNC, the mechanical properties are not negatively affected.

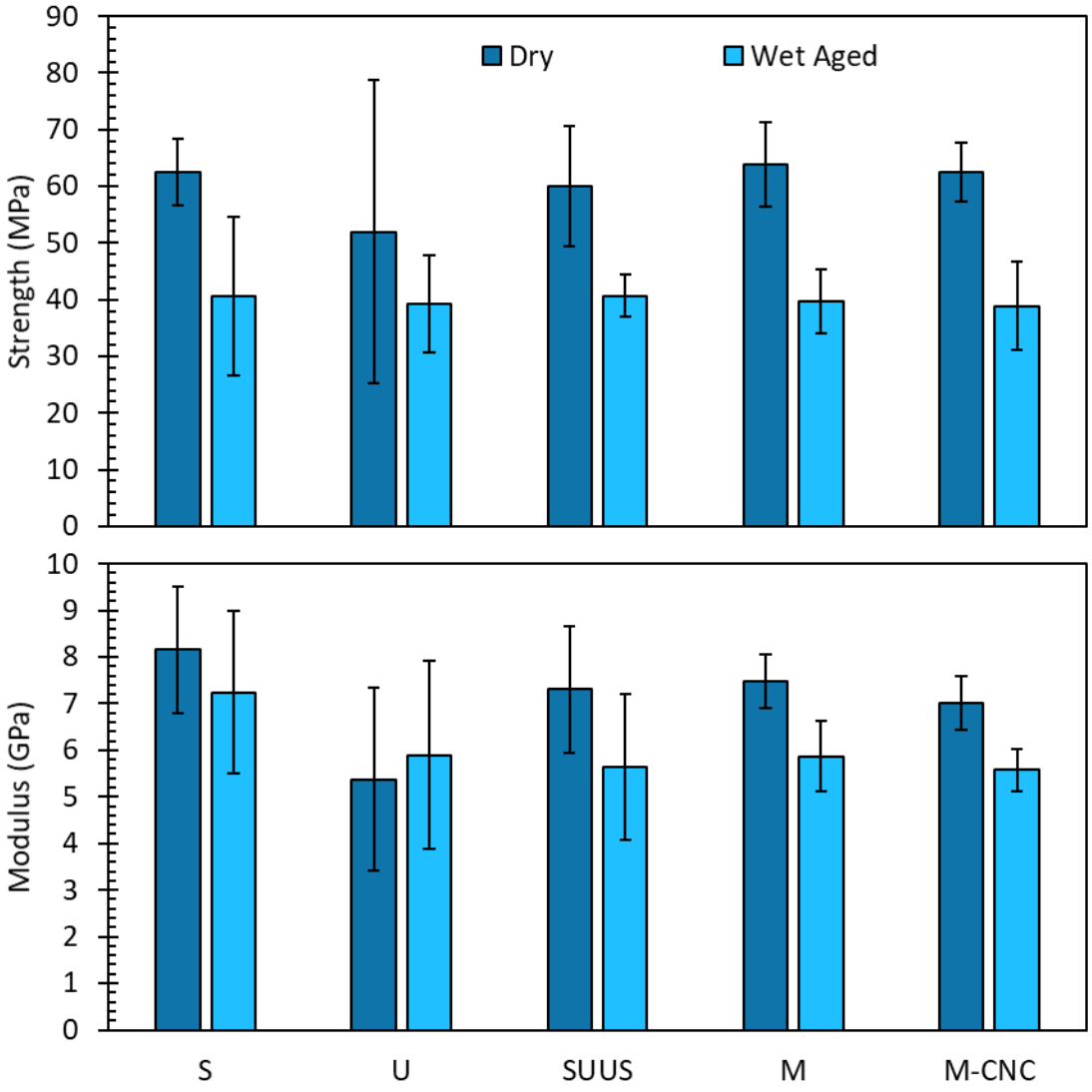

Figure 5.11 Dry and wet aged tensile properties for samples in this study. Error bars are 95% CI.

5.6 Modelling

In developing laminated structures, software tools such as *The Laminator* are useful in predicting laminate properties and aiding in composite design. This study uses classical laminated plate theory to predict tensile and flexural modulus, while Tsai-Hill theory is used to predict tensile strength. Variation between experimental data and theoretical models can usually be traced to the assumptions bound within the model. These calculations assume the material properties for S and U as listed in Section 5.3. And that the composite is a plate 5.5 mm in thickness (the average SUUS plate thickness), with 52% of that thickness being S formulation and 48% being U formulation in an A-B-B-A arrangement. Relative thickness values are determined by a rule of mixtures calculation from the densities of the SUUS composite and the monolithic composites S and U, and assuming no difference in void content between S, U, and SUUS. The model assumes a poisons ratio of 0.30 for all materials, a value selected based on values found in literature [5]. Laminate strength is taken from a first ply failure case.

Table 5.3 outlines the mechanical properties of the SUUS composite as well as the values predicted from the models. Both untreated and wet aged samples are in good agreement with the predicted tensile values, all falling within the 95% CI. The well predicted behavior is an indication of the quality of the classical lamination theory model as well as the quality of the manufacturing processes needed to generate the composite. The flexural modulus is ~10% lower than what would be predicted by the model. This deviation could be due to variations in the load distribution between the experimental and theoretical or the presence of shear forces on the specimen during testing. In both the untreated and wet aged case, the predicted strength value is lower than the average

experimental value. Overall, the model is in good agreement with the experimental values and indicates that classical lamination theory can be used effectively to predict composite properties for functionally graded SMC composites.

Table 5.3 Comparison of experimental and theoretical values for tensile strength (σ_t), tensile modulus (E_t), and flexural modulus (E_f) of the functionally graded composite SUUS. Error bars are 95% CI.

Material	σ_t (MPa)	E_t (GPa)	E_f (GPa)
Experimental	60.0±10.6	7.3±1.4	7.0±0.4
Experimental wet aged	40.7±3.7	5.7±1.6	-
Lamination theory	52.2	6.8	7.8
Lamination theory wet aged	37.0	5.9	-

5.7 Conclusions

Functionally graded SMC composites were developed and validated by various methods, (mechanical testing, density measurements, microscopy, environmental conditioning). SMC composites with $CaCO_3$, HGS, and CNC were also generated and tested in a similar manner. Measurements of functionally graded SMC indicated good interlaminar bonding, and comparable mechanical properties to a singular composite formulation with similar density (1.48 and 1.51 g/cm^3 for SUUS and M respectively). The functionally graded design of the composite increased the specific tensile modulus by 14% and the specific tensile strength by 22% over the S baseline. Analysis of flexural testing

stress strain curves and optical microscope images of fracture patterns revealed a shift in fracture behavior from the more rapid catastrophic type of failure of S, to a gradual type of failure in SUUS and U. Environmental conditioning of samples revealed no significant difference between SUUS, M, and M-CNC materials. These results were taken to indicate that there was not significant crack formation between the S and U layers of the SUUS composite during water absorption as that would have led to a significant spike in water uptake, and a dramatic reduction in mechanical properties. Similarly, the lack of a difference in behavior between M and M-CNC indicates that the addition of 1 phr freeze dried NaCNC did not negatively affect the composite properties. Further studies are needed to investigate the specific mechanisms of water absorption and mechanical degradation in these composites. Classical laminate theory was used to compare the SUUS experimental behavior with theoretical calculations. The collected mechanical data showed good agreement with the model further indicating the efficacy of the processing techniques used. This study provided key insights into the processing-structure-property relationships of functionally graded composites, syntactic foam composites, and the use of CNC in SMC. These results from this fundamental study should prove useful for commercial manufacturers interested in developing novel techniques for reducing density of SMC composites.

CHAPTER 6. CONCLUSIONS & FUTURE WORK

This chapter will outline the major conclusions of each prior chapter and provide a discussion on how these points illuminate the overall objectives of the thesis. Following the conclusions is a discussion on questions that have been revealed during the work and comments on future studies and experiments.

6.1 Chapter Conclusions

The primary goal of this thesis was to develop novel methods for lightweighting PR based composites, this was to be achieved by either (i) substitution of some material with a light but strong material, (ii) reduce the density of the composite by adding ultra-light weight materials such as hollow glass spheres, (iii) design a functionally graded composite, or (iv) a combination of i-iii. Each chapter aimed to address some or all these points and do so via a fundamental approach.

6.1.1 Chapter 3: Cellulose Nanocrystal Reinforced Polyester Composites

- Dispersing freeze-dried CNC in PR via probe sonication proved inadequate for producing a completely nanodisperse system as observed by light microscopy and electron microscopy. The study continued using the CNC-PR composite system with ~100 μm sized, flakelike CNC agglomerates. Mechanical performance improvements were still achieved despite the large CNC agglomerate within the PR matrix.

- Tensile and flexural modulus of freeze-dried CNC-PR composites were 50% and 20%, respectively, higher than the baseline PR, but tensile strength was decreased by as much as 40% relative to the baseline PR.
- Dynamic mechanical analysis of CNC-PR composites demonstrated that the 1 wt% PhCNC and 1 wt% MCNC composite had a 66% and 61% increase in E'_g and a 65% and 48% increase in E'_r over the PR baseline, respectively.

6.1.2 Chapter 4: Nanoreinforced Syntactic Foams

- HGS were successfully coated with both NaCNC and PhCNC as observed by SEM, XPS, and TGA.
- Spray dried NaCNC and HGS did not have any interaction effect when combined in a PR matrix as measured by mechanical testing, and environmental testing.
- PhCNC coated HGS-PR composites had 33% higher E'_g, 41% higher E'_r, but a 40% lower tensile strength relative to the uncoated HGS-PR composite as measured by DMA.
- Maximum water uptake for NaCNC coated HGS-PR composites was 50% lower than that of uncoated HGS-PR composites and 28% lower than MS treated HGS-PR composites.

6.1.3 Chapter 5: Syntactic Foam SMCs

- A functionally graded SMC composite was manufactured utilizing a syntactic foam core. The tensile, flexural, and water uptake behavior of the functionally graded composite was comparable to that of a fully syntactic foam composite.

- Failure phenomenon and crack behavior of the functionally graded composite was dictated by the behavior of the core material rather than the surface material.
- The addition of 1 phr freeze-dried NaCNC to the resin did not substantially change the processing behavior of the system as compared to a formulation without NaCNC. Furthermore, 1 phr NaCNC was not sufficient to significantly impact the physical properties of the composite.
- Classical lamination theory and Tsai-Hill failure criteria models showed good agreement with the experimental data (e.g., flexural modulus, tensile modulus, and tensile strength,) indicating that the system behaved similar to an idealized laminated composite (e.g. good interlaminar bonding, linear stress distribution, and minimal residual stresses).

6.1.4 Dissertation Conclusions Summary

Characterization of surface modified CNC-PR composites showed that probe sonication was not enough to overcome CNC-CNC agglomerate adhesion even among CNC which were surface modified with bulky methyl(triphenyl) phosphonium cations. Mechanical testing via dynamic mechanical analysis, tensile testing, and flexural testing revealed that the addition of PhCNC and MCNC had the strongest effect of increasing the elastic moduli of the composite when compared to the baseline PR. The increase in the case of the PhCNC was attributed to the more favorable PhCNC-PR interactions as compared to SCNC-PR interactions. In the case of the MCNC, it was hypothesized that crosslinking could have occurred between the PR matrix through the unsaturated maleic surface group.

Surface coating of HGS and the resulting HGS-PR composites showed the promising capability of multiscale hierarchical structures for generating low density composites while also mitigating some of the detrimental effects of increased HGS loading, specifically reducing maximum water uptake. The mechanical consequences of CNC coating on HGS were mixed when observed via tensile testing, equivalent elastic modulus, but decreased tensile strength vs untreated HGS-PR composites. Measurements taken by DMA provided a clearer distinction between composite specimens: revealing that the PhCNC coated HGS had enhanced performance over the untreated HGS-PR composites both at lower and elevated temperature conditions. Furthermore, a reduction in the T_β peak of the tan(δ) curve indicates the restriction of lower energy rotations of the polymer network upon addition of CNC coated HGS to the PR matrix.

The final study provided a framework for developing lightweight SMC composites using functionally graded composites, HGS, and CNC. Characterization of the functionally graded composite indicated that the processing method provided good adhesion between individual layers without significant mixing of the material between layers. The functionally graded composite had similar performance to a composite comprised of a single material formulation; however, the surface properties of the functionally graded composite are expected to perform more similarly to that of a commercial standard formulation which provides a higher quality finish and better water barrier properties than the lower density reinforced syntactic foam SMC. It was also noted that the flexural failure behavior of the functionally graded composite was more characteristic of the ultra-low density material than the standard density material. The addition of 1 phr freeze-dried

NaCNC did not have a significant effect on the processing behavior of the material, or the final composite mechanical and hygrothermal behavior.

In conclusion, the processing techniques and material systems developed here provide a guide to future studies and applications which aim to reduce part weight without sacrificing critical to customer properties such as strength, resistance to water damage, and performance at elevated temperatures. This work could prove useful to products in various sectors including automotive, aerospace, naval, and household goods. The materials-process-structure-properties relationships within these systems was explored through various techniques and a fundamental investigation was completed.

6.2 Future Work

6.2.1 Optimization of CNC Drying Method for Maximizing Dispersion Quality

Further work on adjustments to drying procedures for CNC could lead to enhanced dispersion quality in the PR. Other studies have found a benefit to maximizing specific surface area of the dried CNC aerogels to mechanical properties and dispersion quality for CNC-polymer nanocomposites [87, 95, 96]. Preliminary work was conducted to adjust freeze drying parameters and enhance CNC aerogel specific surface area, and the outcome is utilized in Chapter 3.

Such study would likely involve adjusting CNC concentration (~0.1-5 wt% in DIW), CNC dispersion freezing conditions (liquid nitrogen vs. low temperature freezer, freezing as droplets vs. bulk freezing), adding dispersants (tert-butanol, ion exchanged counterions), and adjusting drying conditions (shelf temperature, drying time).

Additionally, to keep the study within the aim of commercial scalability, collaboration and/or access to larger scale lyophilization equipment is necessary.

Characterization of the as dried CNC aerogels would be necessary. SEM and cross polarized light microscopy would be useful in characterizing the aerogel structure, and individual aerogel macroparticle size. Brunauer-Emmet-Teller (BET) gas adsorption or a similar method should also be useful in quantifying the specific surface area of the CNC aerogels.

To determine the permeability of PR into the CNC aerogel, and the dispersion level of CNC in the PR matrix, various techniques would be useful. SEM imaging of fracture surfaces or sectioned surfaces can provide morphological characterization of the CNC-PR composite structure. Cross polarized light microscopy can provide adequate characterization of the agglomerated CNC in the PR. Further testing with DMA and tensile testing can also provide some insight into the interphase regions between CNC and PR. The CNC aerogel with the highest degree of porosity and specific surface area would be expected to have the largest interphase region by volume, as the exposed surface area of CNC should be the greatest. Complete nanodispersion of CNC by this method is possible but still unlikely as CNC-CNC interactions are incredibly strong relative to CNC-polymer interactions [36, 87, 95, 96].

6.2.2 Scaleup of HGS Coating Process to SMC Pilot Production

CNC coated HGS-PR composites were shown to be an enhancement over untreated HGS-PR composites at the lab scale; however, to fully validate this method for reinforced

syntactic foam composites, a pilot scale production run should be completed. Optimization, repeatability, and capability of this process should be addressed.

With respect to further optimization and validation of the CNC coated HGS composites various parameters could be adjusted. During the coating step the parameters of interest are the relative amount of CNC, HGS, and dispersing solvents (DIW, ethanol, or others), the conditions of the silane hydrolysis reaction (temperature, time, pH), and drying temperature and time. Adjusting these variables could lead to an improvement in the consistency of surface quality across various HGS particles, and a reduction of any fracturing of HGS, and HGS agglomeration. Mixing methods for combining HGS into polymer resins has already been explored across conventional two phase (HGS-matrix) syntactic foam studies.

Quantitative validation of the process optimization should also be carried out. SEM analysis combined with gas pycnometery would be useful in describing the degree of HGS fracture during processing, and in determining the change in particle density, if any. Surface analysis methods such as BET, and XPS. FTIR should also be useful for determining chemical interactions and covalent bonding between the HGS and CNC.

Testing of the bulk composites manufactured from CNC coated HGS would be tested in a similar manner to Chapter 5. Mechanical tests, such as compressive testing, tensile testing, flexural testing, and impact testing, should provide good insights into the elastic and failure behavior of the generated reinforced syntactic foam composites. Dynamic mechanical analysis and thermogravimetric analysis could also be used to

characterize the thermal behavior of the composites. Water uptake testing of these composites would also provide good insight into the environmental performance.

Such a study would provide an excellent template for future use of CNC coated HGS in commercially used syntactic foam systems, as well as a strong fundamental understanding of the micromechanical behavior of the composite, and the HGS-matrix interactions.

6.2.3 Further Testing of CNC Coated HGS-PR Composites

Although scale up of lab-based ideas is always an exciting prospect, further testing of the limited CNC coated HGS-PR composite would be eminently useful in investigating the effects of CNC on the HGS-PR interphase. The tests outlined here would be useful for potential scale up of these concepts to industrially relevant processes such as SMC. Additionally, the testing completed in Chapter 4 does not fully encompass some of the benefits of using syntactic foam composites such as decreasing thermal conductivity of the material.

To understand the consequences of CNC coatings on HGS further mechanical testing such as compressive testing, and fracture toughness testing would be useful. Syntactic foam composites are useful in part due to their low density and so have been utilized as fillers in structures in submersible vehicles where large hydrostatic pressures are present [140]. The impact properties of these composites would also be of interest for use in aerospace structures or defence applications. The thermal behavior of these composites (coefficient of thermal expansion, and thermal resistivity) would also be of interest for “under the hood” applications in the automotive sector, where the thermal

gradient can be on the order of 80-90°C. Further understanding of the specific degradation mechanisms during water adsorption should also be considered. In accelerated hygrothermal conditioning, HGS are prone to leeching of minerals and eventual rupture [132]. Testing should be conducted to determine if the CNC coating altogether prevents this behavior, mitigates it, or has not effect.

6.2.4 Further Studies of Functionally Graded SMC

The study outlined in Chapter 5 provided an initial foray into functionally graded SMC and their design. Further examination of the limits of this technique could prove insightful for the fundamental mechanics of SMC processing and compression molding and provide relevant information for commercial applications that aim to develop novel, lightweight SMC structures.

Even when discussing conventional SMC processing the number of potential process variables allows for a tremendous design space; however, during the work in Chapter 5 a handful variables rose to prominent interest. Adjusting the GF content between the layers of the material could provide novel structures (e.g. ≥30 vol% GF in the outer plies and ≤10 vol% GF in the inner plies). The "volume" of the removed GF in the inner plies could be replaced by more HGS. This should further enhance the bending strength of the composite without sacrificing surface properties. Such an experiment may be structured so that several composites of varying GF gradients, but similar overall density are generated, tested, and compared to theoretical calculations. Another possible functionally graded configuration could involve the use of woven fiber mats in addition to a chopped fiber mat.

Further testing on the composites discussed in Chapter 5 would also prove useful in further exploring the fundamental behavior of the functionally graded composite. Surface roughness analysis of the sanded composite by a standard method would provide key data for industry. Environmental conditioning on specifically manufactured composites (i.e. composites that follow the “Thin Specimen” criteria of ASTM D5229) [90]. Computer tomography of the functionally graded SMC sample could also be conducted to better examine the microstructure of the composite and better determine any defects within the composite that may arise from the processing.

REFERENCES

1. Nicolais, L., *Wiley Encyclopedia of Composites*. 2011, John Wiley & Sons.

2. Biron, M., *The Plastics Industry*, in *Thermoplastics and Thermoplastic Composites*, M. Biron, Editor. 2018, William Andrew Publishing. p. 31-132.

3. Mazumdar, S., *Composites manufacturing: materials, product, and process engineering*. 2001: CrC press.

4. Gutowski, T.G.P., *Advanced composites manufacturing*. 1997, New York: New York : John Wiley & Sons.

5. Mallick, P.K., *Fiber-Reinforced Composites*. Dekker Mechanical Engineering. 2007: CRC Press. 638.

6. Kandelbauer, A., et al., *Unsaturated Polyesters and Vinyl Esters*, in *Handbook of Thermoset Plastics*, H. Dodiuk and S.H. Goodman, Editors. 2014, William Andrew Publishing: Boston. p. 111-172.

7. Yalcin, B., *Hollow Glass Microspheres in Sheet Molding Compounds*, in *Hollow Glass Microspheres for Plastics, Elastomers, and Adhesives Compounds*. 2015, Elsevier. p. 123-145.

8. ASADI, A., et al. *Comparative Study of Lightweight Glass Fiber and Basalt Fiber Sheet Molding Compound (SMC) Composites Containing Cellulose Nanocrystals*. in *Proceedings of the American Society for Composites—Thirty-second Technical Conference*. 2017.

9. Asadi, A., et al., *Lightweight sheet molding compound (SMC) composites containing cellulose nanocrystals.* Composite Structures, 2017. **160**: p. 211-219.

10. Asadi, A., et al., *Introducing cellulose nanocrystals in sheet molding compounds (SMC).* Composites Part A: Applied Science and Manufacturing, 2016. **88**: p. 206-215.

11. Favier, V., et al., *Mechanical percolation in cellulose whisker nanocomposites.* Polymer Engineering & Science, 1997. **37**(10): p. 1732-1739.

12. Du, F., et al., *Nanotube Networks in Polymer Nanocomposites: Rheology and Electrical Conductivity.* Macromolecules, 2004. **37**(24): p. 9048-9055.

13. Breuer, O. and U. Sundararaj, *Big returns from small fibers: A review of polymer/carbon nanotube composites.* Polymer Composites, 2004. **25**(6): p. 630-645.

14. Vaia, R.A. and H.D. Wagner, *Framework for nanocomposites.* Materials Today, 2004. **7**(11): p. 32-37.

15. Lin, Y., et al., *Polymeric Carbon Nanocomposites from Carbon Nanotubes Functionalized with Matrix Polymer.* Macromolecules, 2003. **36**(19): p. 7199-7204.

16. Luo, J., *Characterization and modeling of mechanical behavior of polymer/clay nanocomposites.* Composites Science and Technology, 2003. **63**(11): p. 1607-1616.

17. Kornmann, X., et al., *Nanocomposites based on montmorillonite and unsaturated polyester.* Polymer Engineering & Science, 1998. **38**(8): p. 1351-1358.

18. Favier, V., et al., *Nanocomposite materials from latex and cellulose whiskers.* Polymers for Advanced Technologies, 1995. **6**(5): p. 351-355.

19. Moon, R.J., et al., *Cellulose nanomaterials review: structure, properties and nanocomposites.* Chem Soc Rev, 2011. **40**(7): p. 3941-94.

20. Asadi, A. and K. Kalaitzidou, *Process-Structure-Property Relationship in Polymer Nanocomposites*, in *Experimental Characterization, Predictive Mechanical and Thermal Modeling of Nanostructures and their Polymer Composites*, F. Marotti de Sciarra and P. Russo, Editors. 2018, Elsevier. p. 25-100.

21. Dufresne, A., *Dynamic mechanical analysis of the interphase in bacterial polyester/cellulose whiskers natural composites.* Composite Interfaces, 2012. **7**(1): p. 53-67.

22. Hu, L., et al., *Effect of coupling treatment on mechanical properties of bacterial cellulose nanofibre-reinforced UPR ecocomposites.* Materials Letters, 2009. **63**(22): p. 1952-1954.

23. Ansari, F., M. Skrifvars, and L. Berglund, *Nanostructured biocomposites based on unsaturated polyester resin and a cellulose nanofiber network.* Composites Science and Technology, 2015. **117**: p. 298-306.

24. Kargarzadeh, H., et al., *Toughened polyester cellulose nanocomposites: Effects of cellulose nanocrystals and liquid epoxidized natural rubber on morphology and mechanical properties.* Industrial Crops and Products, 2015. **72**: p. 125-132.

25. Kargarzadeh, H., et al., *Cellulose nanocrystal: A promising toughening agent for unsaturated polyester nanocomposite.* Polymer, 2015. **56**: p. 346-357.

26. Kargarzadeh, H., et al., *Cellulose nanocrystal reinforced liquid natural rubber toughened unsaturated polyester: Effects of filler content and surface treatment on its morphological, thermal, mechanical, and viscoelastic properties.* Polymer, 2015. **71**: p. 51-59.

27. Chirayil, C.J., et al., *Nanofibril reinforced unsaturated polyester nanocomposites: Morphology, mechanical and barrier properties, viscoelastic behavior and polymer chain confinement.* Industrial Crops and Products, 2014. **56**: p. 246-254.

28. Gao, C., et al., *Mechanical, moisture absorption, and photodegradation behaviors of bacterial cellulose nanofiber- reinforced unsaturated polyester composites.* Advances in Polymer Technology, 2011. **30**(4): p. 249-256.

29. DiLoreto, E., et al., *Freeze dried cellulose nanocrystal reinforced unsaturated polyester composites: challenges and potential.* Cellulose, 2019. **26**(7): p. 4391-4403.

30. Vu, C.M., et al., *Micro-fibril cellulose as a filler for glass fiber reinforced unsaturated polyester composites: Fabrication and mechanical characteristics.* Macromolecular Research, 2017. **26**(1): p. 54-60.

31. Kargarzadeh, H., et al., *Recent developments on nanocellulose reinforced polymer nanocomposites: A review.* Polymer, 2017. **132**: p. 368-393.

32. Lavoratti, A., L.C. Scienza, and A.J. Zattera, *Dynamic-mechanical and thermomechanical properties of cellulose nanofiber/polyester resin composites.* Carbohydr Polym, 2016. **136**: p. 955-63.

33. Goswami, J., et al., *The Effect of Cellulose Nanocrystal Coatings on the Glass Fiber-Epoxy Interphase.* Materials (Basel), 2019. **12**(12): p. 1951.

34. Reale Batista, M.D. and L.T. Drzal, *Carbon fiber/epoxy matrix composite interphases modified with cellulose nanocrystals.* Composites Science and Technology, 2018. **164**: p. 274-281.

35. Peng, S.X., et al., *Enhanced dispersion and properties of a two-component epoxy nanocomposite using surface modified cellulose nanocrystals.* Polymer, 2017. **112**: p. 359-368.

36. Fox, D.M., et al., *Simultaneously Tailoring Surface Energies and Thermal Stabilities of Cellulose Nanocrystals Using Ion Exchange: Effects on Polymer Composite Properties for Transportation, Infrastructure, and Renewable Energy Applications.* ACS Appl Mater Interfaces, 2016. **8**(40): p. 27270-27281.

37. Asadi, A., et al., *Improving the interfacial and mechanical properties of short glass fiber/epoxy composites by coating the glass fibers with cellulose nanocrystals.* Express Polymer Letters, 2016. **10**(7): p. 587-597.

38. Abraham, E., et al., *Highly Modified Cellulose Nanocrystals and Formation of Epoxy-Nanocrystalline Cellulose (CNC) Nanocomposites.* ACS Appl Mater Interfaces, 2016. **8**(41): p. 28086-28095.

39. Uribe, B.E.B., A.J.F. Carvalho, and J.R. Tarpani, *Low-cost, environmentally friendly route to produce glass fiber-reinforced polymer composites with microfibrillated cellulose interphase.* Journal of Applied Polymer Science, 2016. **133**(46).

40. Lu, T., et al., *Effect of surface modification of bamboo cellulose fibers on mechanical properties of cellulose/epoxy composites.* Composites Part B: Engineering, 2013. **51**: p. 28-34.

41. Tang, L. and C. Weder, *Cellulose whisker/epoxy resin nanocomposites.* ACS Appl Mater Interfaces, 2010. **2**(4): p. 1073-80.

42. Gabr, M.H., et al., *A study on mechanical properties of bacterial cellulose/epoxy reinforced by plain woven carbon fiber modified with liquid rubber.* Composites Part A: Applied Science and Manufacturing, 2010. **41**(9): p. 1263-1271.

43. Gabr, M.H., et al., *Effect of microfibrillated cellulose on mechanical properties of plain-woven CFRP reinforced epoxy.* Composite Structures, 2010. **92**(9): p. 1999-2006.

44. Rusli, R. and S.J. Eichhorn, *Determination of the stiffness of cellulose nanowhiskers and the fiber-matrix interface in a nanocomposite using Raman spectroscopy.* Applied Physics Letters, 2008. **93**(3): p. 033111.

45. Wang, W.-J., W.-W. Wang, and Z.-Q. Shao, *Surface modification of cellulose nanowhiskers for application in thermosetting epoxy polymers.* Cellulose, 2014. **21**(4): p. 2529-2538.

46. Chirayil, C.J., et al., *Rheological behaviour of nanocellulose reinforced unsaturated polyester nanocomposites.* Int J Biol Macromol, 2014. **69**: p. 274-81.

47. Helfferich, F.G., *Ion Exchange*. 1995: Courier Corporation. 624.

48. Zheng, T. and S. Pilla, *Melt Processing of Cellulose Nanocrystal Filled Composites: Towards Reinforcement and Foam Nucleation.* Industrial & Engineering Chemistry Research, 2020.

49. Kargarzadeh, H., et al., *Handbook of Nanocellulose and Cellulose Nanocomposites*. 2017, Somerset, GERMANY: John Wiley & Sons, Incorporated.

50. Uribe, B.E.B., et al., *TEMPO-oxidized cellulose nanofibers as interfacial strengthener in continuous-fiber reinforced polymer composites.* Materials & Design, 2017. **133**: p. 340-348.

51. Gupta, N., et al., *Applications of Polymer Matrix Syntactic Foams.* Jom, 2013. **66**(2): p. 245-254.

52. Gregl, B., *Glass microspheres produce lower weight SMC.* Reinforced Plastics, 1997. **34**(3617/97): p. 34-37.

53. Gregl, B.V., et al., *Formulation Advancements in Hollow-Glass Microspheres Filled SMC*, in *SAE Technical Paper Series*. 1999.

54. Larson, L.D., et al., *SMC Glass Microspheres as a Low-Density*

Alternative to Traditional Fillers. 1998: p. 1-5.

55. Ferreira, J.A.M., C. Capela, and J.D. Costa, *A study of the mechanical behaviour on fibre reinforced hollow microspheres hybrid composites.* Composites Part A: Applied Science and Manufacturing, 2010. **41**(3): p. 345-352.

56. Ferreira, J.A.M., C. Capela, and J.D. Costa, *Dynamic Mechanical Analysis of Hybrid Fibre/Glass Microspheres Composites.* Strain, 2011. **47**(3): p. 275-280.

57. Gupta, N., D. Pinisetty, and V.C. Shunmugasamy, *Reinforced polymer matrix syntactic foams: effect of nano and micro-scale reinforcement*. 2013: Springer Science & Business Media.

58. Marur, P.R., *Numerical estimation of effective elastic moduli of syntactic foams.* Finite elements in analysis and design, 2010. **46**(11): p. 1001-1007.

59. Bardella, L., et al., *A critical evaluation of micromechanical models for syntactic foams.* Mechanics of Materials, 2012. **50**: p. 53-69.

60. Marur, P.R., *Influence of imperfect interface on the elastic moduli of syntactic foams.* Computational materials science, 2009. **46**(2): p. 327-332.

61. Marur, P.R., *Effective elastic moduli of syntactic foams.* Materials Letters, 2005. **59**(14-15): p. 1954-1957.

62. Tagliavia, G., M. Porfiri, and N. Gupta, *Analysis of hollow inclusion–matrix debonding in particulate composites.* International Journal of Solids and Structures, 2010. **47**(16): p. 2164-2177.

63. Huang, R. and P. Li, *Elastic behaviour and failure mechanism in epoxy syntactic foams: The effect of glass microballoon volume fractions.* Composites Part B: Engineering, 2015. **78**: p. 401-408.

64. Hamarneh, A., *DSM proposes new roads to weight reduction.* Reinforced Plastics, 2014. **58**(3): p. 19-21.

65. Deepthi, M., et al., *Mechanical and thermal characteristics of high density polyethylene–fly ash cenospheres composites.* Materials & Design, 2010. **31**(4): p. 2051-2060.

66. Bharath Kumar, B.R., et al., *Effect of particle surface treatment and blending method on flexural properties of injection-molded cenosphere/HDPE syntactic foams.* Journal of Materials Science, 2016. **51**(8): p. 3793-3805.

67. Li, G. and N. Jones, *Development of rubberized syntactic foam.* Composites Part A: Applied Science and Manufacturing, 2007. **38**(6): p. 1483-1492.

68. Karthikeyan, C.S. and S. Sankaran, *Effect of Absorption in Aqueous and Hygrothermal Media on the Compressive Properties of Glass Fiber Reinforced Syntactic Foam.* Journal of Reinforced Plastics and Composites, 2016. **20**(11): p. 982-993.

69. Karthikeyan, C.S., et al., *Processing and compressive strengths of syntactic foams with and without fibrous reinforcements.* Journal of Applied Polymer Science, 2001. **81**(2): p. 405-411.

70. Gupta, N., et al., *Correlation of Processing Methodology to the Physical and Mechanical Properties of Syntactic Foams With and Without Fibers.* Materials Characterization, 1999. **43**(4): p. 271-277.

71. Herrera-Ramírez, L.C., M. Cano, and R.G. de Villoria, *Low thermal and high electrical conductivity in hollow glass microspheres covered with carbon nanofiber–polymer composites.* Composites Science and Technology, 2017. **151**: p. 211-218.

72. Zegeye, E.F. and E. Woldesenbet, *Processing and mechanical characterization of carbon nanotube reinforced syntactic foams.* Journal of Reinforced Plastics and Composites, 2012. **31**(15): p. 1045-1052.

73. Zhang, L., J. Zhang, and D.-Y. Wang, *Hierarchical layered double hydroxide nanosheets/phosphorus-containing organosilane functionalized hollow glass microsphere towards high performance epoxy composite: Enhanced interfacial adhesion and bottom-up charring behavior.* Polymer, 2020. **210**: p. 123018.

74. Paul, D., et al. *Analysis of syntactic foam–GFRP sandwich composites for flexural loads*. in *Journal of Physics: Conference Series*. 2018. IOP Publishing.

75. Li, R., et al., *Surface modification of hollow glass microsphere and its marine-adaptive composites with epoxy resin.* 2020. **29**: p. 2633366X20974682.

76. Pacaphol, K., D.J.S. Aht-Ong, and C. Technology, *The influences of silanes on interfacial adhesion and surface properties of nanocellulose film coating on glass and aluminum substrates.* 2017. **320**: p. 70-81.

77. Gupta, N. and E. Woldesenbet, *Characterization of Flexural Properties of Syntactic Foam Core Sandwich Composites and Effect of Density Variation.* Journal of Composite Materials, 2005. **39**(24): p. 2197-2212.

78. Gupta, N. and E. Woldesenbet, *Compressive fracture features of syntactic foams-microscopic examination.* Journal of Materials Science, 2002. **37**(15): p. 3199-3209.

79. El-Hadek, M.A. and H.V. Tippur, *Dynamic fracture parameters and constraint effects in functionally graded syntactic epoxy foams.* International Journal of Solids and Structures, 2003. **40**(8): p. 1885-1906.

80. Gupta, N., S.K. Gupta, and B.J. Mueller, *Analysis of a functionally graded particulate composite under flexural loading conditions.* Materials Science and Engineering: A, 2008. **485**(1-2): p. 439-447.

81. Kishore, R. Shankar, and S. Sankaran, *Gradient syntactic foams: Tensile strength, modulus and fractographic features.* Materials Science and Engineering: A, 2005. **412**(1-2): p. 153-158.

82. Reid, M.S., M. Villalobos, and E.D. Cranston, *Benchmarking Cellulose Nanocrystals: From the Laboratory to Industrial Production.* Langmuir, 2017. **33**(7): p. 1583-1598.

83. Wang, R., et al., *Tailored and Integrated Production of Carboxylated Cellulose Nanocrystals (CNC) with Nanofibrils (CNF) through Maleic Acid Hydrolysis.* ChemNanoMat, 2017. **3**(5): p. 328-335.

84. Jiang, F. and Y.L. Hsieh, *Assembling and redispersibility of rice straw nanocellulose: effect of tert-butanol.* ACS Appl Mater Interfaces, 2014. **6**(22): p. 20075-84.

85. ASTM, *Test Method for Tensile Properties of Plastics*. 2014, ASTM International: West Conshohocken, PA.

86. ASTM, *Standard Test Methods for Flexural Properties of Unreinforced and Reinforced Plastics and Electrical Insulating Materials*. 2017, ASTM International: West Conshohocken, PA.

87. Khoshkava, V. and M.R. Kamal, *Effect of cellulose nanocrystals (CNC) particle morphology on dispersion and rheological and mechanical properties of polypropylene/CNC nanocomposites.* ACS Appl Mater Interfaces, 2014. **6**(11): p. 8146-57.

88. ASTM, *Standard Test Method for Glass Transition Temperature (DMA Tg) of Polymer Matrix Composites by Dynamic Mechanical Analysis (DMA)*. 2015, ASTM International: West Conshohocken, PA.

89. ASTM, *Standard Test Methods for Density and Specific Gravity (Relative Density) of Plastics by Displacement*. 2013, ASTM International.

90. ASTM, *Test Method for Moisture Absorption Properties and Equilibrium Conditioning of Polymer Matrix Composite Materials*. 2014, ASTM International: West Conshohocken, PA.

91. Halpin, J. and N. Pagano, *The laminate approximation for randomly oriented fibrous composites.* Journal of Composite Materials, 1969. **3**(4): p. 720-724.

92. Jones, R.M., *Mechanics of composite materials*. 1998: CRC press.

93. Pister, K. and S. Dong, *Elastic bending of layered plates.* Journal of the Engineering Mechanics Division, 1959. **85**(4): p. 1-10.

94. Reissner, E. and Y. Stavsky, *Bending and stretching of certain types of heterogeneous aeolotropic elastic plates.* 1961.

95. Khoshkava, V. and M. Kamal, *Effect of drying conditions on cellulose nanocrystal (CNC) agglomerate porosity and dispersibility in polymer nanocomposites.* Powder technology, 2014. **261**: p. 288-298.

96. Kamal, M.R. and V. Khoshkava, *Effect of cellulose nanocrystals (CNC) on rheological and mechanical properties and crystallization behavior of PLA/CNC nanocomposites.* Carbohydr Polym, 2015. **123**: p. 105-14.

97. De France, K.J., T. Hoare, and E.D. Cranston, *Review of hydrogels and aerogels containing nanocellulose.* Chemistry of Materials, 2017. **29**(11): p. 4609-4631.

98. Han, J., et al., *Self-assembling behavior of cellulose nanoparticles during freeze-drying: effect of suspension concentration, particle size, crystal structure, and surface charge.* Biomacromolecules, 2013. **14**(5): p. 1529-40.

99. Khare, K.S., F. Khabaz, and R. Khare, *Effect of carbon nanotube functionalization on mechanical and thermal properties of cross-linked epoxy-carbon nanotube nanocomposites: role of strengthening the interfacial interactions.* ACS Appl Mater Interfaces, 2014. **6**(9): p. 6098-110.

100. Ma, P.C., J.-K. Kim, and B.Z. Tang, *Effects of silane functionalization on the properties of carbon nanotube/epoxy nanocomposites.* Composites Science and Technology, 2007. **67**(14): p. 2965-2972.

101. Arslan, D., et al., *Effect of preparation method on the properties of polylactide/cellulose nanocrystal nanocomposites.* Polymer Composites, 2020. **41**(10): p. 4170-4180.

102. Tsai, H. and J. Kardos, *The Halpin-Tsai Equations.* Polym. Eng. Sci, 1976. **16**: p. 344-352.

103. Munson-McGee, S.H., *Estimation of the critical concentration in an anisotropic percolation network.* Phys Rev B Condens Matter, 1991. **43**(4): p. 3331-3336.

104. Ashraf, M.A., et al., *Effects of Size and Aggregation/Agglomeration of Nanoparticles on the Interfacial/Interphase Properties and Tensile Strength of Polymer Nanocomposites.* Nanoscale Res Lett, 2018. **13**(1): p. 214.

105. Tanaka, F. and T. Iwata, *Estimation of the elastic modulus of cellulose crystal by molecular mechanics simulation.* Cellulose, 2006. **13**(5): p. 509-517.

106. Reising, A.B., R.J. Moon, and J.P. Youngblood, *Effect of particle alignment on mechanical properties of neat cellulose nanocrystal films.* Journal of Science & Technology for Forest Products and Processes: Volume 2, Number 6, 2012; pp. 32-41., 2012. **2**(6): p. 32-41.

107. Zhang, S., et al., *Soy protein isolate-based films reinforced by surface modified cellulose nanocrystal.* Industrial Crops and Products, 2016. **80**: p. 207-213.

108. Qian, S., et al., *Effects of bamboo cellulose nanowhisker content on the morphology, crystallization, mechanical, and thermal properties of PLA matrix biocomposites.* Composites Part B: Engineering, 2018. **133**: p. 203-209.

109. Sanchez-Garcia, M.D. and J.M. Lagaron, *On the use of plant cellulose nanowhiskers to enhance the barrier properties of polylactic acid.* Cellulose, 2010. **17**(5): p. 987-1004.

110. Cao, X., et al., *New nanocomposite materials reinforced with cellulose nanocrystals in nitrile rubber.* Polymer Testing, 2013. **32**(5): p. 819-826.

111. Goertzen, W.K. and M. Kessler, *Dynamic mechanical analysis of fumed silica/cyanate ester nanocomposites.* Composites Part A: Applied Science and Manufacturing, 2008. **39**(5): p. 761-768.

112. Putz, K.W., et al., *Effect of cross-link density on interphase creation in polymer nanocomposites.* Macromolecules, 2008. **41**(18): p. 6752-6756.

113. Benoit, D., et al., *One-Step Formation of Functionalized Block Copolymers.* Macromolecules, 2000. **33**(5): p. 1505-1507.

114. Suo, A., et al., *Synthesis and properties of carboxymethyl cellulose-graft-poly(acrylic acid-co-acrylamide) as a novel cellulose-based superabsorbent.* Journal of Applied Polymer Science, 2007. **103**(3): p. 1382-1388.

115. Haque, E., et al., *Scalable coating methods for enhancing glass fiber–epoxy interactions with cellulose nanocrystals.* Cellulose, 2021: p. 1-16.

116. Garbassi, F., et al., *A quantitative and qualitative assessment of the bonding of 3-methacryloxypropyltrimethoxysilane to filler surfaces using XPS and SSIMS (FABMS) techniques.* Journal of colloid and interface science, 1987. **117**(1): p. 258-270.

117. Pantano, C.G. and T. Wittberg, *XPS analysis of silane coupling agents and silane-treated E-glass fibers.* Surface and interface analysis, 1990. **15**(8): p. 498-501.

118. Yin, Y., et al., *Cellulose nanocrystals functionalized with amino-silane and epoxy-poly (ethylene glycol) for reinforcement and flexibilization of poly (lactic acid): material preparation and compatibility mechanism.* Cellulose, 2018. **25**(11): p. 6447-6463.

119. Edward DiLoreto, A.B., Kyriaki Kalaitzidou. *Glass Fiber Reinforced Polyester Syntactic Foam*. in *American Society for Composites*. 2019. Atlanta, GA.

120. Tall, K., et al., *Influence of hollow glass microspheres on the mechanical and physical properties and cost of particle reinforced polymer composites.* Proceedings of the Estonian Academy of Sciences, 2012. **61**(3): p. 160-165.

121. Shutov, F.A., *Syntactic polymer foams.* Chromatography/foams/copolymers, 1986: p. 63-123.

122. Porfiri, M. and N. Gupta, *Effect of volume fraction and wall thickness on the elastic properties of hollow particle filled composites.* Composites Part B: Engineering, 2009. **40**(2): p. 166-173.

123. Menard, K.P. and N. Menard, *Dynamic mechanical analysis.* Encyclopedia of Analytical Chemistry: Applications, Theory and Instrumentation, 2006: p. 1-25.

124. Derrien, K. and P. Gilormini, *The effect of applied stresses on the equilibrium moisture content in polymers.* Scripta Materialia, 2007. **56**(4): p. 297-299.

125. Kasturiarachchi, K.A. and G. Pritchard, *Water absorption of glass/epoxy laminates under bending stresses.* Composites, 1983. **14**(3): p. 244-250.

126. Gupta, N. and E. Woldesenbet, *Hygrothermal studies on syntactic foams and compressive strength determination.* Composite Structures, 2003. **61**(4): p. 311-320.

127. Dhakal, H., Z. Zhang, and M. Richardson, *Effect of water absorption on the mechanical properties of hemp fibre reinforced unsaturated polyester composites.* Composites Science and Technology, 2007. **67**(7-8): p. 1674-1683.

128. Abdelmouleh, M., et al., *Modification of cellulose fibers with functionalized silanes: Effect of the fiber treatment on the mechanical performances of cellulose-thermoset composites.* Journal of Applied Polymer Science, 2005. **98**(3): p. 974-984.

129. Boinard, E., et al., *Influence of resin chemistry on water uptake and environmental ageing in glass fibre reinforced composites-polyester and vinyl ester laminates.* Journal of materials science, 2000. **35**(8): p. 1931-1937.

130. Apicella, A., et al., *The water ageing of unsaturated polyester-based composites: influence of resin chemical structure.* Composites, 1983. **14**(4): p. 387-392.

131. Ellis, B. and M. Found, *The effects of water absorption on a polyester/chopped strand mat laminate.* Composites, 1983. **14**(3): p. 237-243.

132. Sauvant-Moynot, V., N. Gimenez, and H. Sautereau, *Hydrolytic ageing of syntactic foams for thermal insulation in deep water: degradation mechanisms and water uptake model.* Journal of materials science, 2006. **41**(13): p. 4047-4054.

133. Grosjean, F., et al., *Comprehensive analyses of syntactic foam behaviour in deepwater environment.* Journal of Materials Science, 2009. **44**(6): p. 1462-1468.

134. Strauchs, A., et al. *The impact of water absorption on the dielectric properties of syntactic foam*. in *2010 10th IEEE International Conference on Solid Dielectrics*. 2010. IEEE.

135. Chen, Y., et al., *A novel route to modify the interface of glass fiber-reinforced epoxy resin composite via bacterial cellulose.* International Journal of Polymeric Materials and Polymeric Biomaterials, 2014. **63**(4): p. 221-227.

136. Dankovich, T.A. and D.G. Gray, *Contact angle measurements on smooth nanocrystalline cellulose (I) thin films.* Journal of adhesion science and technology, 2011. **25**(6-7): p. 699-708.

137. Espino-Perez, E., et al., *Designed cellulose nanocrystal surface properties for improving barrier properties in polylactide nanocomposites.* Carbohydr Polym, 2018. **183**: p. 267-277.

138. Berman, A.E., *Reinforced Syntactic Foam SMC Composites for Automotive Lightweighting*. 2020, Georgia Institute of Technology.

139. Berman, A., et al., *Hollow glass spheres in sheet molding compound composites: Limitations and potential.* Polymer Composites, 2020: p. e25900.

140. Gupta, N., et al., *Applications of polymer matrix syntactic foams.* Jom, 2014. **66**(2): p. 245-254.